การพัฒนาตัวรับรู้ชีวภาพฐานกระดาษสำหรับการตรวจวัดสารบ่งชี้ทางชีวภาพ

นางสาวนิภาพรรณ ฤาชา

วิทยานิพนธ์นี้เป็นส่วนหนึ่งของการศึกษาตามหลักสูตรปริญญาวิทยาศาสตรดุษฎีบัณฑิต
สาขาวิชาวิทยาศาสตร์มหโมเลกุล
คณะวิทยาศาสตร์ จุฬาลงกรณ์มหาวิทยาลัย
ปีการศึกษา 2557

DEVELOPMENT OF PAPER-BASED BIOSENSOR FOR BIOMARKER DETECTION

Miss Nipapan Ruecha

A Dissertation Submitted in Partial Fulfillment of the Requirements
for the Degree of Doctor of Philosophy Program in Macromolecular Science
Faculty of Science
Chulalongkorn University
Academic Year 2014

Thesis Title	DEVELOPMENT OF PAPER-BASED BIOSENSOR FOR BIOMARKER DETECTION
By	Miss Nipapan Ruecha
Field of Study	Macromolecular Science
Thesis Advisor	Professor Orawon Chailapakul, Ph.D.
Thesis Co-Advisor	Nadnudda Rodthongkum, Ph.D.

Accepted by the Faculty of Science, Chulalongkorn University in Partial Fulfillment of the Requirements for the Doctoral Degree

.....Dean of the Faculty of Science
(Professor Supot Hannongbua, Dr.rer.nat.)

THESIS COMMITTEE

.....Chairman
(Associate Professor Voravee Hoven, Ph.D.)

.....Thesis Advisor
(Professor Orawon Chailapakul, Ph.D.)

.....Thesis Co-Advisor
(Nadnudda Rodthongkum, Ph.D.)

.....Examiner
(Associate Professor Nuanphun Chantarasiri, Ph.D.)

.....Examiner
(Assistant Professor Varawut Tangpasuthadol, Ph.D.)

.....External Examiner
(Assistant Professor Weena Siangproh, Ph.D.)

นิภาพรรณ ฤาชา : การพัฒนาตัวรับรู้ชีวภาพฐานกระดาษสำหรับการตรวจวัดสารบ่งชี้ทางชีวภาพ (DEVELOPMENT OF PAPER-BASED BIOSENSOR FOR BIOMARKER DETECTION) อ.ที่ปรึกษาวิทยานิพนธ์หลัก: ศ. ดร.อรวรรณ ชัยลภากุล, อ.ที่ปรึกษาวิทยานิพนธ์ร่วม: ดร.นาฏนัดดา รอดทองคำ, 105 หน้า.

วิทยานิพนธ์ฉบับนี้มุ่งเน้นการพัฒนาไบโอเซนเซอร์ชนิดใหม่สำหรับการตรวจวิเคราะห์สารบ่งชี้ทางชีวภาพที่มีความไวสูงในสารตัวอย่างทางชีวภาพ โดยสามารถแบ่งออกเป็น 2 ส่วน ในส่วนแรก คือ การพัฒนาตัวรับรู้ชีวภาพให้มีความไวโดยใช้วัสดุนาโนคอมพอสิตของกราฟีนและพอลิแอนิลีน สารบ่งชี้ทางชีวภาพเช่น คอเลสเทอรอล และโลหะหนัก เช่น สังกะสี แคดเมียม และตะกั่ว ในของเหลวทางชีวภาพ ได้ถูกวิเคราะห์เชิงปริมาณโดยใช้ตัวรับรู้ที่นำเสนอในวิทยานิพนธ์นี้ ในส่วนที่สอง คือแอคทีพเปเปอร์ชิพสำหรับการตรวจวัดสารหลายชนิดทางเคมีไฟฟ้า ประกอบด้วยกลูโคส โดปามีน และกรดยูริก สารโคบอลต์(II)ทาโลไซยานีน อนุภาคนาโนของทอง และกราฟีนออกไซด์ที่ถูกรีดิวซ์ ถูกใช้เพื่อการดัดแปรขั้วไฟฟ้าสำหรับเพิ่มความไวในการตรวจวัดของตัวรับรู้ทางชีวภาพ พารามิเตอร์ของระบบการตรวจวัดทางเคมีไฟฟ้าได้รับการปรับให้มีความเหมาะสมเพื่อให้ได้ภาวะที่เหมาะสมที่สุดในการตรวจวิเคราะห์สารบ่งชี้ทางชีวภาพ โดยความไวของตัวรับรู้ชีวภาพที่ถูกพัฒนาขึ้นก็ได้ถูกอภิปรายไว้ ณ ที่นี้ด้วย ยิ่งไปกว่านั้นได้มีการศึกษาผลของวัสดุที่ใช้ในการสร้างตัวรับรู้ ประกอบด้วย กระดาษ และ ฟิล์มพลาสติก จากผลการทดลองพบว่าตัวรับรู้ฐานกระดาษมีความเหมาะสมสำหรับการตรวจวัดสารชีวโมเลกุล ในทางตรงกันข้ามตัวรับรู้ฐานพลาสติกให้ผลที่ดีในการตรวจวัดโลหะหนักด้วยเทคนิคสแควร์เวฟแอนอดิกสทริปปิงโวลแทมเมทรี นอกจากนี้ได้มีการศึกษาประสิทธิภาพของการตรวจวิเคราะห์ ได้แก่ ช่วงความเป็นเส้นตรง ขีดจำกัดต่ำสุดในการตรวจวัดและตรวจปริมาณ (LOD และ LOQ) การตรวจซ้ำ ความแม่น ในส่วนของความจำเพาะเจาะจงต่อการตรวจวัดของตัวรับรู้ชีวภาพที่ถูกพัฒนาขึ้น ได้ถูกศึกษาโดยการใส่สารรบกวนที่พบทั่วไปในตัวอย่างจริงลงในระบบวิเคราะห์ ซึ่งพบว่าความถูกต้องและความเที่ยงของตัวรับรู้ชีวภาพที่พัฒนาขึ้นอยู่ในช่วงที่สามารถยอมรับได้สำหรับการตรวจวิเคราะห์สารบ่งชี้ทางชีวภาพ โดยให้ขีดจำกัดต่ำสุดในการตรวจวัดอยู่ในระดับต่ำมาก คือ 1 ไมโครโมลาร์ สำหรับคอเลสเทอรอล 0.5 ไมโครโมลาร์สำหรับโดปามีน 5 ไมโครโมลาร์สำหรับกรดยูริก 1 ไมโครกรัมต่อลิตรสำหรับสังกะสี และ 0.1 ไมโครกรัมต่อลิตรสำหรับตะกั่วและแคดเมียม นอกจากนี้ตัวรับรู้ชีวภาพที่ถูกพัฒนาขึ้นยังประสบความสำเร็จในการประยุกต์ใช้ในการตรวจวิเคราะห์สารบ่งชี้ทางชีวภาพที่สนใจในตัวอย่างของเหลวทางชีวภาพ เช่น เซรั่มมนุษย์ได้อีกด้วย

สาขาวิชา วิทยาศาสตร์มหโมเลกุล ลายมือชื่อนิสิต .....

ปีการศึกษา 2557 ลายมือชื่อ อ.ที่ปรึกษาหลัก .....

ลายมือชื่อ อ.ที่ปรึกษาร่วม .....

5373933223 : MAJOR MACROMOLECULAR SCIENCE
KEYWORDS: ELECTROCHEMICAL BIOSENSER / GRAPHENE-POLYANILINE NANOCOMPOSITE / HEAVY METALS / CHOLESTERAL / HUMAN SERUM / BIOMARKER / DOPAMINE / GLUCOSE / URIC ACID

NIPAPAN RUECHA: DEVELOPMENT OF PAPER-BASED BIOSENSOR FOR BIOMARKER DETECTION. ADVISOR: PROF. ORAWON CHAILAPAKUL, Ph.D., CO-ADVISOR: NADNUDDA RODTHONGKUM, Ph.D., 105 pp.

This dissertation focused on the development of novel biosensor for sensitive determination of biomarkers in biological samples, which can be divided into 2 sections. The first section is the development of sensitive biosensor using graphene-polyaniline nanocomposite. Biomarkers (*i.e.* cholesterol) and heavy metals (*i.e.* Zn (II), Cd (II) and Pb (II)) in biological fluids were determined by this proposed biosensor. The second section is active paper chip for electrochemical multiprobe detection of glucose, dopamine and uric acid. Cobalt (II) phthalocyanine, gold nanoparticle and reduced graphene oxide were used to modify the electrode for the improvement of biosensor sensitivity. The experimental parameters in the electrochemical detection were optimized to provide the best condition for biomarker determination. The sensitivity of these developed biosensors was discussed. Moreover, the influence of substrate materials used for making a sensor including paper and plastic film were investigated and optimized. The results showed that paper-based sensor is suitable for biomolecule detection. On the other hand, plastic-based sensor showed a good result for heavy metals detection using square wave anodic stripping voltammetry. In addition, the analytical performances such as linearity, limit of detection and quantitation (LOD and LOQ), reproducibility and accuracy of these biosensors were studied. The selectivity of the developed biosensor was demonstrated for common interferences. The results showed acceptable range of accuracy and precision for biomarker detection. A very low detection limit was observed at 1.0 μM for cholesterol, 0.5 μM for dopamine, 5.0 μM for uric acid, 1.0 ppb for Zn (II) and 0.1 ppb for Pb (II) and Cd (II). Moreover, the developed biosensors were successfully applied to detect the target biomarkers in biological fluid samples such as human serum.

Field of Study: Macromolecular Science
Academic Year: 2014

Student's Signature .....
Advisor's Signature .....
Co-Advisor's Signature .....

ACKNOWLEDGEMENTS

I would like to express my deepest appreciation to my advisor, Professor Dr. Orawon Chailapakul for her suggestion, advice, guidance, encouragement and excellent support, which have helped me to overcome problems encountered during different phase of my Ph.D. degree.

I would also like to thank my co-advisor, Dr. Nadnudda Rodthongkum for encouragement, guidance and giving a new knowledge, which provided me to solve all problems.

I would like to thank to Professor Dr. Charles S. Henry from Colorado State University, USA. I am extremely grateful for his kind support, encouragement and suggestion throughout my 1 year in his research group. I also express to Professor Dr. Kwanwoo Shin for his constructive advice me to complete my work in a limited time.

I would also like to thank Associate Professor Dr. Voravee Hoven, Associate Professor Dr. Nuanphun Chantarasiri and Assistant Professor Dr. Varawut Tangpasuthadol for serving on my committee. Special thanks to Assistance Professor Dr. Weena Siangproh. She gave me the opportunity and constantly provided contribution and excellent advice with kindness.

I would like to express appreciation in financial support during my Ph.D. from Chulalongkorn University Dutsadi Phiphat Scholarship, Ratchadaphiseksomphot Endowment Fund 2013 of Chulalongkorn University (CU-56-640-HR and R_011_2556) and the Thailand Research Fund (TRF).

I would like to give a special thanks to Miss Pornpen Sae-ung, Miss Sunatda Arayachukiat and all members in Electrochemical and Optical Spectroscopy Research Unit. It has been enjoyable moment with you all. I appreciated friendship with you all. Moreover, I would like to special thanks to Mr. Navagan Rachanark for motivation encouragement and support.

Finally, I would like to thank my family for their encouragement and unconditional love.

CONTENTS

Page

Page

Page

Page

Page

LIST OF TABLES

LIST OF FIGURES

LIST OF ABBREVIATIONS

A	ampere
A	electrode area
AA	ascorbic acid
ASV	anodic stripping voltammetry
AE	auxiliary electrode
Ag/AgCl	silver/silver chloride
Bi	bismuth
BSA	bovine serum albumin
Ce	cerium
ChOx	Cholesterol oxidase
CoPc	cobalt phthalocyanine
C_O	concentration of oxidized species
C_R	concentration of reduced species
CE	counter electrode
Cd	cadmium
Cys	cysteine
CNT	carbon nanotube
CPE	carbon paste electrode
Cr	chromium
Cu	copper
CV	cyclic voltammetry
CZE	capillary zone electrophoresis

D	diffusion coefficient
DA	dopamine
DPV	differential-pulse voltammetry
E^0	standard potential
E_p	peak potential (V)
$E_{p,a}$	anodic peak potential
$E_{p,c}$	cathodic peak potential (V)
E_{app}	applied potential (V)
E_{dep}	deposition potential (V)
eCD	electrochemical compact-disk
F	faraday constant (96487 coulombs)
$Fe(CN)_6^{3-}$	ferricyanide
$Fe(CN)_6^{4-}$	ferrocyanide
Fe	iron
g	gram
G	graphene
Glu	glucose
GOx	glucose oxidase
Hg	mercury
h	hour
i.d.	inter diameter
ICP-MS	inductively-coupled plasma-mass spectrometry
i_p	peak current (A)
$i_{p,a}$	anodic peak current (A)

$i_{p,c}$	cathodic peak current (A)
LOD	limit of detection
LOQ	limit of quatification
MCE	microchip capillary electrophoresis
mol	mole
mV	millivolt
min	minute
M	molar
mM	millimolar
mL	milliliter
nm	nanometer
nM	nanomolar
n	number of electron
Ni	nickel
NE	norepinephrine
o.d.	outer diameter
OSHA	The Occupational Health Administration
PA	paracetamol
PAD	paper-based analytical device
PANI	polyaniline
PBS	phosphate buffer saline
Pb	lead
PELs	permissible exposure limits
ppm	part per million

ppb	part per billion
PM	particular matter
R^2	coefficient
RE	reference electrode
RSD	relative standard deviation
rpm	round per minute
SD	standard deviation
SDS	sodium dodecyl sulfate
SPCE	screen-printed carbon electrode
S/B	signal to background
S/N	signal to noise
SEM	scanning electron microscopy
SWV	square-wave voltammetry
T	Kelvin temperature
TCA	trichloroacetic acid
TEM	transmission electron microscopy
UA	uric acid
V	volt
$\boldsymbol{v}$	scan rate
^{o}C	degree Celsius
µL	microliter
µM	micromolar
µg	microgram
µm	micrometer (micron)

CHAPTER I
INTRODUCTION

1.1 Introduction

The development of an accurate, sensitive and low-cost biosensor is very crucial for early stage screening of disease biomarkers. Recently, miniaturized analytical device (*e.g.* paper and polymer based device) has become an important tool in many research fields including biotechnology, medical science, forensic science as well as environmental science [1]. Traditional substrates (*i.e.,* silicon, glass and ceramic) have been previously reported for biosensor fabrication, however; the manufacturing cost is still very high for underdeveloped country [2, 3]. Other substrate materials, such as cellulose filter paper, commercial paper and plastic film have been used an the alternative materials for biosensor applications due to low price [4, 5] compared to other traditional substrates [6]. Therefore, low-cost materials, which are paper and plastic film, are selected as the substrates for biosensor fabrication in this research.

Various materials for electrode surface modifications have been explored for increasing the sensitivity of electrochemical biosensors. Nanomaterials, such as carbon-based nanoparticles and metallic nanoparticles were used to increase the surface area and sensitivity of biosensors. One common approach is incorporating of graphene into the working electrode to increase both surface area and electrochemical conductivity [7]. Moreover, graphene can improve the charge transfer of the modified electrode [8-10].

In the term of biosensor fabrication, graphene-based polyaniline (G/PANI) nanocomposites have attracted more attention than pure graphene because the composite form is more compatible for electrode fabrication and further functionalization [11, 12]. Polyaniline also has excellent electrochemical properties, good environmental stability, and it is easily synthesized. Thus, PANI has been used for a variety of electronic, optical, and electrochemical applications [8, 13]. G/PANI

nanocomposites are prepared by physical mixing and in situ chemical oxidation polymerization [14]. For modification of biosensor, electrospraying of G/PANI nanocomposites on the working electrode were selected to increase the surface area of electrode [12]. Compared to thin-film electrodes prepared by drop-casting, G/PANI droplet-like modified electrodes prepared by electrospraying offer a higher specific surface area which potentially enhance the sensor sensitivity [11].

For paper-based biosensor, the flow of the sample solution in paper is commonly controlled by the competition between attractive and repulsive capillary forces but there are some limitations. Thus, active paper chip that the fluidic operation on the paper is controlled by implementing an electric input via electrowetting technique [15] was also studied in this dissertation. For active paper chip, the drop of solution can move on a chip by adjusting the electric field with an external voltage to control the electrowetting-induced surface tension between the drop and electrode under hydrophobic coated surface of active paper chip. The drop movement on active paper chip can be controlled by mixing and incubating before moving to the detection zone.

In this dissertation, paper and plastic based biosensors with low cost and simple operation were developed for the determination of target analytes in relevant real samples. The development of novel electrochemical biosensors in this dissertation can be devided into 3 main parts as followings;

1. Novel Paper-Based Cholesterol Biosensor Using Graphene/

Polyvinylpyrrolidone/Polyaniline Nanocomposite

2. Sensitive Electrochemical Sensor using a Graphene-Polyaniline

Nanocomposite for Simultaneous Detection of Zn (II), Cd (II) and Pb (II)

3. Active Paper Chips for Electrochemical Multi-probe Detections

These developed systems were successfully used to sensitively and selectively quantify target analytes. Various optimal conditions were investigated to

achieve the best analytical performances of the system. Eventually, the successful application of these systems for the detection of analyte in real samples are accomplished.

1.2 Research Objective

The two main goals of this dissertation are shown below:

1. To develop and evaluate a low-cost electrochemical biosensor for sensitive and selective detection of biomarkers.
2. To apply these proposed systems for the determination of target analytes in real biological samples.

1.3 Scope of Research

Biosensors were initially designed to obtain the suitable platform for each assay. The optimizations of experimental conditions that affect the performance of target analytes detection were investigated. The analytical performances of these systems including linear working range, limits of detection and quantification (LOD and LOQ), repeatability and reproducibility were examined under optimal conditions. The selectivity of these systems was tested using various common interferences. In addition, these systems were then applied to measure analytes in relevant samples. Finally, all of the results were discussed in this dissertation.

CHAPTER II

THEORY AND LITERATURE REVIEW

In this chapter, the fundamentals of sensors are discussed. In the second part of this chapter, the aspects of microchip capillary electrophoresis and electrochemical detection are explained. The discussions in this chapter refer to the basic principles of microchip used in the subsequent chapters.

2.1 Sensor

2.1.1 Principle

The “biosensor” is a device consisting of two combination parts which are bio-element, and sensor-element. The basic concepts of a biosensor can be illustrated in Figure 2.1 [16].

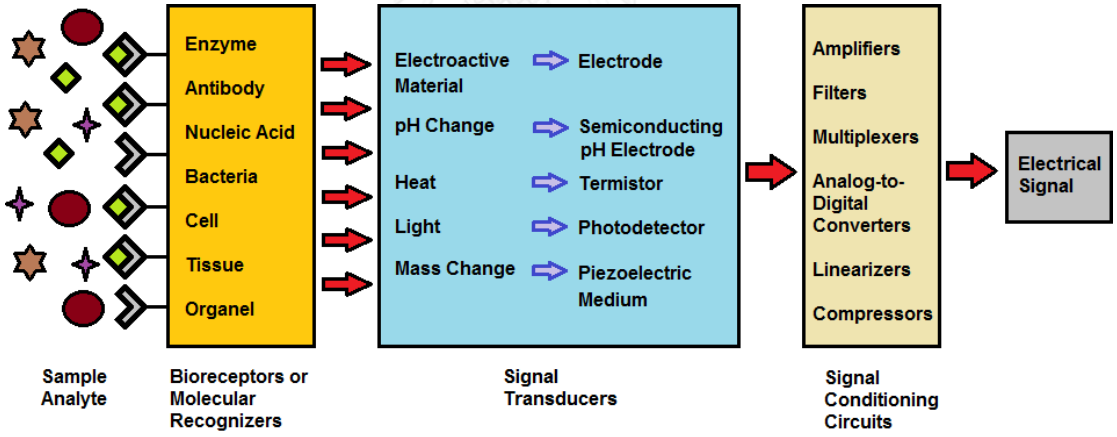

Figure 2.1 A schematic representation of biosensors [16].

Specific bio elements such as enzyme or antibody recognize a specific analyte and the sensor element transduces the change in the biomolecule into an electrical signal. The bio element is a very specific to the analyte to which it is sensitive depending on the transducing mechanism used, the sensors can be separated into many types of sensor such as resonant sensor,

optical-detection sensor, thermal-detection sensor, ion-sensitive FET (ISFET) sensor, and electrochemical sensor [17]. For electrochemical sensors, it can be further classified based on the parameter measured, such as conductimetric, amperometric, and potentiometric sensors. Biosensors can be applied in biomedical, industry, and military as shown in Figure 2.2. The major application is in blood glucose sensing because of its abundant market requirement. However, biosensors have tremendous potential for commercialization in other application fields as well. In spite of this potential commercial adoption has been slow because of several technological difficulties. For example, due to the presence of biomolecule along with semiconductor material, biosensor contamination is a major issue [18].

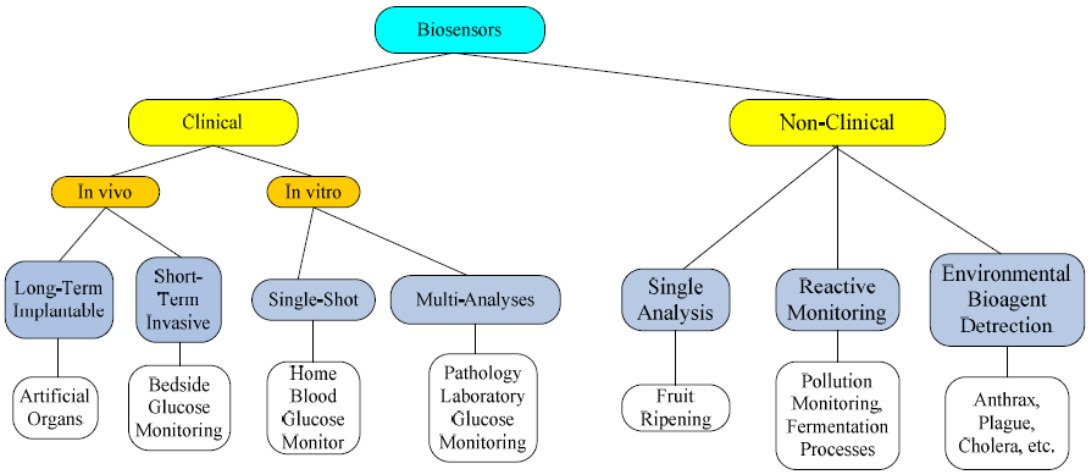

Figure 2.2 Potential applications of biosensors [18].

Common types of sensors such as optical-detection biosensors

2.1.1.1 Optical-detection Biosensors

The output transduced signal that is measured is light for this type of biosensor. The biosensor can be made based on optical diffraction or electrochemiluminescence. In optical diffraction based devices, a silicon wafer is coated with a protein via covalent bonds.

The wafer is exposed to UV light through a photo-mask and the antibodies become inactive in the exposed regions. When the diced wafer chips are incubated in an analyte, antigen-antibody bindings are formed in the active regions, thus creating a diffraction grating. This grating produces a diffraction signal when illuminated with a light source such as laser. The resulting signal can be measured or can be further amplified before measuring for improved sensitivity.

2.1.1.2 Thermal-detection Biosensors

This type of biosensor is exploiting one of the fundamental properties of biological reactions, namely absorption or production of heat, which in turn changes the temperature of the medium in which the reaction takes place. They are constructed by combining immobilized enzyme molecules with temperature sensors. When the analyte comes in contact with the enzyme, the heat reaction of the enzyme is measured and is calibrated against the analyte concentration. The total heat produced or absorbed is proportional to the molar enthalpy and the total number of molecules in the reaction. The measurement of the temperature is typically accomplished via a thermistor, and such devices are known as enzyme thermistors. Their high sensitivity to thermal changes makes thermistors ideal for such applications. Unlike other transducers, thermal biosensors do not need frequent recalibration and are insensitive to the optical and electrochemical properties of the sample. Common applications of this type of biosensor include the detection of pesticides and pathogenic bacteria.

2.1.1.3 Ion-Sensitive Biosensors

These are semiconductor FETs having an ion-sensitive surface. The surface electrical potential changes when the ions and the semiconductor interact. This change in the potential can be

subsequently measured. The Ion Sensitive Field Effect Transistor (ISFET) can be constructed by covering the sensor electrode with a polymer layer. This polymer layer is selectively permeable to analyte ions. The ions diffuse through the polymer layer and in turn cause a change in the FET surface potential. This type of biosensor is also called an ENFET (Enzyme Field Effect Transistor) and is primarily used for pH detection.

2.1.1.4 Electrochemical Biosensors

Electrochemical biosensor is mainly used for the detection of hybridized DNA, DNA-binding drugs, glucose concentration, etc. The underlying principle for this class of biosensors is that many chemical reactions produce or consume ions or electrons which in turn cause some change in the electrical properties of the solution which can be sensed out and used as measuring parameter. Electrochemical biosensors can be classified based on the measuring electrical parameters as: (1) conductimetric, (2) amperometric and (3) potentiometric sensors.

2.1.2 Enzymatic Biosensor

The specific binding capabilities and catalytic activity of enzyme make them popular bioreceptors. Analyte recognition is enabled through several possible mechanisms. For enzymetic biosensors, the enzyme converts the analyte into a product that is sensor-detectable and then detecting enzyme inhibition or activation by the analyte [19], or monitoring modification of enzyme properties resulting from interaction with the analyte [20]. The advantages of enzymetic biosensor are ability to catalyze a large number of reactions, potential to detect a group of analytes and suitability with several different transduction methods for detecting the analytes. Many kinds of biological compounds such as glucose, uric acid, and cholesterol were detected via enzymatic biosensor.

For development of enzymatic biosensor, enzyme immobilization onto self-assembled monolayer fabricated micro-device or bio-chip is usually the primary step in the fabrication of enzymatic biosensor. The selection of immobilization method is essential to achieve the best performance of a biosensor. Normally, biological catalysts as enzymes can promote the transformation of chemical species in living systems. These biological molecules, consisting of thousands of atoms in precise arrangements, are able to catalyze the multitude of different chemical reactions occurring in biological living cells. The principle of enzymatic biosensor is described in Figure 2.3.

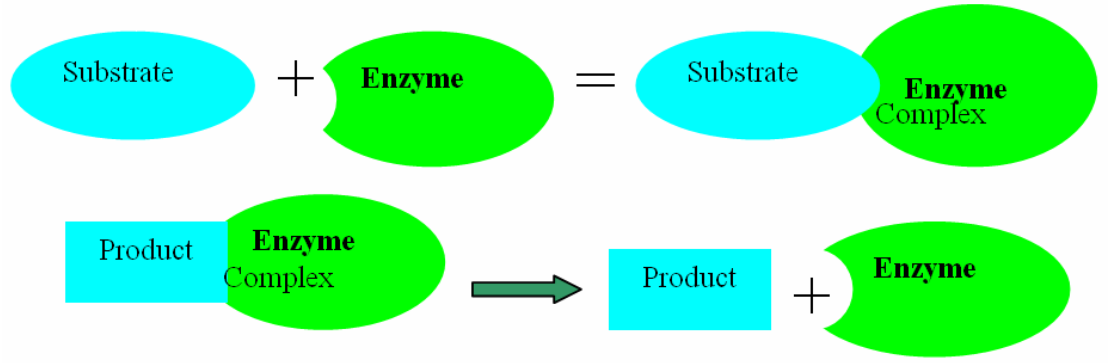

Figure 2.3 The principle of enzymatic biosensor

2.1.3 Metal Sensor

Conventional measurement of heavy metals such as lead (Pb^{2+}), cadmium (Cd^{2+}) and zinc (Zn^{2+}) is typically accomplished using atomic absorption spectrophotometry (AAS) [21], inductively-coupled-plasma mass spectrometry (ICP-MS) [22], or mass spectrometry (MS) [23], which are highly sensitive, but very expensive techniques. Complicated operation and long time-delay for sample processing and assessment also prevent these methods from being used more frequently. Electrochemical detection, alternatively, is an inexpensive detection motif that has recently been incorporated in low-cost sensors for trace metal analysis [24-27]. Square-wave anodic stripping voltammetry is a commonly employed technique for heavy

metal ions due to its high sensitivity and low (~nM-pM) detection limits [28, 29], a result of a pre-concentration step that accumulates the analyte on the electrode surface. The bulk and expense of bench top potentiostat can also be reduced using handheld device, which can improve the utility of electrochemical detection in a point-of-care setting [29].

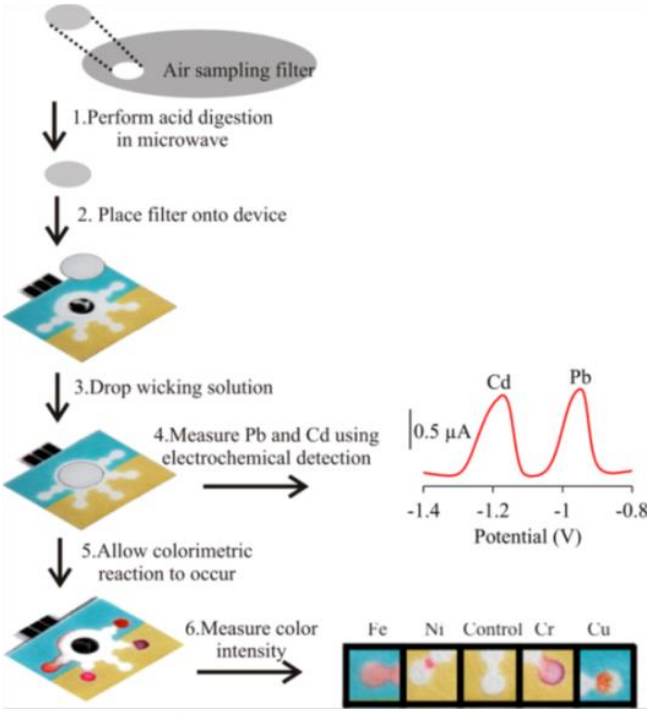

Figure 2.4 Schematic drawing of the fabrication procedure for paper-based analytical devices and ASV detection of Pb (II) and Cd (II) [27]

2.2 Fabrication Method

2.2.1 Wax-printing

Paper-based sensors are fabricated by penetrating materials to form hydrophobic into hydrophilic cellulose paper [30, 31]. To create hydrophobic barriers in the paper-based sensor, many methods were used for fabrication such as photoresist, plotting, plasma oxidation and cutting, however; there have their own set of advantages and limitations. Therefore, wax-printing method is suited for fabrication the paper-based sensor because it can perform a large number (<100) of paper-based sensors in a single batch [31].

For using wax-printing fabrication, the wax was patterned as a hydrophobic wall in hydrophilic paper using a commercially solid wax-printer and hot plate. The fabrication process involves two operations including the printing patterns of wax on the hydrophilic surface of paper and the melting wax into the porous capillary paper to form complete hydrophobic barriers as showed in Figure 2.5 [31]. The advantages of this method are easy, rapid, inexpensive and particularly well-suited for producing large numbers of patterned paper-based sensor [32].

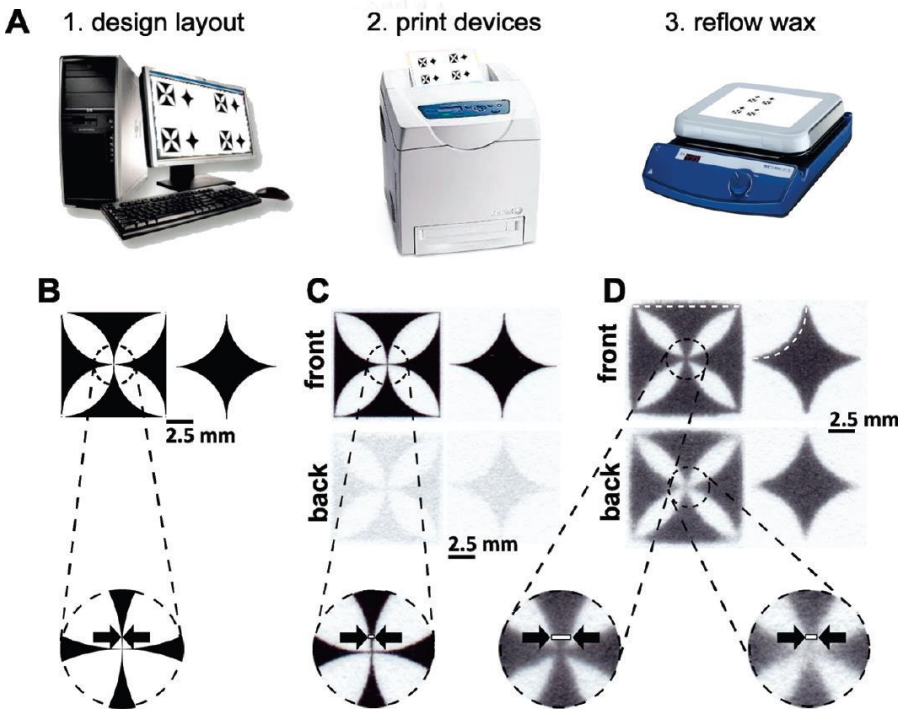

Figure 2.5 Patterning wax patterned paper-based sensor by wax printing method. (A) Schematic of the basic steps (1-3) required for wax printing. (B) Digital image of test designs. (C) Images of the test design printed on filter paper (Whatman no. 1) using the solid wax printer. (D) Images of the test design after heating the wax [31].

2.2.2 Intjet-printing

Inkjet printing has become a useful and feasible technology in a lot of industrial fields for accurately depositing very small quantities (tens of picoliters) of materials at defined spots on the surface of a wide variety of substrates [33, 34]. Moreover, it is a single step process which does not require highly qualified professionals or an important amount of facilities, in contrast to photolithography. Inkjet printing is a suitable technology for scale industry mass production. Therefore, its time saving, low cost and flexibility will probably establish inkjet printing technology as one of the most suitable printing technologies in the future [35]. Furthermore, modern inkjet printing devices have multiple print heads which are able to print different kinds of ink simultaneously, being able to print both the hydrophobic barrier of the pattern and the sensor reagent, and, in contrast with other printing technologies like plotting, the place, time and quantity of liquid deposition can be controlled precisely. In addition, inkjet printing can be used to deposit a wide variety of materials, such as inorganic particles or biological species, on paper. It becomes a promising alternative technology for the fabrication of simple patterned paper-based sensor for simultaneous multi-analyte detection [36].

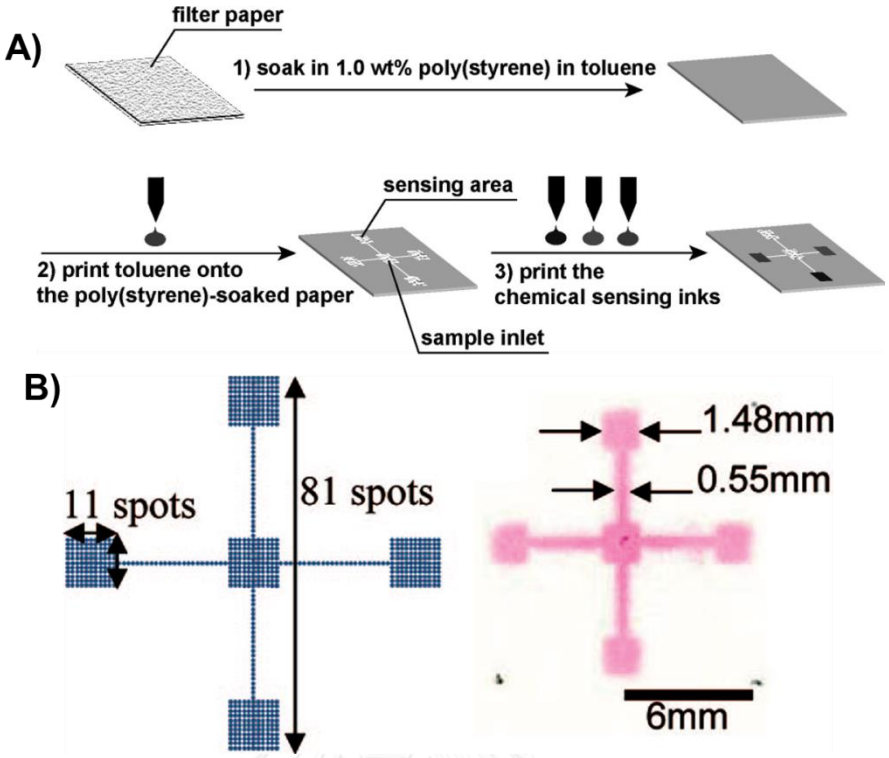

Figure 2.6 A) Schematic of the fabrication process of the inkjet-printed microfluidic multi-analyte chemical sensing paper featuring microfluidic channels connecting a central sample inlet area with three different sensing areas and a reference area. Patterning of paper using inkjet etching of poly(styrene) with toluene: (B) outline of the printing pattern (interspot distance 150 μm), and inkjet etched pattern colored with a color ink to visualize the structure. Fifteen identical patterns were printed onto a single 10 cm × 8 cm filter paper [33].

2.2.3 Screen-printing

Screen-printing method is a printing technique that uses a woven mesh to support an ink-blocking stencil to receive a desired image. The attached stencil forms open areas of mesh that transfer ink or other printable materials which can be pressed through the mesh as a sharp-edged image onto a substrate [37]. Screen-printing is a well-known, inexpensive method for printing images on clothing and other everyday materials as well as creating electrodes [38, 39]. Printing screens are cheap widely available around the

world. To create the patterned paper, wax screen-printing method was used to fabricate as showed in Figure 2.7 [40]. Inexpensive wax can be purchased anywhere in the world, and is environmentally friendly. Furthermore, the wax screen-printing method is accomplished without the use of a clean room, UV lamp, organic solvents, or sophisticated instrumentation. This method requires only a hot plate (or similar heated surface) making it ideal for fabrication of paper-based sensor in developing countries [41].

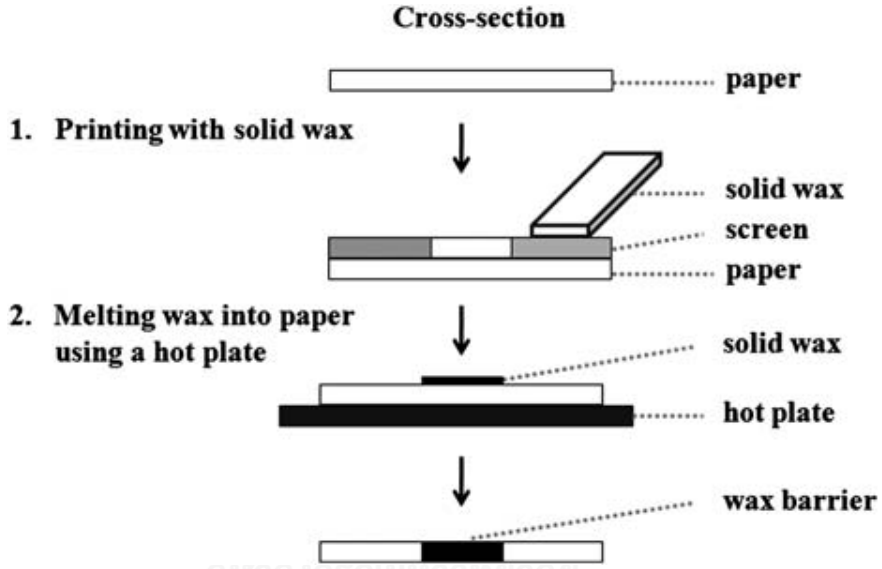

Figure 2.7 Schematic diagram of the fabrication step for wax screen-printing method [40].

In addition, the advent of screen-printing technology has opened new exciting opportunity to apply electrochemical techniques for environmental and clinical analyses for outside a centralized laboratory. Using screen-printing technology, the mass production makes screen-printed electrodes (SPEs) with consistent chemical performance. Besides the need for controlling the chemical nature of the measure media, SPEs may be the most appropriate electrochemical sensors for in situ analysis because of their linear output, low power requirement, quick response, high sensitivity and ability to operate at

room temperature [4, 37]. Moreover, screen-printed carbon electrodes have many attractive advantages for ECD including low cost, disposability, flexibility in design, ease of chemical modification, and ability to produce with minimal outside technology.

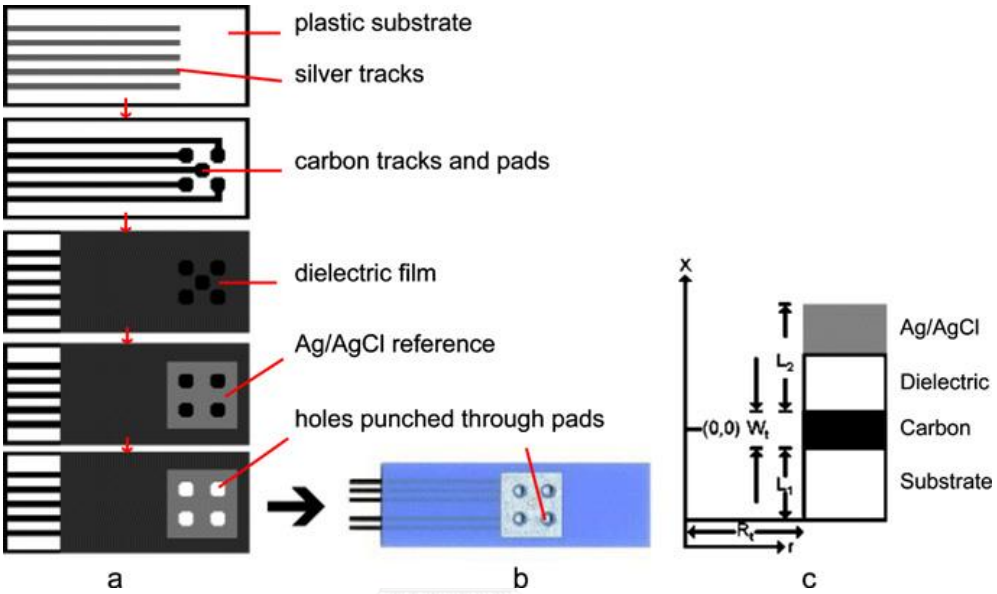

Figure 2.8 Schematics of (a) side view illustrating the method for manufacturing well SPEs, (b) image of a well electrode strip, and (c) a vertical section cut through the center of the well containing the coordinate system used for the well electrode simulation. [37]

2.4 Electrochemical Detection

Electrochemical detection has been broadly used and integrated in the microfluidic device and sensor. In this detection mode, electrodes are electrochemically responsible to investigate the relationship between electrical response (current, potential, or charge) and electroactive components of interest. This detection method has various outstanding advantages [42, 43] such as

(i) low cost

(ii) portable instrumentation

(iii) high sensitivity

(iv) fast operation

(v) easy to miniaturize

(vi) low power requirements

(vii) independence of sample turbidity

The conventional electrochemical cell consisted of 2 main parts including supporting electrolyte and electrode. The supporting electrolyte is a medium containing inert chemical species which do not react with analyte. It usually provides a constant ionic strength, low solution resistance, and low electromigration effect within the electrochemical cell.

Electrode is an electrical conductor immersed in the testing solution which is required at least 2 electrodes. The working electrode (WE) is used for the measurement of electroactive analyte while the reference electrode (RE) serves a constant and stable potential. Moreover, the counter electrode (CE) or auxiliary electrode (AE) might be additionally used in the electrochemical cell to minimize the electrical flowing through the RE. A general redox reaction at electrode surface is described as following equation 2.1.

$$R \leftrightarrow O + ne^- \quad (\mathbf{2.1})$$

Where R and O are reduced and oxidized forms of the electroactive species, which either are soluble in solution or absorbed on the electrode surface. The relationship between the concentrations of electroactive species and potential can be described by Nernst Equation (equation 2.2) [44-46].

$$E = E^0 + 2.3(RT/nF) \log (C_O/C_R) \quad (\mathbf{2.2})$$

Where E^0: Standard potential of the redox reaction

R: Gas constant (8,314 J K^{-1} mol^{-1})

T: Temperature (Kelvin, K)

n: number of electrons

F: Faraday constant (96487 C/mol))

C_O: Concentration of oxidized form

C_R: Concentration of reduced form

Moreover, conventional electrochemical cells are divided into 2 types

(i) Galvanic cell (potentiometric technique) uses a spontaneous reaction to provide electrical work which generally refers to “potentiometry”, based on the change of electrochemical potential in the nonappearance of current state.

(ii) Electrolytic cell (potentiostatic technique) consumes electrical energy from an external source which generally refers to “voltammetry”. Voltammetry (a potentiostatic or controlled-potential technique) is based on a dynamic (nonzero-current) process which measure the resulting current obtained from oxidation/reduction reaction of analyte as a function of potential. Generally, a potentiostat instrument is used in this technique to apply a time-dependent potential to an electrochemical cell across a couple of electrodes [17]. This technique deals with charge transfer process at the interface between electrode and solution. An important electrochemical information about the thermodynamics and kinetics of chemical reactions is obtained which can be used to determine and identify an electroactive analyte in testing solution [37].

In this dissertation, some electrochemical methods were used as an electrochemical sensing in the presented sensor platforms such as cyclic voltammetry (CV), square-wave voltammetry (SWV), and amperometry. In addition, electrochemical impedance spectroscopy (EIS) was performed to investigate the electrochemical characterization of modified electrodes. Next section attempts to give an overview of these techniques.

2.4.1 Square-wave Voltammetry (SWV)

Square-wave voltammetry (SWV) is one of the pulse techniques which is imposed on a staircase waveform. This SWV method is known for its higher electrochemical sensitivity than normal sweeping and other pulse techniques

[47]. Figure 2.9 shows the SW potential waveform. The forward pulse of SW is coincident with the staircase step in the time. The reverse cycle of the SW decreases the half way of the staircase step. The SW peak current is measured twice at the beginning and the end of a pulse. As shown in Figure 2.9, the resulting curve is termed as square-wave voltammogram. The SWV responses (peak height and width) rely on the main optimization of SW parameters including scan rate and staircase step.

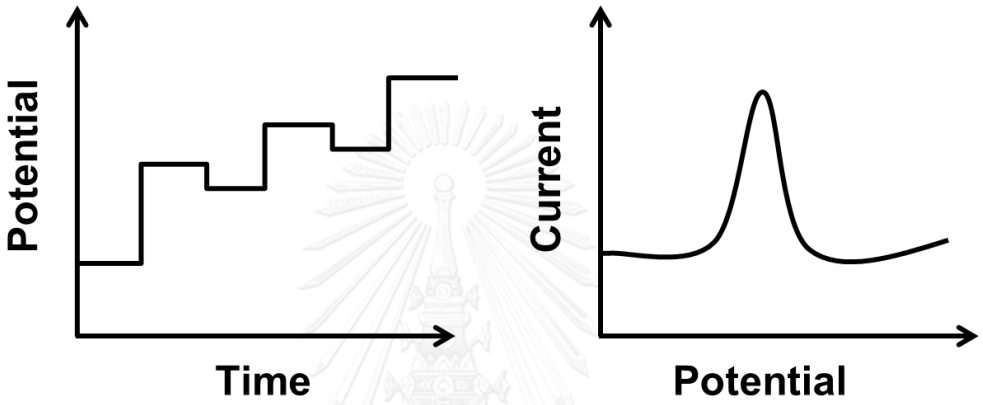

Figure 2.9 Potential excitation waveforms and output electrochemical responses for square-wave voltammetry.

2.4.2 Cyclic Voltammetry (CV)

Cyclic voltammetry is a common electrochemical method for investigating qualitatively electrochemical information (thermodynamics and kinetics) of heterogeneous electron transfer reactions and coupled chemical reactions of electroactive species. The excitation signal for this method is a linear potential sweeping using triangular potential excitation waveforms. The potential of WE is linearly swept in both forward and reverse directions. As shown in the Figure 2.10, the potential is scanned between two potential values at a constant scan rate. When the potential increased to V_2, the scan is reversed and the voltage is scanned backward to V_1 [48].

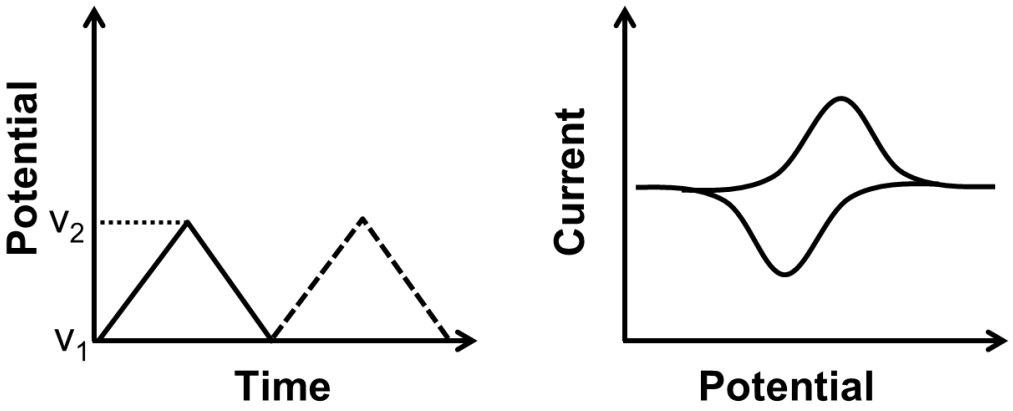

Figure 2.10 Potential excitation wave forms and output electrochemical responses for cyclic voltammetry.

The relationship between current (vertical axis) and potential (horizontal axis) is termed as cyclic voltammogram (Figure 2.10). The influence of currents (anodic peak current ($i_{p,a}$) or cathodic peak current ($i_{p,c}$)) on scan rate can be explained by Randles-Sevick equation (equation 2.3) [48].

$$i_p = (2.69 \times 10^5)\, n^{3/2}\, D^{1/2}\, \nu^{1/2}\, A\, C \qquad (2.3)$$

Where
- n: number of electrons
- D: diffusion coefficient ($cm^2\ s^{-1}$)
- ν: scan rate ($mV\ s^{-1}$)
- A: electrode surface area (cm^2)
- C: concentration ($mol\ cm^{-3}$)

In case of reversible redox reaction, a well-defined cyclic voltammogram is observed. The peak separation (ΔE_p) between anodic peak potential ($E_{p,a}$) and cathodic peak potential ($E_{p,c}$) is approximately equal to $\Delta E_p = E_{p,a} - E_{p,c} = 59/n$. The ratio of cathodic-to-anodic peak current ($i_{p,c}/i_{p,a}$) is unity approximately. Moreover, the formal potential (E^O) value should be centered between $E_{p,a}$ and $E_{p,c}$, related to the equation of $E^O = (E_{p,a} + E_{p,c})/2$.

For irreversible reaction, ΔE_p is broadly separated and the reverse peak in the cyclic voltammogram might be vanished. Furthermore, a potential shift is observed while the scan rate is changed.

2.4.3 Stripping techniques

Stripping voltammetry has attached much interest for ultrasensitive detection of trace heavy metals and some organic compounds due to its accumulation step to preconcentrate electroactive analytes on the electrode surface before stripping step. There are at least 2 steps which are preconcentration and stripping steps;

(i) Accumulation step: electroactive analyte is preconcentrated at the surface of electrode by either an anodic, cathodic or an adsorptive process.

(ii)Stripping step: the potential is scanned in order to strip out the accumulated analyte from the electrode surface and then the voltammetric response is obtained.

In case of the deposition potential is hold at appropriate negative potential to occur reduction process of analytes on the electrode surface then potential is scanned to more positive direction in order to occur the oxidation of deposited analytes, this technique is termed as "anodic stripping voltammetry".

2.4.4 Amperometry

Amperometry is an electrochemical technique which the electrode potential is fixed at a constant value, and the result is plotted between current and time. Both potential waveform and chronoamperogram are shown in the Figure 2.11, respectively. This technique has been continuously selected to use as an electrochemical detector in various flow-based and separation systems. At maintained potential, oxidation or reduction reaction of electroactive species at interface between electrode and solution is occurred. The steady-state current is directly proportional to the analyte concentration. Selectivity is accomplished by

the selection of applied potential which can minimize the electrochemical responses of background and interference. The optimization of detection potential is obtained by hydrodynamic voltammetry. The optimal detection potential was found at the highest signal/background (S/B) ratio [49].

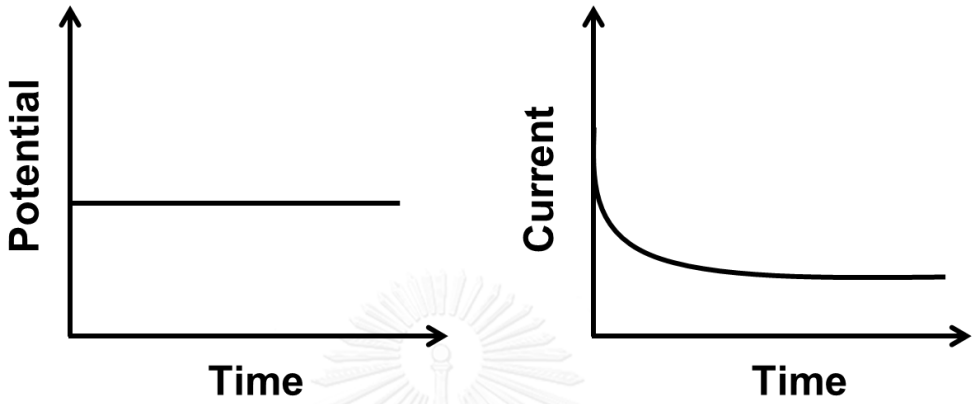

Figure 2.11 Potential excitation waveforms and output electrochemical responses for amperometry [49].

2.4.5 Electrochemical Impedance Spectroscopy (EIS)

The impedance investigation for characterization is generally based on electrochemical impedance spectroscopy which involves the study of resistive and capacitive properties of materials. Electrochemical impedance is based on the perturbation of a system at equilibrium by applying a sinusoidal potential excitation to an electrochemical cell and then measuring the current through the cell [50].

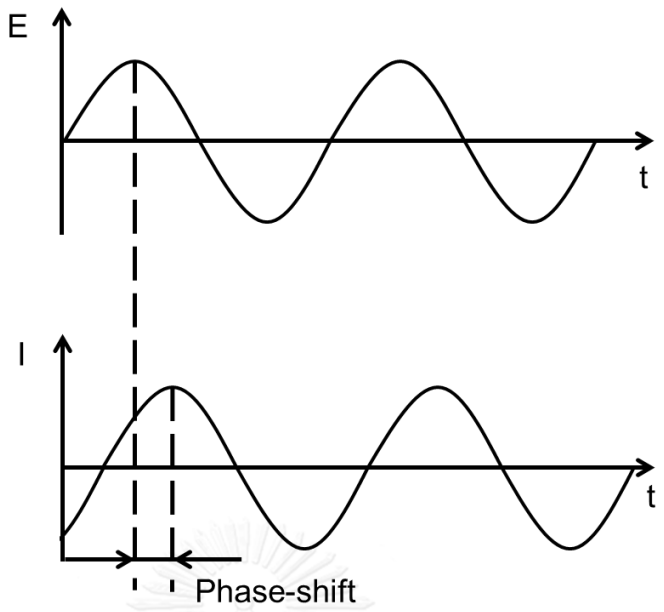

Figure 2.12 Response of sinusoidal current in a linear system

The impedance is then represented as a complex number,

$$Z(\omega) = \frac{E}{I} = Z_o \exp(j\emptyset) = Z_0(\cos\emptyset + j\sin\emptyset) \qquad (2.4)$$

The expression for Z (ω) consists of a real and an imaginary part. The real part is plotted on the X-axis while the imaginary part is plotted on the Y-axis of a chart. This plot is termed as "Nyquist Plot" as shown in Figure 2.13. The impedance can be represented as a vector (arrow) of length |Z|. The angle between this vector and the X-axis, commonly called the "phase angle", is ψ (=arg Z) [51].

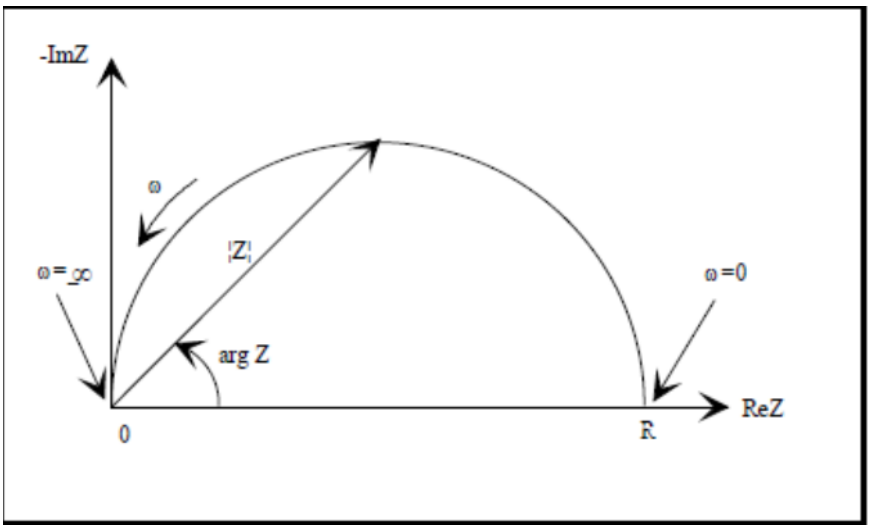

Figure 2.13 Nyquist Plot with Impedance Vector

The Nyquist Plot in Figure 2.13 results obtained from the equivalent circuit as shown in Figure 2.14. The semicircle is characteristic of a single "time constant". Only a portion of a semicircle is often seen [52].

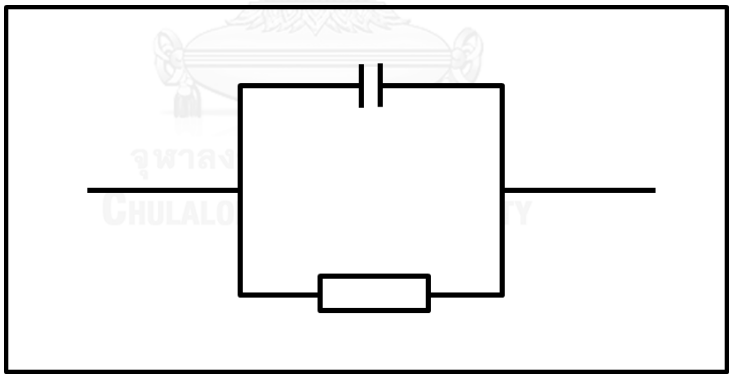

Figure 2.14 Simple equivalent circuit with one time constant

2.5 Electrowetting

Surface tension is an inherently dominant force in the microscale. Electrocapillarity, the modification of surface tension by applying an electric field, has received renewed attention because of its potential usefulness in microfluidics. Pollack et al. demonstrated a microactuator for rapid manipulation of discrete

microdroplets by direct electric control of the surface tension [53]. Electrowetting was first demonstrated by Berge [54]. The general experiment scheme for electrowetting on dielectrics (EWOD) is shown in Figure 2.15.

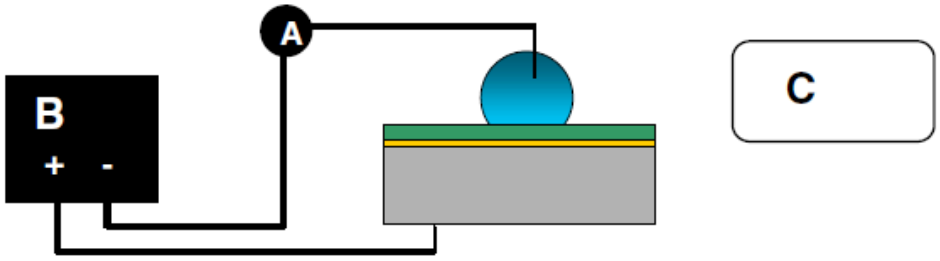

Figure 2.15 Open EWOD experiment. A) amp meter; B) power supply; C) digital camera.

For electrowetting on Dielectric (EWOD), an externally added electrostatic charge may significantly modify the capillary forces at an interface. The notion of electrical control of surface tension, electrocapillary or electrowetting is quite attractive for microdevices because of its inherent effectiveness in microscale and simplicity in implementation. The configuration of the electrode is covered with a thin insulating film as illustrated in Figure 2.16. When an electric voltage is applied, the electric charge changes free energy on the dielectric surface, inducing a change in wettabilty on the surface and contact angle of the droplet. This phenomenon, which we name electrowetting on dielectric (EWOD), has an excellent reversibility with many kinds of dielectric layers compared to the conventional electrowetting, where liquids contact the conductive surface directly [15].

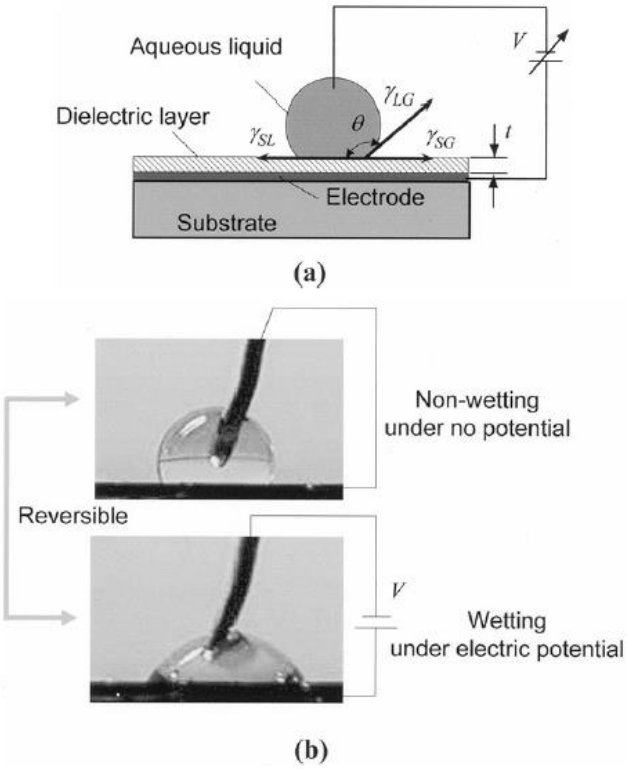

Figure 2.16 Principle of electrowetting on dielectric (EWOD). (a) Schematic configuration. (b) Pictures of basic EWOD demonstration [55].

2.6 Biomarker

Biomarker is a biological or chemical molecules that were found in blood and other body fluids, or tissue that is sign of a condition or disease. In this works, cholesterol, dopamine, uric acid and heavy metal (*e.g.* Zn (II), Pb (II) and Cd (II)) were selected as the biomarkers.

2.6.1 Cholesterol

Cholesterol is a one of the most important of biomarkers for cardiovascular disease and high blood pressure. Cholesterol and its fatty acid esters are one of the main constituents of mammalian cell membrane and are precursors of other biological materials, such as bile acid and steroid hormones. For its regular estimation, development of a biosensor, which allows convenient and rapid determination are under active research and

development. Enzymatic biosensor in the presence of cholesterol oxidase enzyme is normally used for clinical determination of cholesterol.

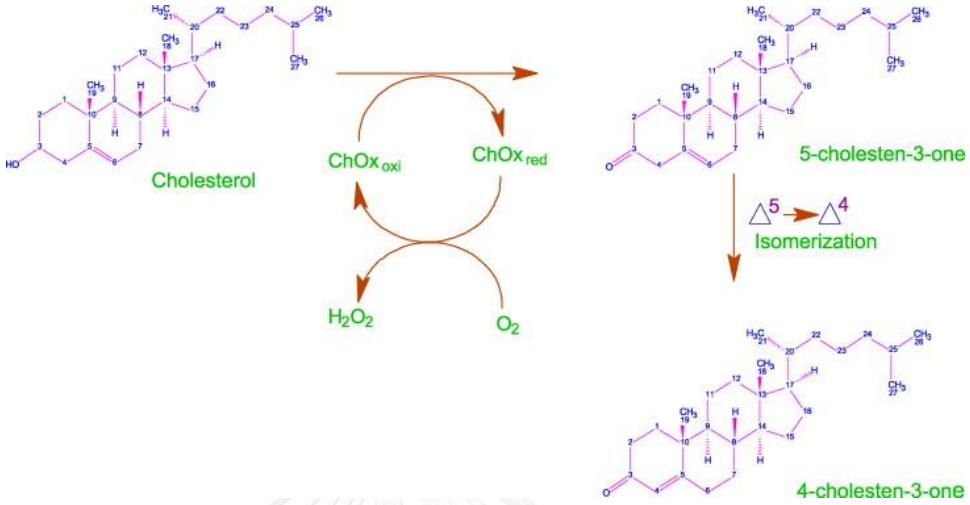

Figure 2.17 Pathway of cholesterol oxidase enzyme reaction [56]

The conventional method for cholesterol detection is spectrophotometry [10, 11]; however, this method is neither low-cost nor suitable for rapid analysis because of its complicated principle. Many electrochemical biosensors have been developed for more sensitive and selective detection of cholesterol by using nanocomposites of metal nanoparticles [28, 30, 31] and carbon based nanomaterial [29, 30]. Ahmad *et al* [28] developed a highly sensitive amperometric biosensor based on Pt-incorporated fullerene-like ZnO hybrid nanospheres. Pt-ZnO nanospheres (PtZONS) with diameters in the range 50-200 nm have been successfully synthesized by electrodeposition on a glassy carbon electrode (GCE). The PtZONS/GCE was functionalized with ChOx by physical adsorption. Nafion/ChOx/PtZONS/GCE-based biosensor exhibits a very high and reproducible sensitivity of 1886.4 mA M^{-1} cm^{-2} to cholesterol with a response time less than 5 s and a linear range from 0.5 to 15 μM. These electrodes

show that the PtZONS not only enhance the sensitivity to cholesterol but it also help to eliminate the interferences at low applied potential.

Dey *et al* [57] developed a highly sensitive amperometric biosensor based on hybrid material derived from nanoscale Pt particles (nPt) and G for the detection of H_2O_2 and cholesterol. This hybrid material modified electrode efficiently catalyzes the electrochemical oxidation of H_2O_2 at the potential of 0.4 V. The cholesterol biosensor was developed by immobilizing ChOx and ChEt on the surface of G—nPt. The bienzyme integrated nanostructure electrode is very sensitive, selective and fast response toward cholesterol. The sensitivity and limit of detection of this electrode toward cholesterol ester are 2.07±0.1 μA (μM cm)$^{-1}$ and 0.2 μM, respectively. This sensor does not suffer from the interference due to other common electroactive species and this system is highly stable.

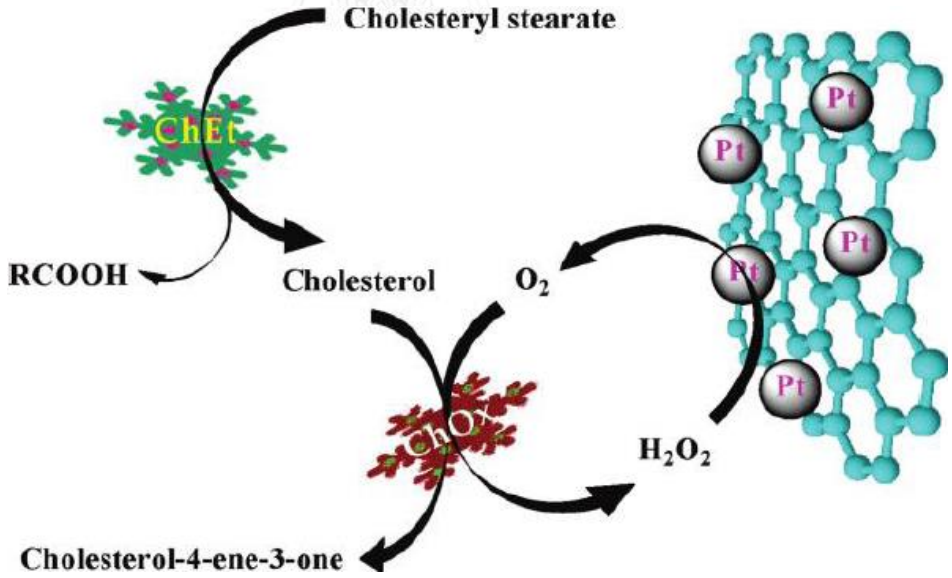

Figure 2.18 Scheme illustrating the biosensing of cholesterol ester with the GNS-nPt-based biosensor [57]

The nanocomposite of poly-(diallyldimethyl-ammonium chloride) with nanoparticles of gold and multiwall carbon nanotubes was developed by Eguílaz [58] to improve response for H_2O_2 and cholesterol detection. This electrode exhibits cholesterol responded in the range of 0.02–1.2 mM with sensitivity of 2.23 μA mM^{-1} and a limit detection of 4.4 μM. Moreover, the use of Nafion thin film to minimize the effect of potential interferences including ascorbic acid and/or uric acid in real samples.

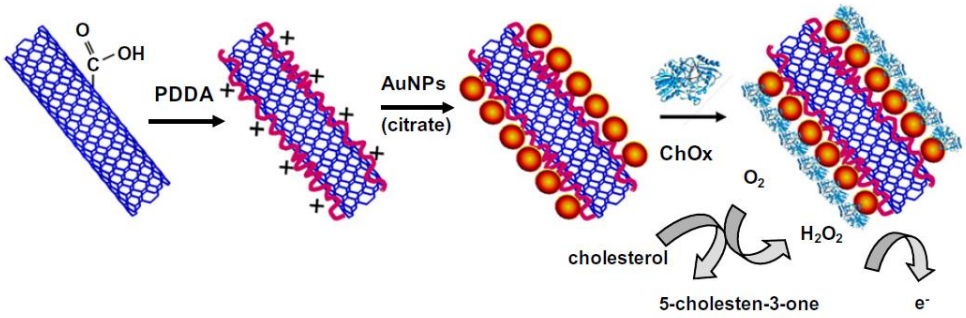

Figure 2.19 Schematic of the steps involved in the preparation of the ChOx/AuNPs/PDDA/MWCNTs/GCE biosensor [58].

To measure the free and total cholesterol, Manjunatha [29] fabricated a cholesterol oxidase (ChOx) and choleserol esterese (ChEt) enzymes immobilized on functionalized graphene (FG) modified graphite electrode (FG/Gr) electrode. For the free cholesterol, ChOx-FG/Gr exhibited sensitive response in a range of 50 to 350 mM with a detection limit of 5 mM. For the total cholesterol determination, ChEt/ChOx-FG/Gr electrode showed the linear range from 50 to 300 mM with a detection limit of 15 mM. The interferences such as glucose, ascorbic acid and uric acid did not affect the desired signal due to the use of a low operating potential. Thus this electrode exhibits good electrocatalytic activity for H_2O_2 determination. The classification of cholesterol in the human blood is shown in Table 2.1.

Table 2.1 Classification of total cholesterol level in the blood [58].

Level ($mg \cdot dL^{-1}$)	**Level** ($mmol \cdot L^{-1}$)	**Interpretation**
< 200	< 5.0	Desirable level corresponding to lower blood cholesterol
200 to 239	5.2 to 6.2	Borderline high blood cholesterol
> 240	> 6.2	High blood cholesterol

2.6.2 Glucose

Glucose is a major source of energy for most cells of the body, including brain cells. To detect glucose level in human blood, the enzymatic assay was usually used by immobilized the enzyme *glucose oxidase* (GOD) on to the surface of working electrode by physically trapping or chemical interaction. The enzyme activity changes depending on the surrounding oxygen concentration. Glucose was reacted with GOD to form gluconic acid while producing two electrons and two protons, thus reducing GOD. The reduced GOD, surrounding oxygen, electrons and protons (produced above) react to form hydrogen peroxide and oxidized GOD (the original form). This GOD can again react with more glucose. The higher the glucose content, more oxygen is consumed. On the other hand, lower glucose content results in more hydrogen peroxide. Hence, either the consumption of oxygen or the production of hydrogen peroxide can be detected by electrochemical detection and can serve as a measure for glucose concentration.

2.6.3 Dopamine and uric acid

Dopamine with IUPAC nomenclature 4-(2-aminoethyl)benzene-1,2-diol, structure given in Figure 2.18, is one of the most neurotransmitter that helps control the brain's reward and pleasure centers. Dopamine also helps regulate movement and emotional responses, and it enables us not only to see rewards, but to take action to move toward them.

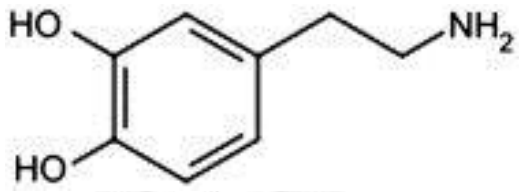

Figure 2.20 Chemical structure of dopamine [59]

In normal health of human, dopamine is found around 50 nmol g^{-1} in the brain and at 0.01–1 μM in extracellular fluids. Abnormal levels of dopamine are related to neurological disorders, such as Parkinson's disease [60], Alzheimer's disease [61], Attention-Deficit Hyperactivity Disorder [62], and Huntington's disease [63]. Previously, various methods have been used for DA detection including liquid chromatography [64, 65], capillary electrophoresis [66, 67], electrogenerated chemiluminescence [68, 69] and mass spectrometry [70]. However, these methods are expensive, generally time-consuming, require expensive instrumentation, and can only be carried out in the laboratory.

Uric acid (UA: 2,4,6-trihydroxypurine) is an end product from purine derivatives in human metabolism), It is a biologically important primary product of purine metabolism in body fluids [71]. The normal level of uric acid in serum is between 240 and 520 μM and 1.4 and 4.4 mM in urinary excretion [72]. Abnormal levels of the UA concentrations in blood is sensitive

indicators of certain pathologic states, including gout, xanthinuria, hyperuricemia, renal failure, toxemia during pregnancy, etc. [73, 74]

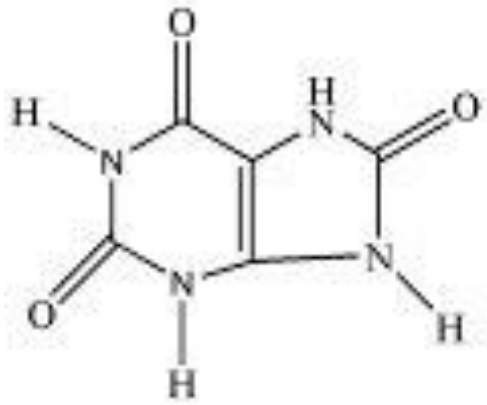

Figure 2.21 Chemical tructure of Uric acid

Over the past decades, many researchers have been developed the method for simultaneous detection of dopamine (DA) and uric acid (UA). The electrochemical method has been considered as a simple, rapid, sensitive and good stability approach for detection of the dopamine and uric acid due to their electrochemical activities [75-77]. The main problem for simultaneous detection of dopamine and uric acid in biological fluids is their oxidation potentials are rather close to each other [76-78], resulting in overlapping of the oxidation peaks on traditional electrodes and the interfering from ascorbic acid. Therefore, it is very important to develop the sensitive and selective biosensors for the simultaneous detection of DA, and UA in complex biological fluids such as blood, serum and urine

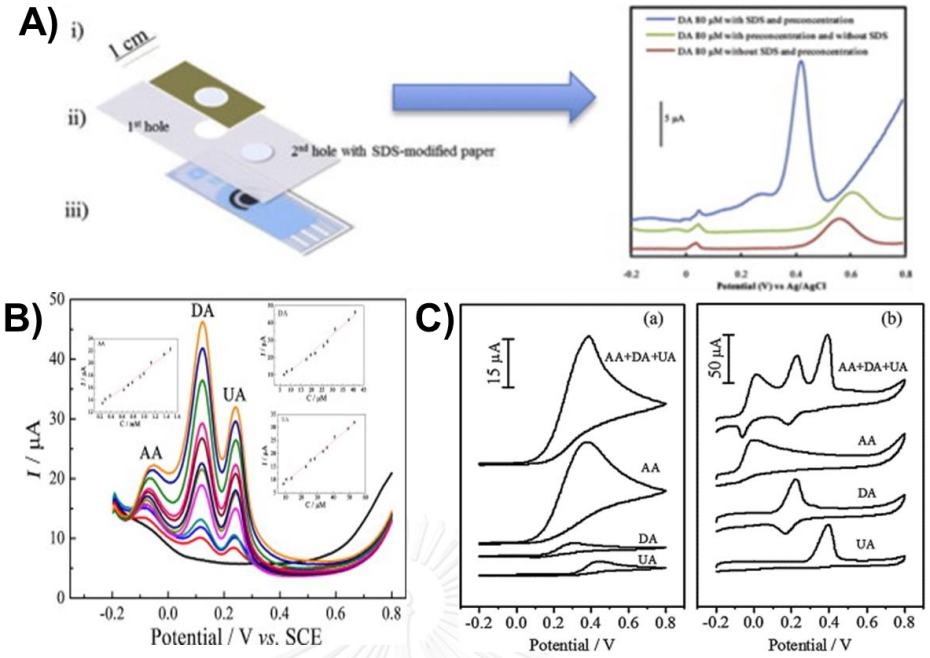

Figure 2.22 A) Paper-based analytical device for determination of dopamine levels in biological [78] and simultaneous detection of ascorbic acid, dopamine and uric acid using B) reduced graphene oxide and Au nanoplates modified glassy carbon electrode [75] and C) reduced graphene oxide modified electrode [76]

2.6.3 Heavy metals

Heavy metals are commonly contaminated in the environment and have long been recognized as a significant threat to human health [79, 80]. Being able to determine metal concentrations in biological fluids such as blood, serum, or urine is of considerable interest in clinical diagnosis because the presence heavy metals, in moderate quantities, is integral for living organisms, but abnormal levels can lead to serious problems [9]. Zn, an essential trace metal, is required for normal function of multiple enzymes, hormones, and transcription-related factors [81, 82]. Public health studies have consistently demonstrated abnormally low zinc levels in critically ill patients as inflammation and infection are associated with reduced serum levels of zinc [83, 84]. Normally, Zinc (Zn) in human body in the range of 2-3

g, and 90% is found in muscle and bone. Other organs such as liver, gastrointestinal tract, kidney, skin, lung, brain, heart and pancreas contain concentration of Zn [85]. Cadmium is a naturally occurring metal often used in industrial processes that has the potential to cause kidney, liver, bone, and blood damage [86-88]. In addition, Pb concentrations in blood as low as 10 μg dL^{-1} have been consistently associated with deficit in IQ and academic achievement [89].

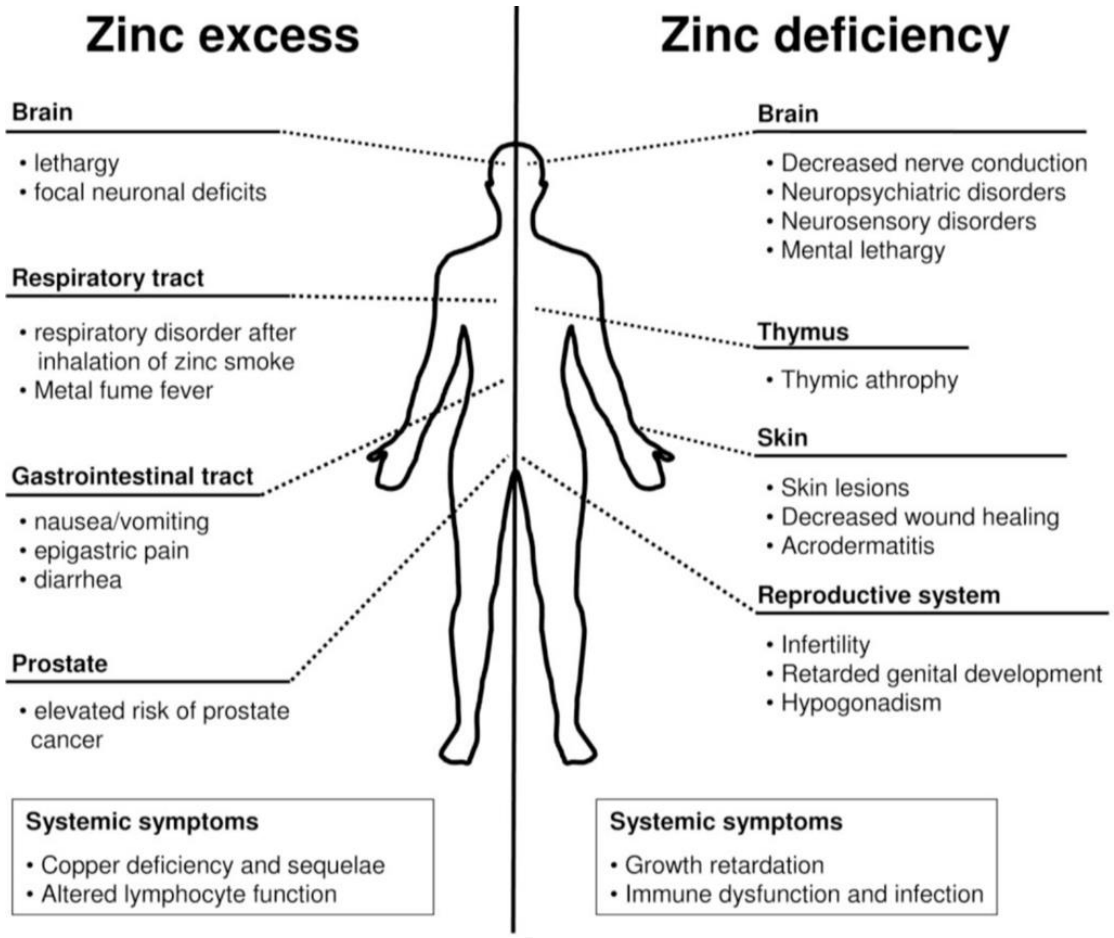

Figure 2.23 The effect of Zn intoxication [85]

CHAPTER III

EXPERIMENTAL

This chapter has separated into 3 parts of the detection of biomarkers including cholesterol, heavy metals and multi-detection (*e.g.* glucose, dopamine and uric acid). It has provided the information of chemical and materials, instruments and equipment and sample preparation.

3.1 Novel Paper-Based Cholesterol Biosensor Using Graphene/ Polyvinylpyrrolidone/Polyaniline Nanocomposite

3.1.1 Chemicals and materials

Filter paper grade No. 1 (size, 46 x 57 cm^2) purchased from Whatman was reduced to letter size. Carbon ink (Electrodag PF-407 C) was obtained from Acheson Colloids Company (Port Huron, MI) and silver/silver chloride ink (Ag/AgCl ink) was purchased from Gwent group (Torfaen, United Kingdom). Graphene (G) nanopowders were purchased from SkySpring Nanomaterials, Inc (Houston, TX). Cholesterol and cholesterol oxidase from *Streptomyces* sp. (418 U mg^{-1}, ChOx), *sodium dodecyl sulfate* (SDS), polyoxyethylene octyl phenyl ether (Triton X-100), camphor-10-sulfonic acid (CSA), polyaniline (PANI), polystyrene (Mw∼180,000; PS), poly (vinyl pyrrolidone) (Mw=10,000; PVP) and trichloroacetic acid (TCA) were obtained from Sigma (St. Louis, MO). Dimethylformamide (DMF), potassium dihydrogen phosphate (KH_2PO_4) and chloroform were purchased from Carlo Erba Reagenti-SDS (*Val de* Reuil, France). Disodium hydrogen phosphate (Na_2HPO_4), potassium chloride (KCl), and sodium chloride (NaCl) were purchased from Merck (Darmstadi, Germany). All solutions were prepared by using high-purity water from Milli-Q Water System (Millipore, USA, R ≥18.2 MΩ cm^{-1}). Phosphate buffered saline (PBS) was prepared by dissolving 0.144% (w/v) Na_2HPO_3, 0.024% (w/v) KH_2PO_4, 0.02% (w/v) KCl, 0.8% (w/v) NaCl in high-purity water. All chemicals were used

as received without further purification. A stock solution of cholesterol was prepared in 5% (w/v) of Triton X-100 and high-purity water and then stored at 4 °C. A stock solution of ChOx was freshly prepared in PBS [90]. For the detection of the cholesterol in a real biological sample, lyophilized human serum (CONSERA), obtained from Nissui Pharmaceutical, was used (Tokyo, Japan).

3.1.2 Apparatus

All electrochemical measurements, including cyclic voltammetry and amperometry, were performed on a CHI 1232A electrochemical analyzer (CH Instruments, Inc., USA). A three electrode system was used for all measurement. The 4 mm in diameter of screen-printed carbon as a working electrode was modified by G/PVP/PANI. An in-house electrospraying system was used for the modification of working electrode. A JSM-6400 field emission scanning electron microscope (Japan Electron Optics Laboratory Co., Ltd, Japan) with an accelerating voltage of 15 kV and a JEM-2100 transmission electron microscope (Japan Electron Optics Laboratory Co., Ltd, Japan) were used for the electrode surface characterization.

3.1.3 Fabrication of paper-based biosensor

Paper-based biosensor was fabricated by using wax-printing method according to a previous report [6]. First, the patterned paper-based biosensor was designed by Adobe Illustrator and then printed onto filter paper (Whatman no. 1) using a wax printer (Xerox Color Qube 8570, Japan). Next, the printed paper-based biosensor was placed on a hot plate at 175 °C for 40 s to melt the wax. The area covered with wax was hydrophobic, and the area without wax was hydrophilic. The block screen was designed with Adobe Illustrator software and fabricated by Chaiyaboon Co. (Bangkok, Thailand). For three electrode system of the paper-based biosensor, a working electrode

(WE) and a counter electrode (CE) were screen-printed in-house using carbon ink. Silver/silver chloride (Ag/AgCl) ink was used as a reference electrode (RE) and a conductive pad.

3.1.4 Electrospraying fabrication of G/PVP/PANI nanocomposites modified paper based biosensor

To modify working electrode using G/PVP/PANI nanocomposites, PANI was firstly doped with CSA to generate a conductive form of PANI and dissolved in chloroform [91]. Then the stock solution of PVP was prepared by dissolving of 2 mg mL^{-1} of PVP in DMF and stirring for 10 min at a room temperature. G dispersion was prepared by the adding 2 mg mL^{-1} of G into the stock solution of PVP and sonicating for 6 h at room temperature. After that, the solutions of PANI and G/PVP were mixed together, and 0.1% (v/v) PS was added into G/PVP/PANI solution. An electrospraying system consists of syringe pump, high-voltage power supply, ground collector, syringe and stainless-steel needle. During electrospraying, the CE and RE, were covered with masks to prevent the electrode modification. The G/PVP/PANI nanocomposite solution was mixed thoroughly in a syringe, and a high voltage was applied to the solution. The nanocomposite solution was electrosprayed onto the WE of a paper-based biosensor attached to a ground collector on a rotating drum. The flow rate was controlled at 1.0 mL h^{-1}, the distance between the needle tip and ground collector was fixed at 5 cm, and the applied high voltage was 6 kV.

3.1.5 Electrochemical measurement

A three-electrode system fabricated on a paper-based biosensor was used throughout the experiment. To control all electroanalytical measurements, a potentiostat (CHI 1207A, CH Instruments, Austin, TX) was used. For the cyclic voltammetric measurements, the potential was scanned

from −0.3 V to +0.8 V for a standard $[Fe(CN)_6]^{3-/4-}$ detection and +0.2 V to +1.0 V for H_2O_2 detection. Hydrodynamic voltammogram was employed to optimize the detection potential for H_2O_2 in a range of +0.2 to +0.8 V. The standard solution of H_2O_2 was dropped in the paper-based device and the current measured at a fixed time with different potentials. For the cholesterol detection, the volume of 418 U mL^{-1} ChOx enzyme was investigated between 0.1 and 1.0 µL. Prior to the detection of cholesterol, an optimum volume of ChOx enzyme was drop-cast and dried onto the surface of the G/PVP/PANI-modified electrode, and amperometry was performed at an optimum detection potential. After that, the anodic current was recorded at the steady state current for 100 s.

3.1.6 Preparation of human serum

Prior to measure cholesterol in standard human serum, 3.0 mL of high purity water was added to the lyophilized human serum, and then the proteins in the serum were precipitated using TCA method [92]. To precipitate protein, 200 µL of human serum, 50 µL of standard cholesterol at different concentration, and 250 µL of 10% (w/v) TCA were mixed together by vortexing for 5 min. Then, the mixed solution was centrifuged at 6000 rpm (Cole-Parmer, USA) for 10 min and the supernatants were kept for further analysis. All samples were analyzed on paper-based sensors using amperometry.

3.2 Sensitive Electrochemical Sensor using a Graphene-Polyaniline Nanocomposite for Simultaneous Detection of Zn(II), Cd(II), and Pb(II)

3.2.1 Materials and Methods

The standards solutions of the all metals including Zn(II), Cd(II), Pb(II) and Bi(III) were purchased from Sigma-Aldrich (St. Louis, MO). Potential

interferences including Mn(II) standard solution, cobalt(II) chloride, iron(III) chloride hexahydrate, copper(II) sulfate pentahydrate and nickel(II) sulfate hexahydrate were obtained from Sigma-Aldrich (St. Louis, MO). For electrochemical detection, carbon ink (E3178, Ercon Incorporated, Wareham, MA) and graphite powder (diameter <20 μm, Sigma-Aldrich, St. Louis, MO) were used as electrode materials. Graphene (G) nanopowders (SkySpring Nanomaterials, Inc, Houston, TX), aniline monomer and polyvinylpyrollidone (PVP) from Sigma-Aldrich, (St. Louis, MO), Nafion® and trimethylsilylated from Aldrich Chem. Co. (Milwaukee, WI) and N,N-dimethylformamide (DMF) (Carlo Erba Reagents, Milano, Italy) were used for electrode modification. The transparency film and filter paper (Grade one) used for electrode fabrication were purchased from Apollo Presentation Products (Booneville, MS) and GE Healthcare Bio-Sciences (Pittsburgh, PA), respectively. Sodium acetate and glacial acetic acid were obtained from Fisher Scientific (Pittsburgh, PA). Milli-Q water from Millipore ($R \geq 18.2\ M\Omega\ cm^{-1}$) was used throughout this experiment. All chemicals were used as received without further purification. For the determination of Zn(II), Cd(II) and Pb(II) in complex biological sample, lyophilized human serum (CONSERA), obtained from Nissui Pharmaceutical, was used (Tokyo, Japan).

3.2.2 Apparatus

All electrochemical measurements, including cyclic voltammetry (CV) and square-wave anodic stripping voltammetriy (SWASV), were performed on a CHI 660B electrochemical analyzer (CH Instruments, Inc., USA). A three electrode system was used and the working electrode was a G/PANI nanocomposite modified screen-printed carbon electrode (3 mm in diameter). An in-house electrospraying system was used for the electrode modification. A 3.0 mL plastic syringe with a 26 G blunt tip needle was loaded with composite solution and inserted into a variable speed syringe pump (Kent Scientific Corp., Torrington, CT, U.S.A.) with a flow rate of 3.0 mL h^{-1}.

Various potentials were applied via a high-voltage power supply (Gamma High Voltage Research, Ormond Beach, FL, U.S.A.). A JSM-6400 field emission scanning electron microscope (Japan Electron Optics Laboratory Co., Ltd, Japan) with an accelerating voltage of 15 kV and Fourier transform infrared spectroscopy (Nicolet 6700) instrument from Nicolet, USA with a frequency of 400–4000 cm^{-1} using TGS detector (32 scans at resolution 4 cm^{-1}) were used for the electrode characterization.

3.2.3 Preparation of G/PANI nanocomposite

A synthetic process of G/PANI nanocomposite was started by dissolving of1.0 g aniline monomers in 1.0 mL concentrated HCl and then adding distilled water to obtain a total volume of 10.0 mL (solution I). Next, G was added into a solution I and sonicated for 2 hr to obtain a dispersed G in aniline monomer solution. For the solution II, 0.8 mL concentrated HCl, 1.0 g ammonium persulfate (APS), and 2.0 g PVP were dissolved in distilled water to obtain a total volume 90.0 mL. Then, solution II was cooled in an ice–water bath for 30 min. After that, solution I was added into solution II under vigorous stirring and the mixture solution was continuously stirred for 4 h to obtain precipitated powder. Finally, the precipitated powder was filtrated and washed with distilled water and ethanol until the filtrated solution became colorless and then precipitated powder on filter paper was dried overnight in an oven at 65 °C. To confirm that G/PANI was completely doped with HCl, the dried powder was re-dispersed in 0.1 M HCl under ultrasonication for 30 min and collected by filtration and drying [93]. The G/PANI preparation is shown in Scheme 3.1A.

3.2.4 Fabrication of electrochemical sensors

The electrochemical sensor was fabricated using a screen-printing method according to a previous report with slight modification [6]. The design

of electrode was firstly created by Adobe Illustrator software and fabricated using screen-printing method. For electrochemical sensor on paper substrate, a patterned paper was created on filter paper (Whatman no. 1) by printing the solid wax onto filter paper using a wax printer (Xerox Color Qube 8870, Japan). Next, the wax patterned on the filter paper was melted at 200 °C for 120 s using hot plate for constructing hydrophobic barriers and hydrophilic channels. Then, patterned paper was used to fabricate the three electrode system by screen-printing method. All electrode including working electrode (WE), counter electrode (CE), and pseudo reference electrode (RE) and conductive pad were screen-printed in-house using carbon ink on transparency film and filter paper. Then, the screen-printed electrode was placed into an oven at 65 °C for 30 min to remove the solvent [11]. Finally, the laser printed of 6 mm diameter hole of packing tape was placed onto a transparency film based device in the middle of sample reservoir to control the area of electrode. For paper-based device, the back side of device was covered with clear packing tape. The fabrication of electrochemical sensor using filter paper and transparency film is shown in Scheme 3.1B.

3.2.5 Electrode modification using G/PANI nanocomposite by casting and electrospraying

Firstly, G/PANI nanocomposite was dispersed in PVP solution prepared by dissolving of 2 mg mL^{-1} of PVP in DMF. Then, G/PANI solution was sonicated using probe sonicator for 2 h at room temperature, and 0.1% (v/v) PS was added into G/PANI solution. For electrode modification by casting, 1.0 µL of the dispersed solution of G/PANI was directly dropped onto working electrode surface, and allowed it to dry completely at room temperature for 10 min. An electrospraying system consisting of syringe pump, high-voltage power supply, ground collector, plastic syringe and stainless-steel needle was used to modify electrode. G/PANI nanocomposite solution was mixed thoroughly in a syringe, and 14.0 kV of high voltage was applied to the

solution. During the electrospraying, the CE and RE were covered with aluminium foil as a mask to prevent the G/PANI solution in electrospraying system. Then, G/PANI solution was sprayed onto the working electrode of electrochemical sensor attached to a ground collector on a collector. The flow rate was controlled at 3.0 mL h^{-1} with 5 cm of the distance between the needle tip and electrode on the colletor. For the detection of heavy metal including Zn(II), Cd(II) and Pb(II), 1.0 µL of Nafion, which is permeable to metal ions, was coated onto G/PANI nanocomposite modified electrode to pre-concentrate metal ions. Electrochemical sensor modifications using G/PANI nanocomposite by casting and electrospraying are shown in Scheme 3.1C.

3.2.6 Electrochemical measurement

Electrochemical performance of the sensors was studied by cyclic voltammetry (CV) and square-wave anodic stripping voltammetry (SWASV). The three-electrode system fabricated on a transparency film and filter paper was used throughout the experiment. A potentiostat (CHI 660B, CH Instruments, Austin, TX) was used to control all electroanalytical measurements. For the cyclic voltammetric measurements of a standard $[Fe(CN)_6]^{3-/4-}$, the potential was scanned from −0.8 V to +0.7 V with a scan rate of 100 mV s^{-1}. SWASV was used for the detection of Zn(II), Cd(II) and Pb(II) after dropping 50.0 µL of standard metals and 2.5 µL of 10.0 ppm Bi(III) in 0.1 M acetate buffer pH 4.5 onto the three electrode system. In the accumulation step, Zn(II), Cd(II) and Pb(II) with the concentration range of 25.0−200.0 µg L^{-1} was accumulated on electrode surface by applying the deposition potential of −1.6 V for 240 s and 0.5 ppm Bi(III) in situ. After 5 s of equilibration time, square-wave voltammograms with a frequency of 10 Hz, a step potential of 5 mV, and pulse amplitude of 25 mV were recorded from −1.8 V to 0 V.

3.2.7 Preparation of human serum

Prior to analysis, 3.0 mL of high purity water was added to the lyophilized human serum purchased from Nissui Phar-maceutical Co., Ltd. (Tokyo, Japan). For the detection of heavy metals, human serum was diluted in a 1:10 ratio with 0.1 M sodium acetate buffer (pH 4.5). According to the product information, the human serum is a complex biological environment, but it does not contain any heavy metal. Thus, standard addition method was used to determine the amount of heavy metals.

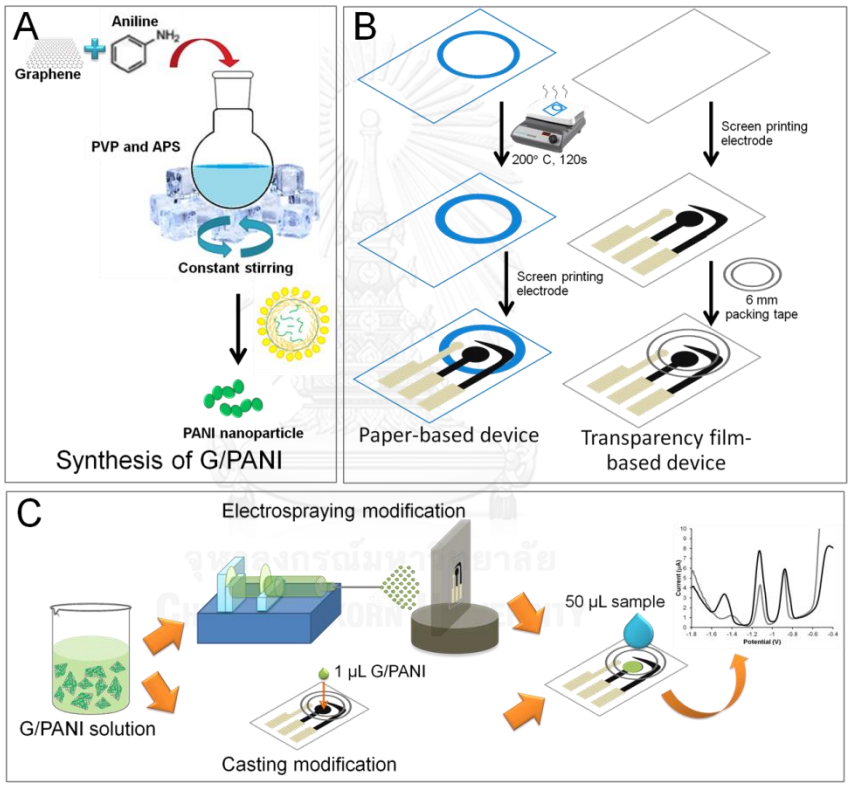

Scheme 3.1 The schematic drawing of A) the preparation procedure for the G/PANI nanocomposite, B) the fabrication of electrochemical sensor and C) modification methods (electrospraying and casting) for electrochemical sensor.

3.3 Active Paper Chips for Electrochemical Multiprobe Detections

3.3.1 Paper chips fabrication

CNT ink was prepared by mixing the CNT with dispersion agent as a non-ionic surfactant with a naphthyl group and used kinetic ball milling. The details of CNT ink fabrication are described in Kwon et al. [94]. The CNT ink was printed on a photo paper using an office inkjet printer (model: EPSON Stylus T10), and the patterned electrodes was designed by Adobe Flash graphic software. After printed CNT electrode, dielectric parylene-C film (Sigma-Aldrich, 1-μm thick) was deposited on paper chip device using chemical vapor deposition method, and then a hydrophobic film of amorphous Teflon (AF 1600, DuPont, 200-nm thick) was coated by spin-coating using 2000 rpm for 30 s. The paper chip devices were then baked at 170 °C for 30 minutes. Finally, 3 μL of silicone oil (Sigma-Aldrich) with a kinetic viscosity of 10 cSt was spin-coated at 2000 rpm for 30 s onto a paper chip with an estimated thickness of approximately 500 nm. The silicone oil is a siloxane polymer with organic CH_3 side chains that was used as a lubricant for adjusting the surface tension of the paper chips.

3.3.2 Screen-printed carbon electrode

Electrodes were screen-printed according to the previous methods, with slight modifications. [11] Electrode designs were created with computer-aided design software (Adobe Illustrator). Three electrodes of the sensor were screen-printed in-house on PET substrate using carbon or cobalt (II) phthalocyanine ink as a working electrode (WE) and counter electrode (CE). Silver/silver chloride (Ag/AgCl) ink was used as the reference electrode (RE) and conductive pads. The screen-printed electrode was dried at 60 °C for 30 min for removing any remaining solvent. For dopamine and uric acid detection, 1 μL graphene oxide ink from Korea Atomic Energy Research Institute (KAERI) was coated on a carbon electrode, and then was reduced to form of graphene via cyclic voltammetry in 0.01 M PBS buffer (pH 3).

Moreover, reduced graphene oxide electrode was modified by deposition of gold nanoparticles.

3.3.3 Apparatus

All electrochemical measurements, including cyclic voltammetry (CV), amperometry and square wave anodic stripping voltammetry (SWASV) were performed using a SP200 BioLogic electrochemical analyzer (Biologic science instrument, France). A three electrode system was used, and working electrodes with 2 mm diameter were CoPc and Au/rGO modified SPCEs. In general, the CV measurements were performed over a potential range from −1.25 to +1.25 V at a scan rate of 100 mV s^{-1} for standard $[Fe(CN)_6]^{3-/4-}$. The amperometry measurements of glucose were performed by applied +0.4 V as a detection potential for 120 s. The optimal parameters for SWASV measurement were found in preliminary trials (data not shown) to be a pulse amplitude of 30 mV, pulse width of 35 ms, square wave frequency of 50 Hz, and a step height of 5 mV for scanning the potential between −0.3 V and 1.0 V (vs. Ag/AgCl). These parameters were used throughout DA and UA measurement.

3.3.4 Electric System for Drop Actuation

Keithley 2400 and 2702 units were used as an electric power source and the multiflex relay, respectively, for switching the power to the each electrode printed on the paper.

3.3.5 Preparation of human serum

Lyophilized human serum from Sigma (St. Louis, MO) was used for analysis of the analyte (glucose, DA and UA) in complex biological sample. Prior to use, 5.0 mL of DI water was added to the lyophilized human serum. To precipitate protein in serum, trichloroacetic acid (TCA) was used by mixing

200 µL of human serum, 50 µL of the mixture of standard glucose, DA and UA at different concentrations, and 250 µL of 10% (w/v) TCA, and then the solutions were completely mixed using vortex for 5 min [78]. After that, the mixture solutions were centrifuged at 6000 rpm (Cole-Parmer, USA) for 10 min, and the supernatants were kept for further analysis. All samples were analyzed using APOC coupled with CoPc and Au/rGO modified electrode.

CHAPTER IV
RESULTS AND DISCUSSION

4.1 Novel Paper-Based Cholesterol Biosensor Using Graphene/ Polyvinylpyrrolidone/Polyaniline Nanocomposite

4.1.1 Optimization electrospraying parameters for Graphene/ Polyvinylpyrrolidone/Polyaniline Nanocomposite (G/PVP/PANI) modification

For electrospraying, the effect of applied voltage, spraying time and G/PANI ratio on the electrochemical conductivity of modified electrodes were investigated and carefully optimized.

4.1.1.1 The effect of voltage for electrospraying

The applied voltage is an important parameter affecting the morphology of G/PVP/PANI on modified electrode. The surface of G/PVP/PANI modified electrode with different applied voltage was characterized by SEM as shown in Figure 4.1A-D. The results showed that when increasing the applied voltage, the morphology of G/PVP/PANI on electrode surface become less uniform. The droplet-like structure was observed when using 6 kV as an applied voltage. Moreover, the currents of 1 mM standard $[Fe(CN)_6]^{3-/4-}$ with different applied voltage in a range of 6 to 12 kV were investigated by of cyclic voltammetry. As shown in Figure 4.1E, the anodic current rapidly decreased with increasing the applied voltage from 6 kV to 10 kV; after that the current became constant. Therefore, 6 kV was selected as an optimized applied voltage for electrospraying fabrication.

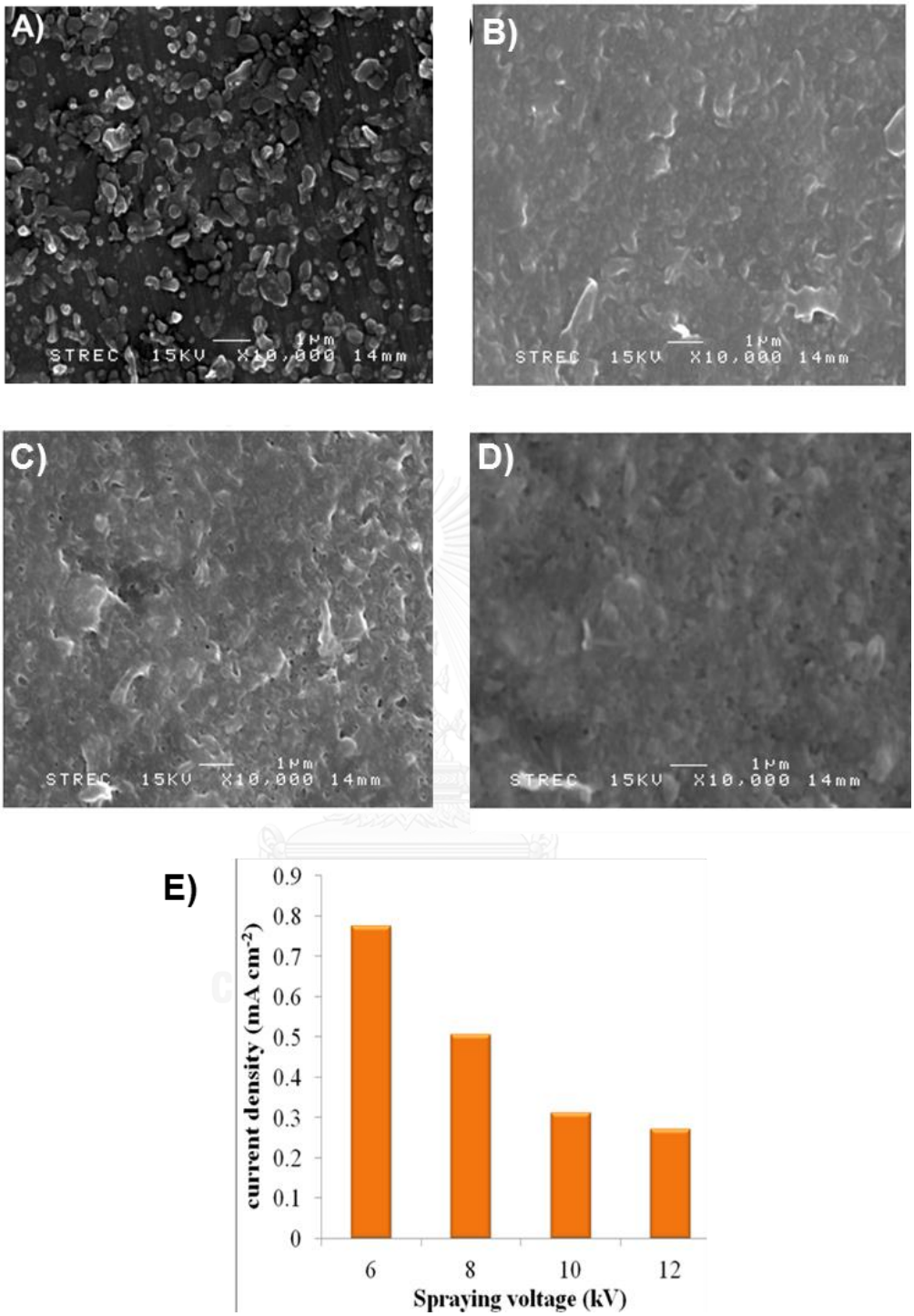

Figure 4.1 SEM images of G/PVP/PANI nanocomposite-modified electrodes using electrospraying method at different applied voltage, (A) 6 kV, (B) 8 kV, (C) 10 kV, and (D) 12 kV and E) anodic current response of 1 mM standard $[Fe(CN)_6]^{3-/4-}$ measured on different applied voltage.

4.1.1.3 The ratio of G/PANI for modified carbon electrode

Figure 4.2 shows the effect of G/PANI ratio for increasing the conductivity of modified electrode for 1 mM standard $[Fe(CN)_6]^{3-/4-}$ detection. The G/PANI ratio was optimized by fixing G ratio and varying PANI ratio from 0.5 to 5. It was found that the anodic current of 1 mM $[Fe(CN)_6]^{3-/4-}$ increased rapidly when increasing the G/PANI ratio from 1:0.5 to 1:1. However, the anodic current tends to decrease once the G/PANI ratio is increased above 1:1. The decreasing in anodic current was probably caused by agglomeration of G within the nanocomposites. Therefore, 1:1 as a G/PANI ratio was selected as an optimized G/PANI ratio for further study.

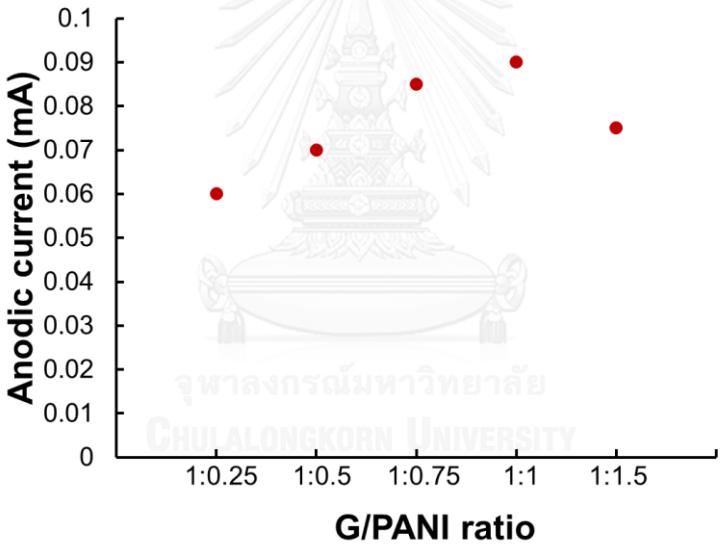

Figure 4.2 A) The effect of ratio of G/PANI on anodic current of 1 mM $[Fe(CN)_6]^{3-/4-}$ at different G/PANI ratio (1:0.25, 1:0.5, 1:0.75, 1:1, and 1:1.5); condition, scan rate 100 mV s^{-1}.

4.1.1.4 The effect of collecting time

For the collection time of electrospraying, G/PANI nanocomposite solutions were collected on different screen-printed carbon electrodes for a time period ranging from 5 to 25 min. The cyclic voltammetry of 1 mM standard $[Fe(CN)_6]^{3-/4-}$ was used to

investigate the electrochemical sensitivity of each modified electrode. The anodic peak currents obtained using different collection time for each of the modified electrodes indicated that the highest electrochemical response was achieved at 5 min collection time (Figure 4.3). The anodic peak currents decreased for longer collection times. This decrease in current was probably caused by the agglomeration of G in nanodroplet on the electrode surface.

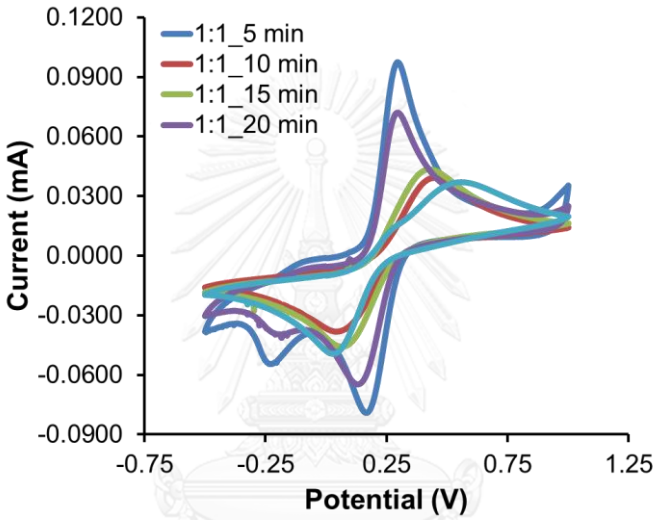

Figure 4.3 Cyclic voltamograms of 1 mM $[Fe(CN)_6]^{3-/4-}$ at different collection times between 5 min and 25 min

4.1.2 Characterization of G/PVP/PANI nanocomposites modified paper-based biosensor

In this study, electrospraying technique was selected for electrode modification to increase the surface area of working electrode. 6 kV of applied voltage, 5 min of spraying time, and 1:1 of G/PANI ratio were selected as optimized parameters. The surface morphology of G/PVP/PANI modified electrode on a paper substrate was characterized by scanning electron microscopy (SEM). Interestingly, the droplet-like structures as a three dimensional of G/PVP/PANI can be uniformly generated on paper electrode

and the average size of each droplet was found to be 160±1.02 nm as shown in Figure 4.4A. In addition, to indicate a well dispersion of G without severe aggregation inside the nanocomposites, TEM and the electron diffraction pattern of G were characterized as shown in Figure 4.4B and inset of Figure 4.4B, respectively. The electron diffraction pattern of G matched very well with the previous report ([95]) confirming that G in droplet was well dispersed.

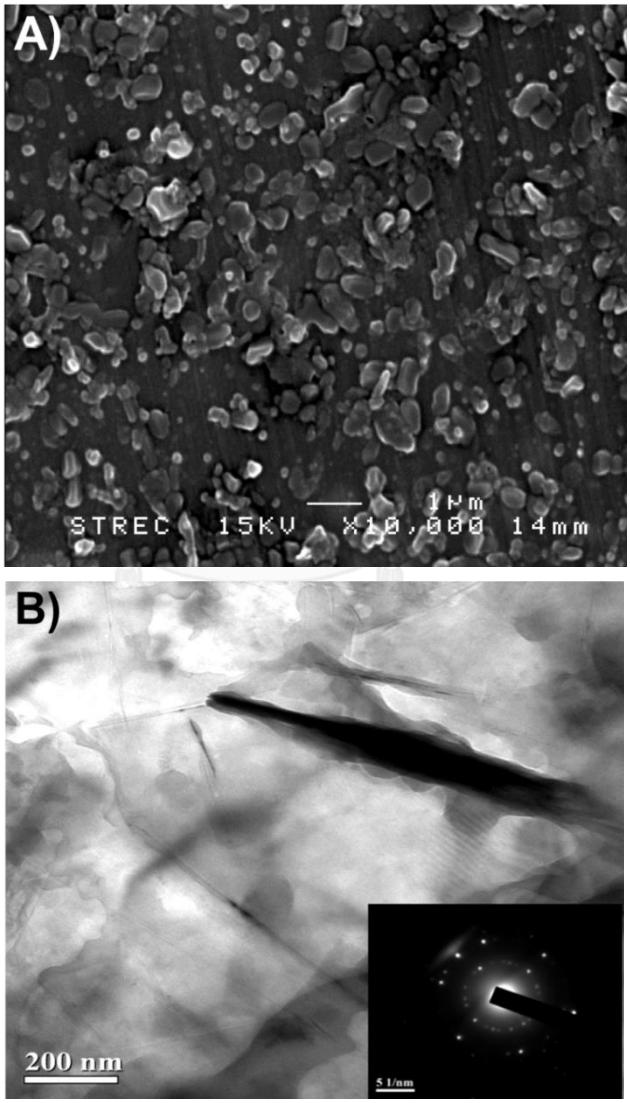

Figure 4.4 A) SEM and B) TEM images of G/PVP/PANI nanocomposite modified electrodes with an electron diffraction pattern of G (inset of 4.4B).

To prepare the nanocomposite of G/polymer, other than PANI conducting media, PVP and PS were selected as graphene stabilizer and carrier polymer for electrospraying, respectively. To investigate the electron transfer process, cyclic voltammetry was performed on different electrodes including G/PVP/PANI, G/PANI, PANI and unmodified carbon electrodes using $[Fe(CN)_6]^{3-/4-}$ as a redox probe. As shown in Figure 4.5, the anodic and cathodic peak currents of $[Fe(CN)_6]^{3-/4-}$ show the well-defined peaks for all electrodes. The highest anodic and cathodic peak currents of $[Fe(CN)_6]^{3-/4-}$ were observed on G/PVP/PANI modified electrode (green line) indicating the high sensitivity of the system. The peak currents gradually decrease for G/PANI, PANI and unmodified carbon electrode, respectively. Compared to PANI modified electrode (purple line), incorporation of G into the nanocomposites can increase both anodic and anodic peak currents of $[Fe(CN)_6]^{3-/4-}$ (red line). Interestingly, the peak-to-peak potential separation (ΔEp) of $[Fe(CN)_6]^{3-/4-}$ measured on G/PANI modified electrode (ΔEp = 0.155; red line) significantly decreases when compared to ΔEp of 0.508 obtained from PANI modified electrode, indicating that the presence of G in the nanocomposites can improve the electron transfer kinetics of the system. Moreover, it can be noticed that using PVP as a stabilizer for G dispersion can further increase the anodic and cathodic peak currents in this sensing system as shown in Figure 4.5 (green line vs red line). Another important advantage of using PVP is decreasing of dispersion time of G from 24 h to 6 h. In general, the long dispersion time is required to prevent the re-aggregation of G to graphite form. Therefore, 2 mg mL^{-1} of PVP in DMF was used as a stabilizer for G dispersion in all further experiments.

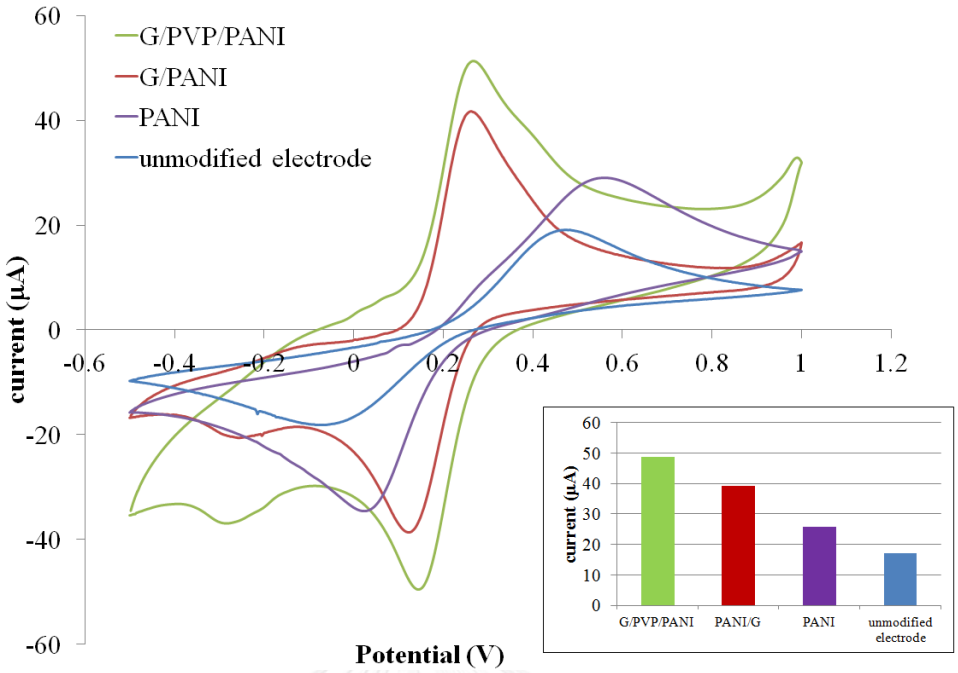

Figure 4.5 Cyclic voltammograms of 2.0 mM $[Fe(CN)_6]^{3-/4-}$ in 0.1 M KCl and anodic current responds (in the inset) measured on different working electrodes of paper-based biosensor

Prior to analysis of hydrogen peroxide and cholesterol, the electrochemical behavior of G/PVP/PANI modified paper-based biosensor was examined using $[Fe(CN)_6]^{3-/4-}$ as a redox probe. 70 µL of the solution of 2.0 mM $[Fe(CN)_6]^{3-/4-}$ in 0.1 M KCl was directly dropped onto the modified electrode surface and the cyclic voltammetric measurements were performed at different scan rates. The relationship between square root of scan rate ($\nu^{1/2}$) and current response was plotted as shown in Figure 4.6. The anodic and cathodic peak currents of $[Fe(CN)_6]^{3-/4-}$ are linearly proportional to the square root of the scan rate in a range of 2 to 100 mV s^{-1}. These results verify that the redox process is controlled by diffusion.

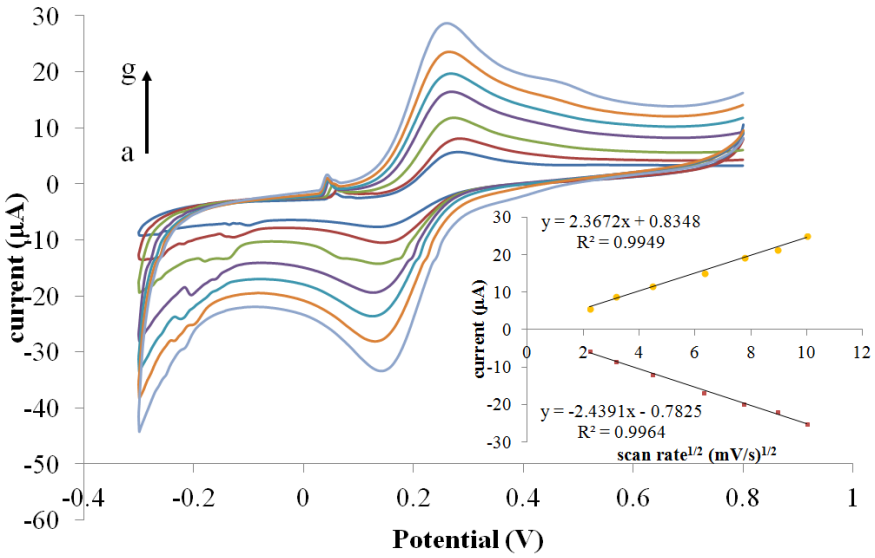

Figure 4.6 Cyclic voltammograms of 1 mM $[Fe(CN)_6]^{3-/4-}$ in 0.1 M KCl on G/PVP/PANI modified electrodes at different scan rates (a) 5, b) 10, c) 20, d) 40, e) 60, f) 80, g) 100 mV s^{-1}). The relationship between the square root of scan rate ($\nu^{1/2}$) and peak currents is shown in an inset.

4.1.3 Detection of hydrogen peroxide and cholesterol

For electrochemical biosensor, determination of H_2O_2 product obtained from cholesterol oxidation can be used for indirect quantification of cholesterol [96]; [97]. In this study, a novel paper-based biosensor based on G/PVP/PANI modified screen-printed carbon electrode was used for sensitive determination of H_2O_2 and cholesterol using cyclic voltammetry and amperometry. The cyclic voltammograms of H_2O_2, measured on G/PVP/PANI modified electrode and unmodified carbon electrode are illustrated in Figure 4.7. A dramatic increase (40 times) in the anodic current signal of H_2O_2 is observed (green line) when compared to an unmodified carbon electrode (red line) indicating that the modified electrode might be a promising tool for sensitive detection of cholesterol.

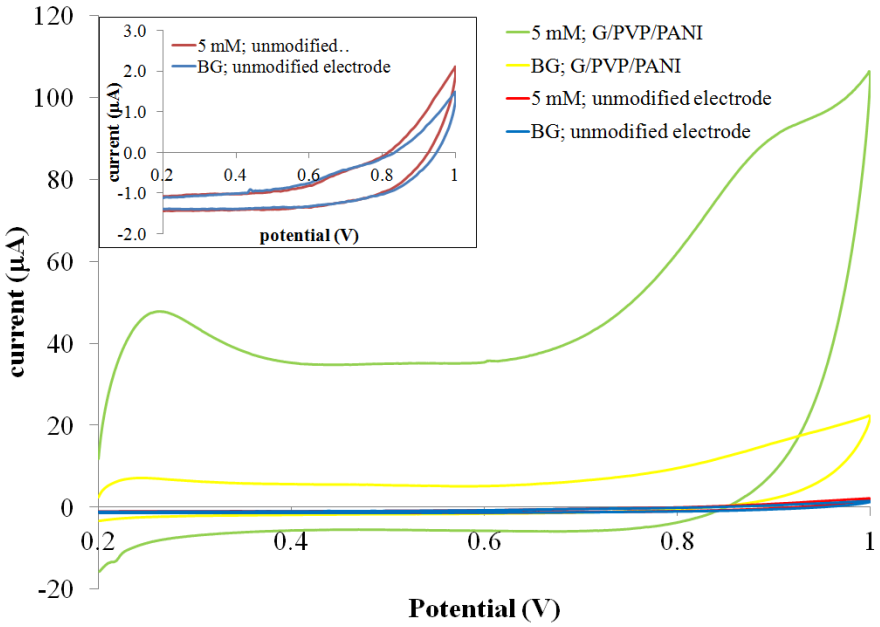

Figure 4.7 Cyclic voltammograms of 5 mM hydrogen peroxide (H_2O_2) in 0.1 M PBS pH 7.0 measured on G/PVP/PANI-modified electrode and unmodified carbon electrode at a scan rate of 100 mV s^{-1}.

Due to the high sensitivity and wide applicability, chronoamperometry was selected for the electrochemical detection of H_2O_2 and cholesterol. Initially, the detection potential was investigated and optimized as shown in Fig. 4.8. A hydrodynamic voltammogram of H_2O_2 was obtained by adjusting the detection potential in a range from +0.2 V to +0.8 V at a sampling time of 100 s. As seen in Figure 4.8, the anodic current signal of H_2O_2 significantly increases as the detection potential increases (blue line); however, the background current also increases (green line). Therefore, a hydrodynamic voltammogram of signal-to-background ratios (S/B) was investigated instead of current signal as shown in Figure 4.8B. The S/B ratio measured at +0.6 V shows the highest sensitivity for H_2O_2; thus, +0.6V was selected as an amperometric detection potential for further experiments.

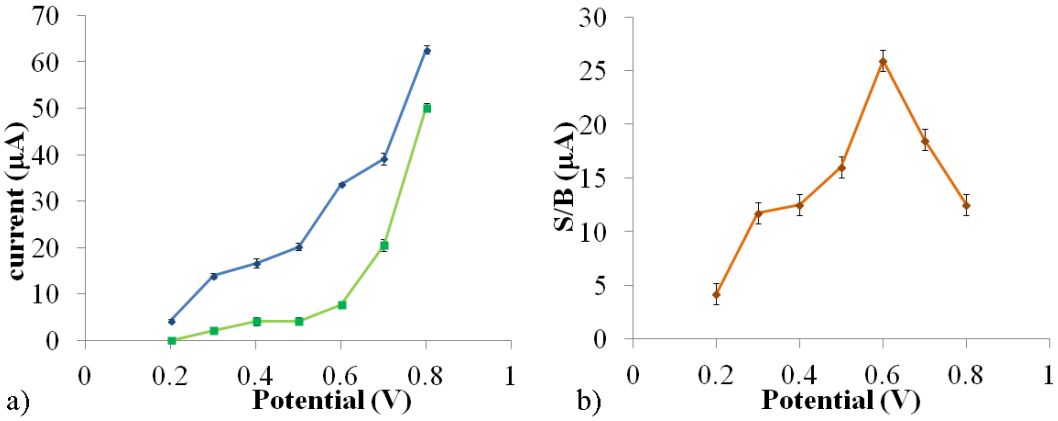

Figure 4.8 (A) Hydrodynamic voltammograms of 1.0 mM H_2O_2 (blue line) and background (green line) in 0.1 M PBS pH 7.0 at a 100 s sampling time measured on a G/PVP/PANI modified paper-based device and (B) Hydrodynamic voltammogram of signal-to-background ratios (S/B) extracted from the data in Figure 4.8A.

For cholesterol biosensor, H_2O_2 is generated from the enzymatic reaction between cholesterol and ChOx as shown in Scheme 4.1. Therefore, it is important to optimize the amount of ChOx on G/PVP/PANI modified paper-based biosensor. In this study, different volumes of ChOx were directly dropped on the modified electrodes and dried out at room temperature for 10 min. The effect of enzyme volume on the anodic current signal of 1 mM cholesterol is shown in Figure 4.9. The anodic currents of cholesterol increase rapidly upon increasing of enzyme volume from 0.1 to 0.4 µL and the currents tend to decrease gradually when the enzyme volume is increased above 0.4 µL. Therefore, the enzyme volume of 0.4 µL was selected as an optimum volume.

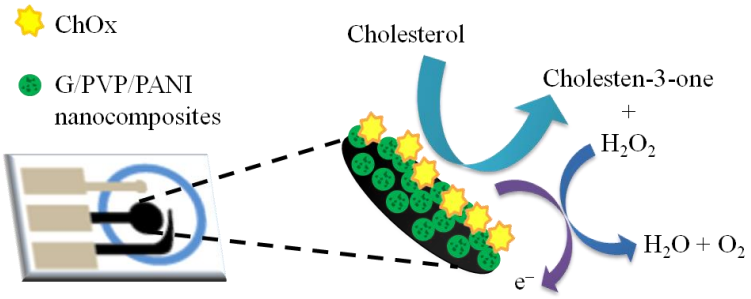

Scheme 4.1 The enzymatic reaction between cholesterol and ChOx on G/PVP/PANI modified paper-based biosensor.

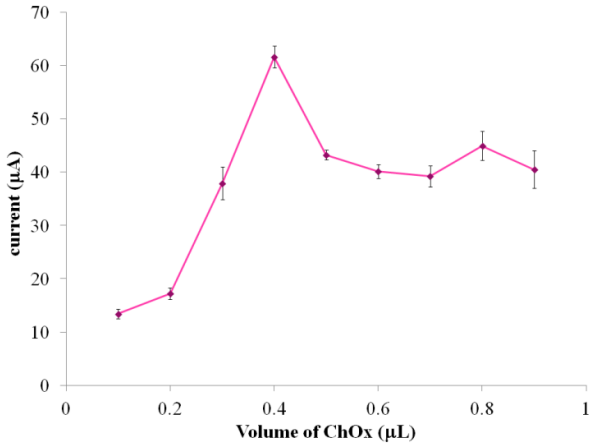

Figure 4.9 The effect of ChOx volume on the anodic current response of 1 mM cholesterol in 0.1 M PBS pH 7.0 at a detection potential of +0.6 V on G/PVP/PANI modified paper-based biosensor.

4.1.4 Analytical performance of G/PVP/PANI nanocomposites modified paper-based biosensor

G/PVP/PANI modified paper-based biosensor was used to measure cholesterol at different concentrations and the amperometric current responses were recorded at a steady state current of 100 s to create a calibration curve of cholesterol. As shown in Figure 4.10, the calibration plot is linearly proportional to cholesterol concentration in a range of 1.93 mg

dL^{-1} (50 μM) to 387 mg dL^{-1} (10 mM) with a correlation coefficient of 0.9994. The detection sensitivity of the system calculated from the slope of linear range was found to be 3490.9 μA mM^{-1} cm^{-2}. Limit of detection (LOD) and limit of quantitation (LOQ) for cholesterol are 38.70 μg dL^{-1} (1 μM) and 1.93 mg dL^{-1}(50 μM), respectively. Previously, it has been reported by the national cholesterol education program (NCEP) that the normal level of total blood cholesterol in human is lower than 200 mg dL^{-1} [98]. This information confirms that our system can be applied for the determination of cholesterol in real biological sample.

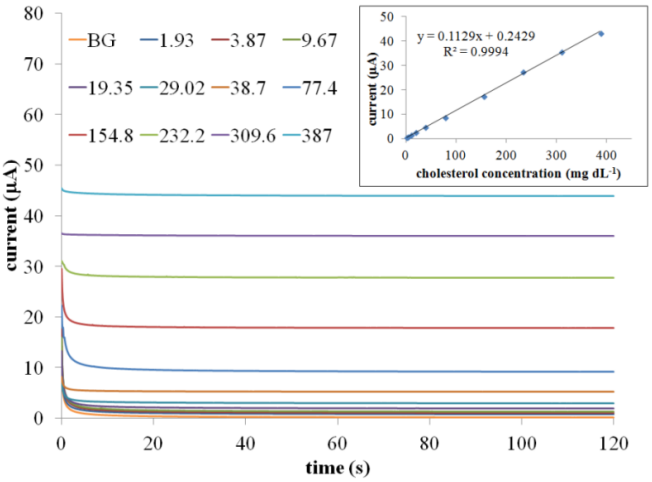

Figure 4.10 Amperometric current responses for the detection of cholesterol in a concentration range of 1.93 mg dL^{-1} (50 μM) to 387 mg dL^{-1} (10 mM) in 0.1 M PBS pH 7.0 with a linear range (inset).

The electrochemical performances of G/PVP/PANI modified electrode were compared to the other modified electrodes used for the detection of cholesterol. As shown in Table 4.1, the proposed electrode shows the highest electrochemical sensitivity, wide linearity and comparable LOD for cholesterol detection. Since the G/PVP/PANI modified paper-based biosensor proposed in this study is easily prepared and inexpensive, it might be a promising tool for cholesterol detection.

Table 4.1 Comparison of various cholesterol biosensors based on nanomaterial/polymer modified electrode

Modified electrode	Detection method	Sensing element	Method of enzyme immobilization	LOD (μM)	Linear range (mM)	Sensitivity ($A(mM^{-1} cm^{-2})^{-1}$	Reference
G/nPt/GCE	Amperometry	ChOx/ChEt	physical adsorption	0.2	0-0.035	2070	[103]
AuNPs/f-G modified GCE	Amperometry	ChOx	physical adsorption	-	0-0.135	314	[97]
AuPt–Ch–IL/GCE	Amperometry	ChOx	cross-linking	10	0.05–6.2 and 6.2–11.2	90.7	[102]
Ti/NPAu/ChOx–HRP–ChE	CV	ChOx/ChEt	Entrapment	12.95	0.97–7.8	29.33	[98]
CSNF–AuNPs/ChOx	Amperometry	ChOx	Physical adsorption	0.5	0.001–0.045	1.02	[101]
AuE/dithiol/AuNPs/MUA/ChOx	CV	ChOx	Covalent attachment	34.6	0.04–0.22	45.96	[100]
ChOx/HRP/AuNPs/PDDA/	Amperometry	ChOx	Physical adsorption	2.2	0.01–1.05	18.6	[58]
$NiFe_2O_4$/CuO/FeO-Ch/ChOx	DPV	ChOx	Physical adsorption	0.0313	0.13–12.95	16.54	[99]
ChOx-FG/G	Amperometry	ChOx	Covalent attachment	5	0.05–0.35	-	[96]
G/PVP/PANI nanocomposites	Amperometry	ChOx	Physical adsorption	1	0.05-10	3490.4	Present work

4.1.5 Interference study

Previously, it has been reported that glucose and ascorbic acid are the common interferences for the detection of cholesterol in complex biological fluids (*e.g.* human serum). Therefore, selective determination of cholesterol in the presence of glucose and ascorbic acid was investigated using the highest anticipated concentrations of glucose (5.3 mM) and ascorbic acid (80 μM) in human serum ([4, 78, 98]). As shown in Figure 4.11A, the amperometric result of a mixture between cholesterol and glucose shows a negligible effect on the current response (blue bar), while an effect of ascorbic acid on the current response is observed (green bar). To solve the problem of ascorbic acid interference, an anionic surfactant of sodium dodecyl sulfate (SDS) was used to coat on the surface of G/PVP/PANI modified electrode. Recently, it has been proven that an electrostatic repulsion between anionic SDS and anionic AA can prevent the interference effect from AA in the detection of target analytes ([78]). In this study, an optimum concentration of SDS was found to be 2 mM, which can prevent the effect of AA interference in a concentration range of 0 to 120 μM in the detection of 3.87 mg dL^{-1} (1 mM) cholesterol (Figure 4.11B)

.

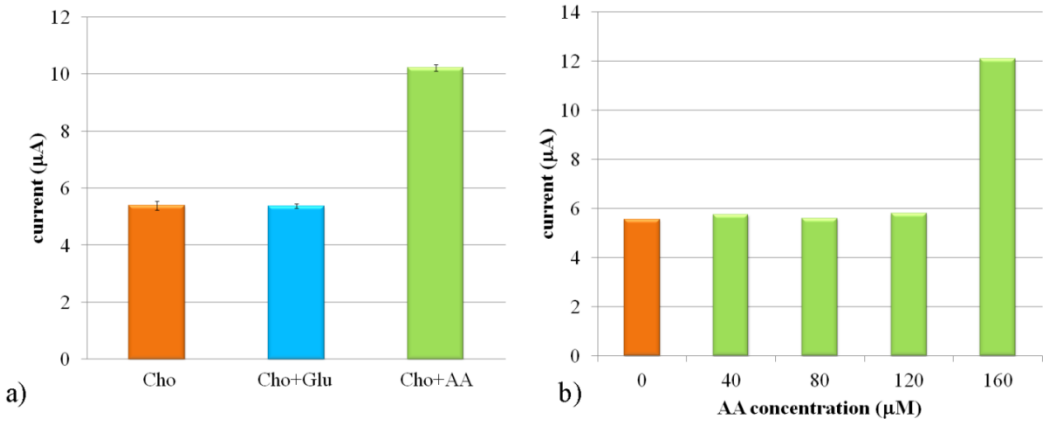

Figure 4.11 A) The interference effect of 5.3 mM glucose (Glu) and 80 µM ascorbic acid (AA) in the detection of 3.87 mg dL^{-1} (1 mM) cholesterol in 0.1 M PBS pH 7.0 and B) The interference effect of different concentration of AA (0 µM, 40 µM, 80 µM, 120 µM, and 160 µM) in the detection of 3.87 mg dL^{-1} (1 mM) cholesterol measured on SDS coated-G/PVP/PANI modified paper-based cholesterol biosensor.

4.1.6 Sample analysis

To test the applicability of this system, G/PVP/PANI modified paper-based biosensor was used for the detection of cholesterol in human serum. The blank human serum samples are the common systems for determination of the accuracy and validation of a new diagnostic assay. Initially, the different concentrations of cholesterol (1.93, 3.87, 9.67, 38.7, and 193.5 mg dL^{-1}) were spiked into the human serum and the proteins in the serum were precipitated by using TCA. After centrifugation, the supernatant was kept for further amperometric analysis on G/PVP/PANI modified paper-based biosensor. The results indicated that the current responses depended on the cholesterol concentration, and the acceptable linearity with a correlation coefficient (R^2) of 0.9998 (n = 3) was achieved. The percentages of recoveries (Table 4.2) were found in a range of 97.9—101.7 % and the RSD was less than 5.0%, verifying that this sensing system is highly accurate.

Table 4.2 Determination of cholesterol in human serum samples (n = 3)

Cholesterol (mg dL^{-1})		% Recovery	% RSD
added	found		
1.93	1.91 ± 0.04	98.9	2.1
3.87	3.79 ± 0.08	97.9	2.1
9.67	9.73 ± 0.30	100.6	3.1
38.7	39.36 ± 1.05	101.7	2.7
193.5	194.06 ± 2.84	100.3	1.4

4.2 Sensitive Electrochemical Sensor using a Graphene-Polyaniline Nanocomposite for Simultaneous Detection of Zn(II), Cd(II), and Pb(II)

4.2.1 Characterization of carbon electrode on the different substrates

The surface roughness of carbon electrodes screen-printed on both paper and plastic surfaces was evaluated by optical profilommetry (Figure 4.12). This non-destructive technique was used because it can effectively resolve small (~nm) feature differences, and is adequate for demonstrating small differences in electrode surface structure. As shown in the Figure 4.12, on paper, the carbon electrode penetrated into the porous capillary network which is why the capillary network is so visible and the electrode nearly indistinguishable from the paper itself. The electrode is highly distinguishable from the plastic substrate, however, because the carbon ink cannot readily penetrate the plastic material. These results suggest that transparency film might be an appropriate substrate for the detection of Zn (II), Cd (II), and Pb (II) in this work. The electrochemical performance of screen-printed carbon electrodes on paper and plastic surfaces, as evaluated by CV, is shown in Figure 4.13. The peak potential difference of the electrode on plastic is lower for paper, indicating that electron transfer kinetics are faster for electrodes screen-printed on plastic. The SWASV responses of Zn (II), Cd (II), and Pb (II) of

carbon electrodes on both substrates are shown in Figure 4.12C indicating that relative high surface roughness of transparency film based device generates a relative high current response for the detection of Zn (II), Cd (II) and Pb (II). Thus, transparency film based device is selected in this work for increasing the electrochemical sensitivity in the detection of Zn (II), Cd (II) and Pb (II).

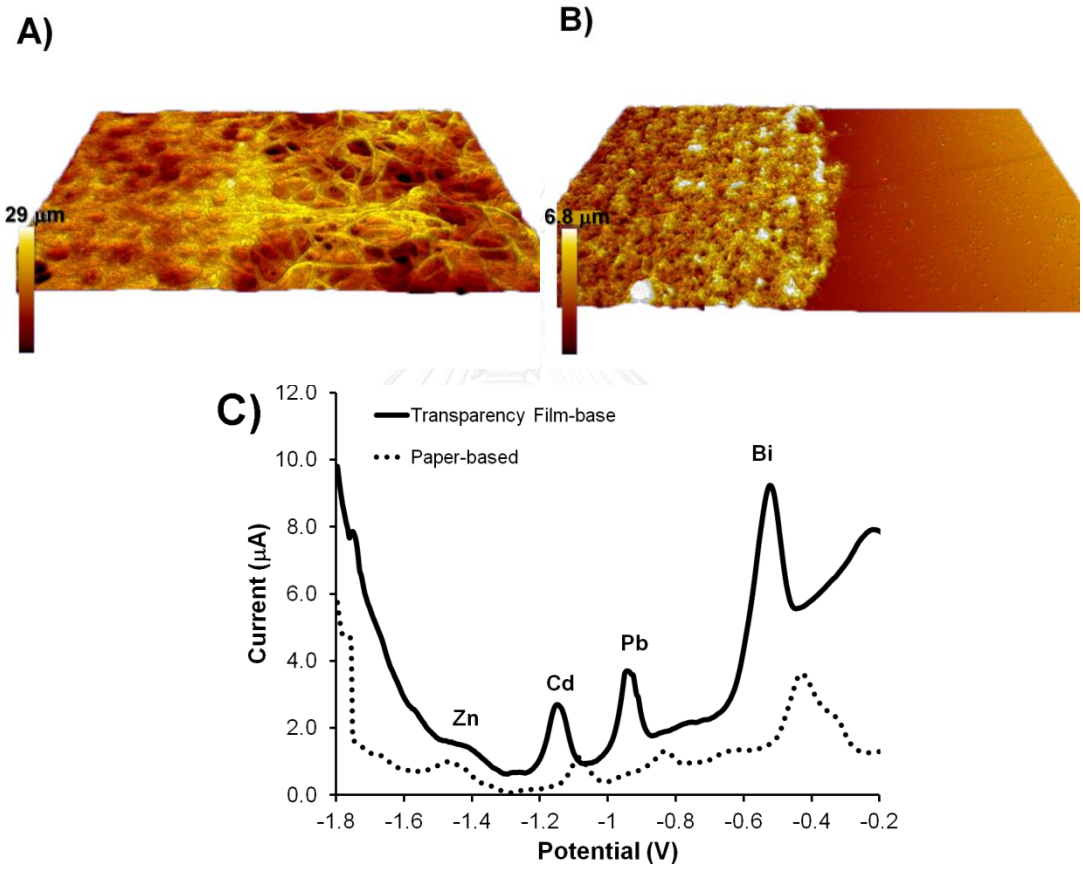

Figure 4.12 Optical profile of a carbon working electrode on (A) filter paper and (B) a plastic transparency film. C) SWASV of 200 µg L^{-1} Zn(II), Cd(II), and Pb(II) in 1.0 M acetate buffer pH 4.5 measured with a carbon electrode (3 mm diameter) on paper and plastic substrates.

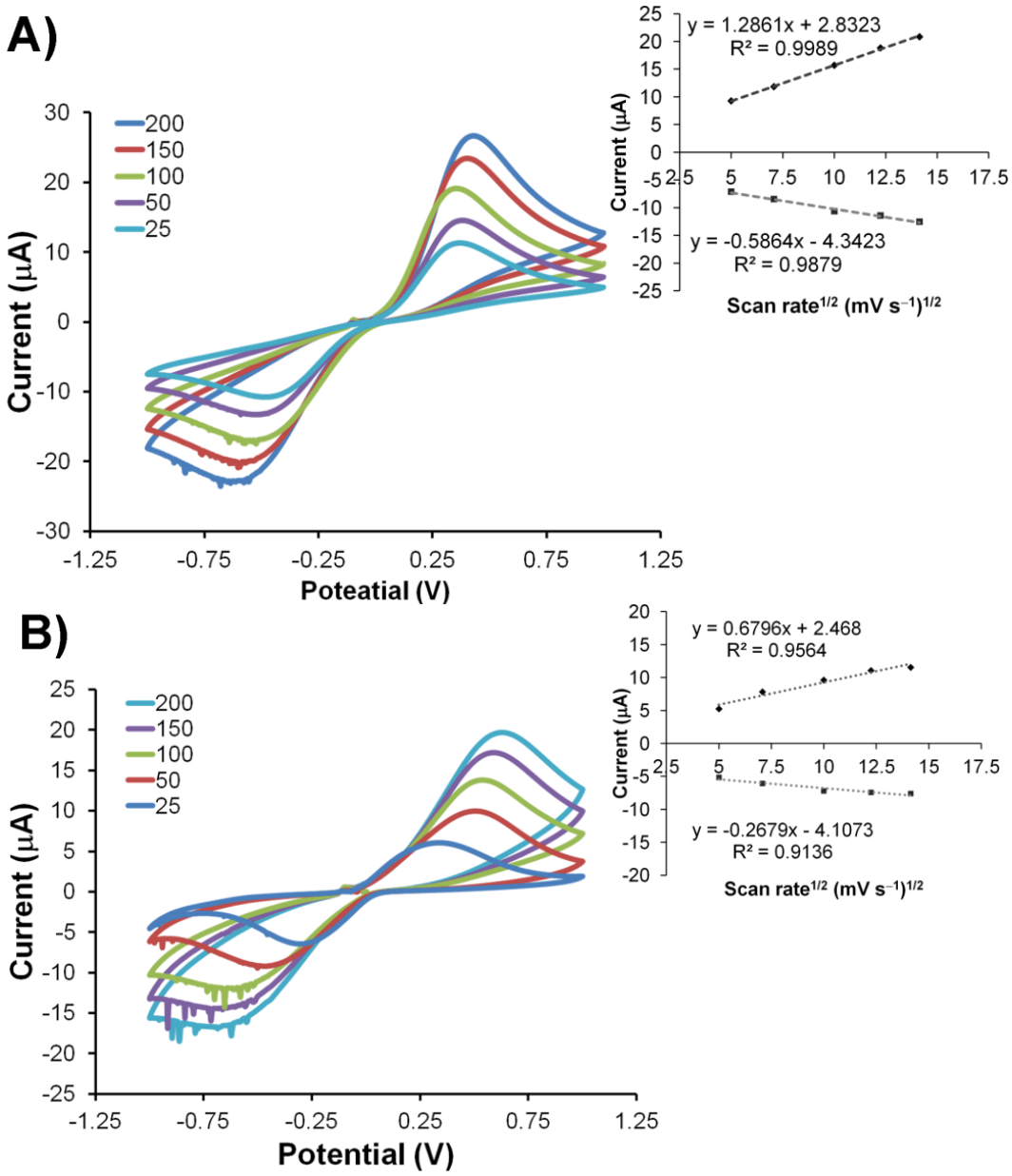

Figure 4.13 Cyclic voltammograms of 2.0 mM $[Fe(CN)_6]^{4-/3-}$ in 0.1 M PBS (pH 7.4) at scan rates of 25, 50, 100, 150 and 200 mV s^{-1} on A) plastic film and B) paper electrodes where the diameter of the working electrode was 2 mm. The anodic and cathodic peak currents are a function of the square root of the scan rate ($\nu^{1/2}$) (inset).

4.2.2 G/PANI nanocomposite characterization

In the preparation of PANI nanoparticles, a mixture of aniline monomer solution was added immediately in the APS solution containing PVP to obtain the granular nanostructure of PANI (Figure 4.14A). PVP was used as a steric stabilizer to increase the dispersion of PANI nanoparticles. To improve the conductivity and electroactivity of PANI nanoparticles, 10 mg of G was added into the aniline monomer solution prior to synthesis step. The morphology of the G/PANI nanocomposite was characterized by scanning electron microscopy (SEM). As seen in Figure 4.14B, the composite of G/PANI was characterized; G sheet was coated with lots of PANI nanoparticles having highly uniform size. The average diameter size of the PANI nanoparticles is approximately 391±8.2 nm. Further characterization information was obtained from the FT-IR spectrum as shown in Figure 4.14C. In a spectrum band of PANI and G/PANI observed at 3206.27 cm^{-1} is due to N—H stretching. The absorption bands of PANI shows at 2923.62, 2923.25, 2923.21 and 2825.55 cm^{-1} are due to asymmetric C—H stretching and symmetric C—H stretching. The obtained band at 1600—1500 cm^{-1} corresponds to C—H stretching in aromatic structures. Absorption bands at 1565.68, 1479.34, and 1485.98 cm^{-1} correspond to C=N stretching in aromatic compounds. The polymer shows absorption bands at 1300—1200 cm^{-1} that confirms the C—N stretching of primary aromatic amines. For the absorption bands of G, the peaks at ~3435.42 cm^{-1} are attributed to –OH bands. The deviations from the characteristic band of G/PANI observed at 1240.22, 1303.32, and 3206.27 cm^{-1} that may be attributed some molecular interaction between G and PANI [104, 105]. These results confirmed that PANI was composited with G.

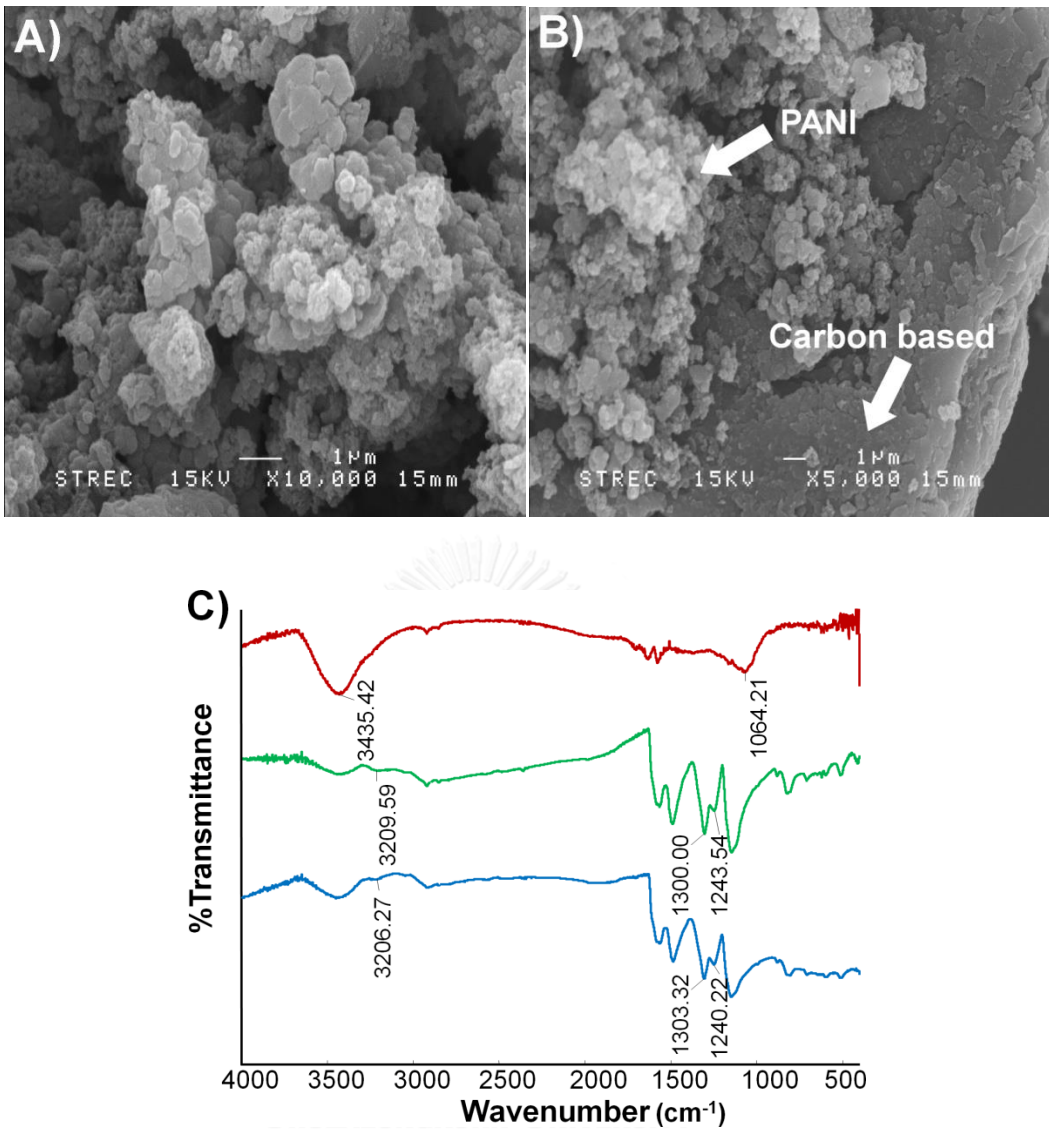

Figure 4.14 Electrode surface characterization, A) SEM micrographs of PANI nanoparticles and B) G/PANI nanoparticles, C) FT-IR spectrum of graphene (red line), PANI (green line), and the G/PANI nanocomposite (blue line).

4.2.3 Characterizati on of G/PANI nanocomposite modified electrode

The incorporation of G into PANI is crucial for improving the properties of the nanocomposites. Casting and electrospraying were used as the fabrication methods for G/PANI nanocomposite on electrode surface. As shown in Figure 4.15, G/PANI nanocomposite modified electrode obtained from both fabrication methods increase the electrochemical sensitivity of

electrode in the simultaneous detection of Zn(II), Cd(II) and Pb(II). However, G/PANI nanocomposite modified electrode prepared by electrospraying shows the higher sensitivity than the one prepared by casting, thus, electrospraying was selected for the modification of G/PANI nanocomposite in this work. Moreover, electrospraying fabrication can generate the uniformed 3D droplet-like structures of G/PANI on the working electrode that can be used to further increase the surface area and thus electrochemical sensitivity of the working electrode. The morphology of the G/PANI nanocomposite modified electrode was characterized by scanning electron microscopy (SEM). SEM image of unmodified electrode (Figure 4.16A) was compared to G/PANI nanocomposite modified electrode under optimal electrospraying conditions (Fig. 5B). Droplet-like structure of G/PANI nanocomposite is relatively distribution on carbon electrode surface leading to highly increase the surface area and sensitivity of this electrode as shown in Figure 5B. For synthesis of G/PANI nanocomposite, the effect of G loading was investigated and optimized by cyclic voltammetry using a standard of $[Fe(CN)_6]^{3-/4-}$ redox couple. As shown in Figure 4.17, the anodic peak currents increased rapidly upon increasing the G loading from 0.0 to 10.0 mg and decreased when the G loading was increased over 10.0 mg. This decrease in oxidative current was caused from a lot of G in G/PANI nanocomposites leading to agglomeration of G.

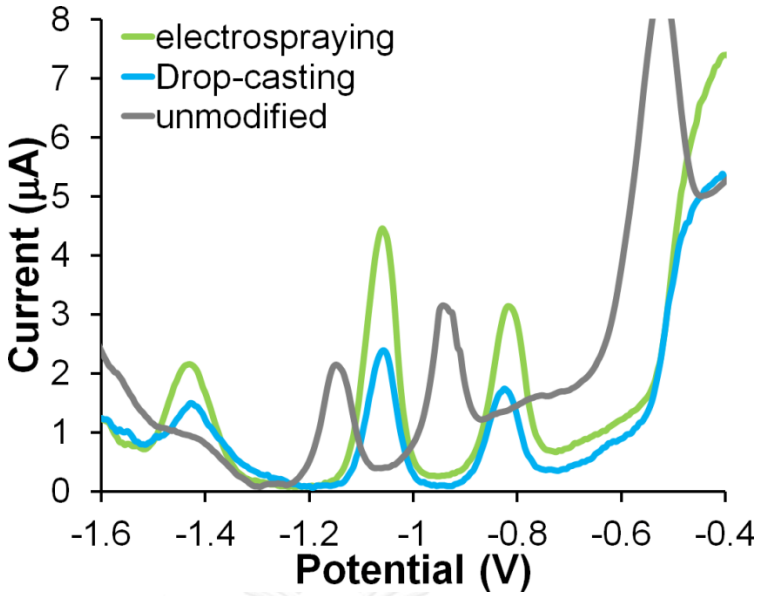

Figure 4.15 SWASV of 200 ppb of Zn(II), Cd(II), and Pb(II) in 1.0 M acetate buffer pH 4.5 measured with an unmodified electrode and a G/PANI nanocomposite-modified electrode via drop-casting and electrospraying

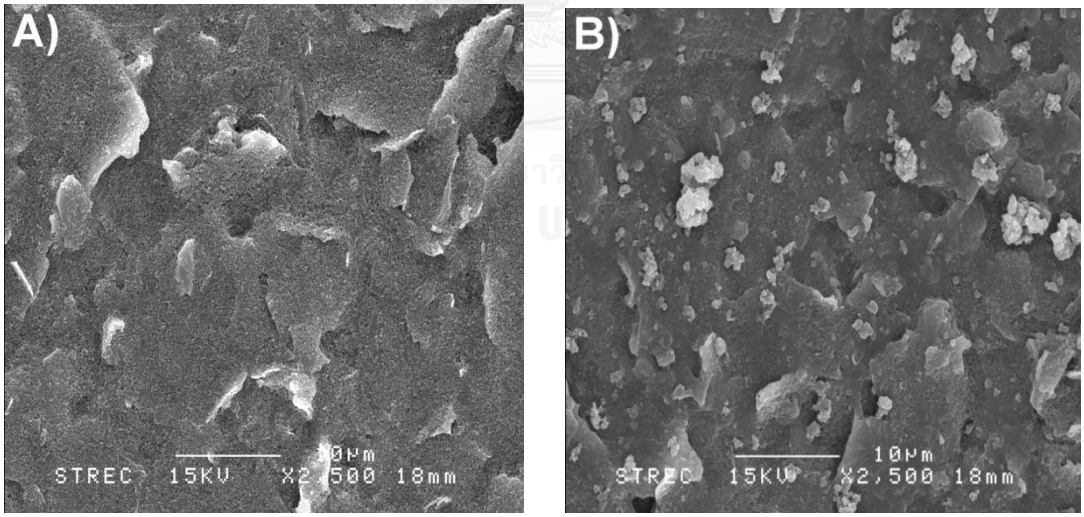

Figure 4.16 SEM of an A) unmodified and B) G/PANI nanocomposite-modified electrode by electrospraying.

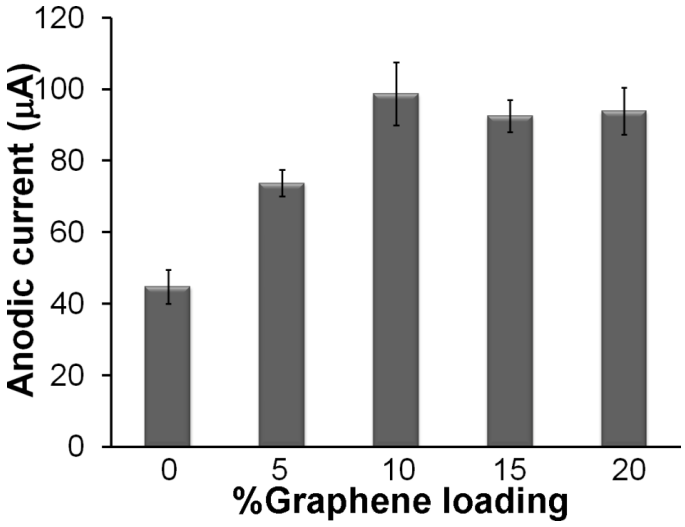

Figure 4.17 Anodic peak currents (i_{pa}) obtained from cyclic voltammetry of 2.0 mM $[Fe(CN)_6]^{3-/4-}$ in 0.1 M KCl using G/PANI nanocomposite-modified electrodes with different graphene loading concentrations (n=5). Error bars represent one standard deviation.

To fabricate G/PANI nanocomposite modified electrode b electrospraying, our previous protocol with slight modification was used [11]. In this study, 14 kV of applied voltage, 5 min of spraying time, and 5 mg mL^{-1} of G/PANI in DMF were selected for all experiment. Cyclic voltammetry using a standard of $[Fe(CN)_6]^{3-/4-}$ redox couple was used to investigate the performance of all electrode including G/PANI, PANI and unmodified carbon electrode as shown in Figure 4.18A. The highest anodic and cathodic currents of $[Fe(CN)_6]^{3-/4-}$ redox couple were observed on G/PANI nanocomposite modified electrode indicating that the cooperation of G and PANI provides the necessary conduction pathways on the surface of electrode and a better electrocatalytic behavior. Moreover, the peak potential difference values (ΔEp) obtained from G/PANI nanocomposite (ΔEp=0.347) and PANI nanoparticles (ΔEp=0.377) modified electrode decreased when compared to ΔEp obtained from unmodified electrode (ΔEp=0.517), indicating that the

presence of G and PANI can improve the electron transfer kinetics of this system.

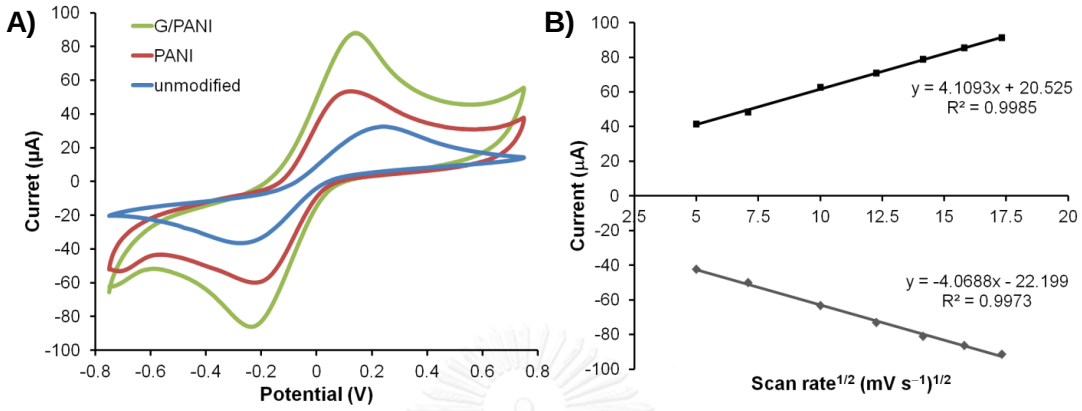

Figure 4.18 A) cyclic voltammograms of 2.0 mM $[Fe(CN)_6]^{3-/4-}$ in 0.1 M KCl and B) the anodic and cathodic peak currents of 2.0 mM $[Fe(CN)_6]^{4-/3-}$ in 0.1 M KCl as a function of the square root scan rate ($\nu^{1/2}$) on G/PANI nanocomposites-modified electrode

Prior to the quantification of Zn(II), Cd(II) and Pb(II), the electrochemical behavior of G/PANI nanocomposite modified electrode was examined using a standard $[Fe(CN)_6]^{3-/4-}$ redox couple. The cyclic voltammograms of $[Fe(CN)_6]^{3-/4-}$ were measured at different scan rates between 25 and 300 mV s^{-1}. As an expected, the anodic and cathodic peak currents of $[Fe(CN)_6]^{3-/4-}$ increased when the scan rate was increased. Moreover, the linearity of the anodic and cathodic peak currents versus the square root of a scan rate between 25 and 300 mV s^{-1} verified that the redox process occurring on this modified electrode is controlled by diffusion process (Figure 4.18B).

In addition, the SWASV of unmodified electrode and the modified electrode using G/PANI nanocomposites and PANI nanoparticles were presented in Figure 4.19. The accumulation process of Zn(II), Cd(II) and Pb(II) was carried out for 240 s at −1.6 V in 0.1 M acetate buffer (pH 4.5). The result

shows very weak peaks current at unmodified electrode and high peaks current at PANI nanoparticle modified electrode. The sharper and higher peak current for Zn(II), Cd(II) and Pb(II) were obtained on the G/PANI nanocomposite modified electrode, demonstrating that the presence of G significantly increases the current response of Zn(II), Cd(II) and Pb(II) leading to enhance the detection sensitivity of electrode.

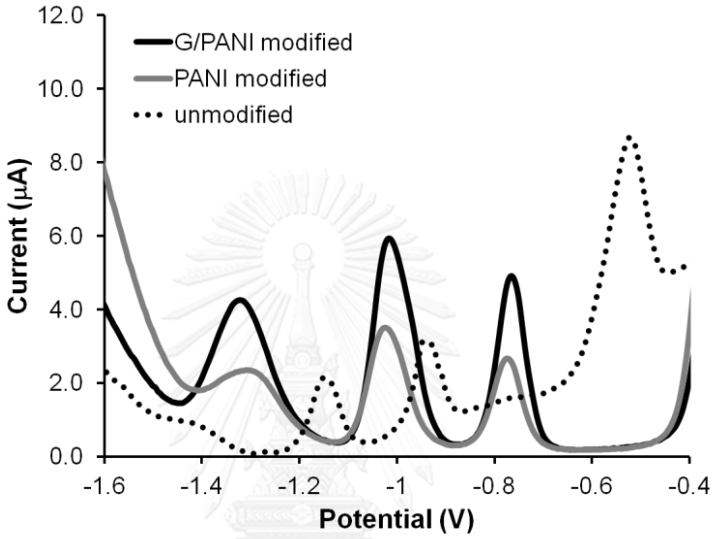

Figure 4.19 SWASV of 200 ppb of Zn(II), Cd(II) and Pb(II) in 1.0 M acetate buffer pH 4.5 measured on unmodified electrode, PANI nanoparticle and G/PANI nanocomposites-modified electrode by electrospraying.

4.2.4 Electrochemical Detection of Zn(II), Cd(II) and Pb(II)

For monitoring a very low levels of Zn(II), Cd(II) and Pb(II) in food, environmental and biological samples, square wave anodic stripping voltammetry (SWASV) is commonly used [9, 106]. To increase the sensitivity of electrode for heavy metal detection, Bismuth (Bi) was used to form a metal-Bi alloy on the electrode surface that facilitates the process of nucleation during to heavy metal ions accumulate leading to enhance the sensitivity of electrodes [25, 107, 108]. In addition, bismuth is a more 'environmentally friendly' material because it has a lower toxicity and widely

used in the many industry including pharmaceutical and cosmetic [109]. Moreover, the presence of the Nafion film on electrode surface may account to improve the sensitivity of electrode since sulfonate groups in the Nafion film are negatively charged and, as a result, the polymeric membrane acts as a cation- exchanger and facilitates the preconcentration of metal cations on electrode surface [108, 110, 111]. The anodic peak currents of three metals using G/PANI and Nafion coated G/PANI nanocomposite modified electrode are shown in Figure 4.20.

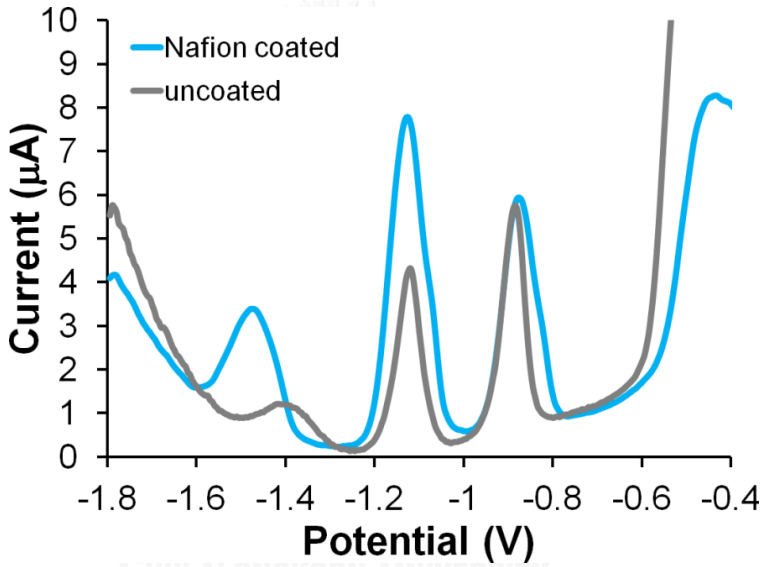

Figure 4.20 SWASV of 200 ppb of Zn(II), Cd(II) and Pb(II) in 1.0 M acetate buffer pH 4.5 measured on G/ PANI nanoparticle and Nafion coated G/PANI nanocomposites-modified electrode.

Under the optimal experimental conditions, Zn(II), Cd(II) and Pb(II) were determined individually and simultaneously at the G/PANI nanocomposite modified electrode using SWASV. The anodic peaks of Zn(II), Cd(II) and Pb(II) were identified at the potentials of −1.31± 0.03, −0.98± 0.04 and −0.75± 0.04 V, respectively. The resulting calibration plots, (Figure 4.21), are linear over a range from 1.0 to 300 µg L^{-1} with the correlation coefficients

exceed 0.98 for all metals. The limits of detection (LOD) from the experiment are 1.0 μg L^{-1} for Zn(II) and 0.1 μg L^{-1} for Cd(II) and Pb(II). Electrochemical performance of the G/PANI nanocomposite-modified electrode was compared with similar systems in the literature for measuring Zn(II), Cd(II), and Pb(II) (Table 4.4).

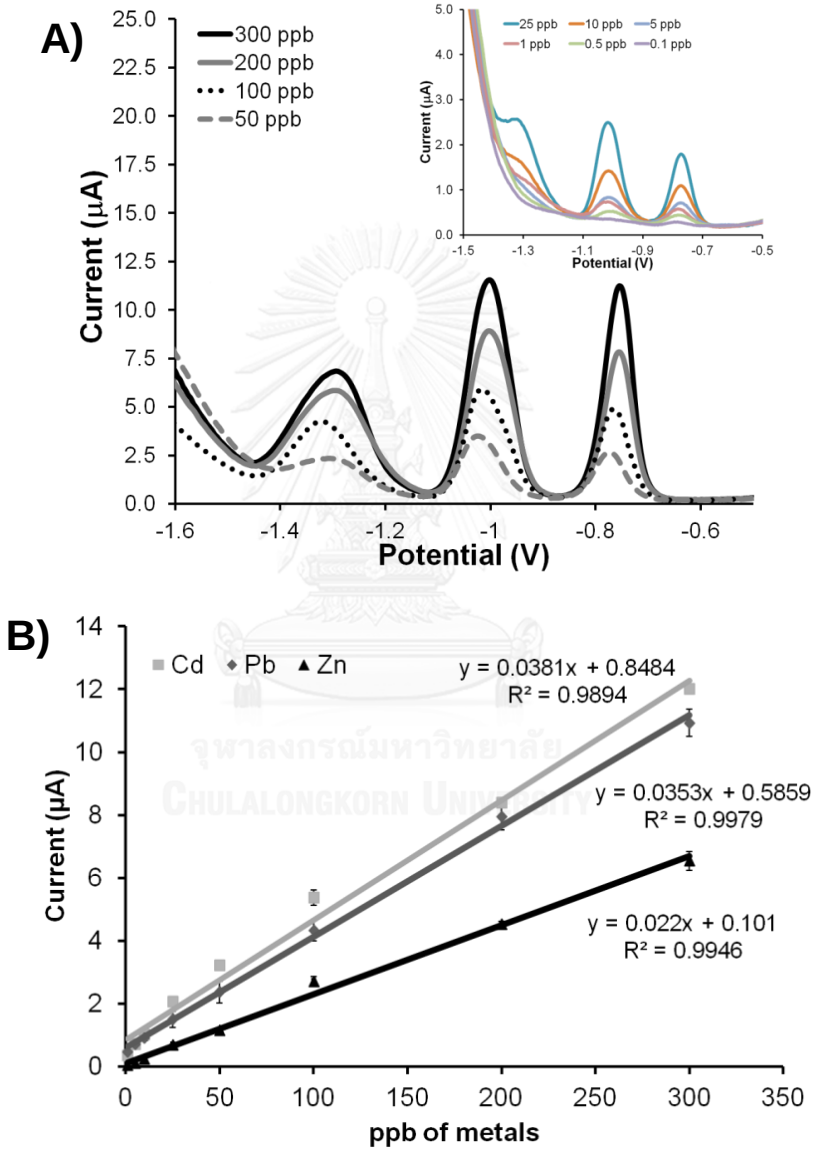

Figure 4.21 A) Square-wave voltammogram showing electrochemical detection of Zn(II), Cd(II) and Pb(II) (B) Representative calibration graph between μg L^{-1} of metal and anodic current of Zn(II), Cd(II) and Pb(II).

Table 4.3 Electrode performance for measuring Zn(II), Cd(II), and Pb(II).

Modified electrode	Detection limit (μg L^{-1})			Linear range (μg L^{-1})			Ref
	Zn	**Cd**	**Pb**	**Zn**	**Cd**	**Pb**	
Bimetallic Hg–Bi/SWNTs composite/GCE	0.23	0.076	0.18	0.5–11	0.5–11	0.5–11	[25]
SnO_2/reduced graphene oxide nanocomposite	–	0.0001015	0.0001839	–	0.0003–0.0012	0.0003–0.0012	[10]
CNTs	–	5–150	5–150	–	1	1	[27]
CNT arrays (CNT thread)	1.4	1.8	1.5	3–9	1.5–4.5	1–4	[112]
bismuth/poly(p-aminobenzene sulfonic acid)	0.62	0.63	0.8	1–110	1–110	1–130	[113]
nitrogen-doped microporous carbon/Nafion/bismuth-film electrode	–	1.5	0.05	–	2–10, 10–100	0.5–10, 10–100	[114]
Bi/Au-GN-Cys/GCE	–	0.1	0.05	–	0.50–40	0.50–40	[115]
Bi/Nafion/PANI-MES/GCE	–	0.04	0.05	–	0.10–20	0.10–30	[116]
Clioquinol/HMDE	0.06	0.06	0.1	0–25	0–15	0–15	[117]
screen-printed carbon nanotubes electrodes	11	0.8	0.2	12–100	2–100	2–100	[26]
Nafion/G/PANI nanocomposite	1.0	0.1	0.1	1–300	1–300	1–300	This work

4.2.5 Interference Study for Zn(II), Cd(II) and Pb(II) detection

Previously, it has been reported that different metals could interfere in the SWASV, so the tolerance ratio for interfering metals was investigated. The concentration of interfering metal ions that generated a change in peak current (less than 5%) was performed as a tolerance ratio [27]. The concentration of interfering metal ions including Mn(II), Cu(II), Fe(III), Fe(II), Co(III) and Ni(II) are shown in Table 4.4. Interestingly, G/PANI nanocomposite modified electrode can prevent the effect of other metal ion interferences indicating that this modified electrode is a selective device for simultaneous detection of Zn(II), Cd(II) and Pb(II).

Table 4.4 Tolerance ratio of interfering metal ions in the electrochemical determination of 200 μg L^{-1} of Pb(II) Cd(II) and Zn(II) on Nafion coated G/PANI-modified electrode

Interfering Metals	5% Tolerance Ratio		
	Zn^{2+}	Cd^{2+}	Pb^{2+}
Cu(II)	25	50	50
Mn(II)	500	500	500
Ni(II)	250	250	200
Fe(II)	250	250	250
Fe(III)	200	200	200
Co(II)	100	100	50

4.2.6 Reproducibility and stability of the modified electrode

The reproducibility and stability of the G/PANI nanocomposites modified electrodes were investigated by measuring SWASV response of 200 μg L^{-1} mixture of Zn(II), Cd(II) and Pb(II) in acetate buffer (pH 4.5) multiple times. The relative standard deviation (RSD) of the anodic peak currents by ten successive measurements was lower than 11.0. In addition, the fabrication reproducibility of modified electrode was investigated from three modified electrodes (RSD $\leq$ 12.3), indicating excellent detection reproducibility. The G/PANI nanocomposite modified electrode was stored for 3 weeks and used to evaluate the stability of the modified electrodes, the anodic current responses retained 82% of initial response. Hence, this modified electrode is verified the good reproducibility and stability of the modified electrodes. Moreover, this proposed electrode can be reused for more than ten replicates with high reproducibility (RSD $\leq$ 17.1).

4.2.7 Sample analysis

To evaluate the applicability of this approach, Nafion coated G/PANI nanocomposite modified electrode was used for the detection of Zn(II), Cd(II) and Pb(II) in human serum by using standard addition method. The blank human serum sample is generally used to determine the accuracy and validation of a new diagnostic assay. Initially, human serum was diluted in a 1:10 ratio with sodium acetate buffer (pH 4.5), and spiked with three different concentrations of Zn(II), Cd(II) and Pb(II), and then it was dropped onto Nafion coated G/PANI nanocomposite modified electrode for analysis of Zn(II), Cd(II) and Pb(II). Each sample was detected three times and the average of three results was determined. The analytical of these results was summarized in Table 4.5. The recovery ranged from 93.8 to 109.7% and the RSD (n = 3) was below 9.0% indicating this system is highly accurate. The results indicated that Nafion coated G/PANI nanocomposite modified electrode is highly

accurate for the detection of Zn(II), Cd(II) and Pb(II) in biological fluids such as human serum. (In a healthy adult blood levels of Zn, Cd and Pb are typicall at or below 900 μg L^{-1} (18 μM), 29.7 μg L^{-1} and 200 μg L^{-1} (1 μM), respectively [118].

Table 4.5 Determination of Zn(II), Cd(II), and Pb(II) in human serum samples (n = 3)

Added Concentration (μg L^{-1})	Measured Concentration (μg L^{-1})			% Recovery	% RSD
	Zn(II)	Cd(II)	Pb(II)		
10.0	9.41±0.5	10.7±0.5	10.6±0.4	94.1—106.5	4.0—4.8
20.0	19.5±1.7	20.2±1.7	18.8±1.1	93.8—101.1	3.4—8.5
50.0	51.1±2.2	54.9±4.8	52.7±3.0	102.3—109.	4.3—8.8

4.3 Active Paper Chips for Electrochemical Multiprobe Detections

4.3.1 Paper Chips Design

APOC for electrochemical multiprobe detection is a novel approach for rapid and automatic detection of biomarkers including glucose, DA and UA. To reduce overall analysis time and cost, APOC was designed to allow electrochemical detection of multiple biomarkers continuously. The main idea to develop this approach is ability to automatically detect three biomarkers using only single sheet of APOC. Two designed paper-chips are shown in Figure 4.22A-B. Paper-chip was designed to allow detection of multiple analytes using 2 types of modified electrode including CoPc and rGO electrode. The designed paper-chip included with 4 sections as import, active actuation, detection and export. The key to this development is the ability to

allow distinct chemical reactions to occur for each analysis using the high sensitive electrode. In the import section, it has 3 ports for sample, reagent and cleaning solution. The enzyme reagent was moved to react with sample (glucose) and then incubated for 4 min. Next, the mixed solution was controlled to move to the detection zone by applying the voltage to paper-chip electrode. After detection, cleaning solution was moved to the detection zone to merge with detecting solution. Then, the detecting solution was expended to touch with moving pad. Finally, detecting solution was moved from electrode.

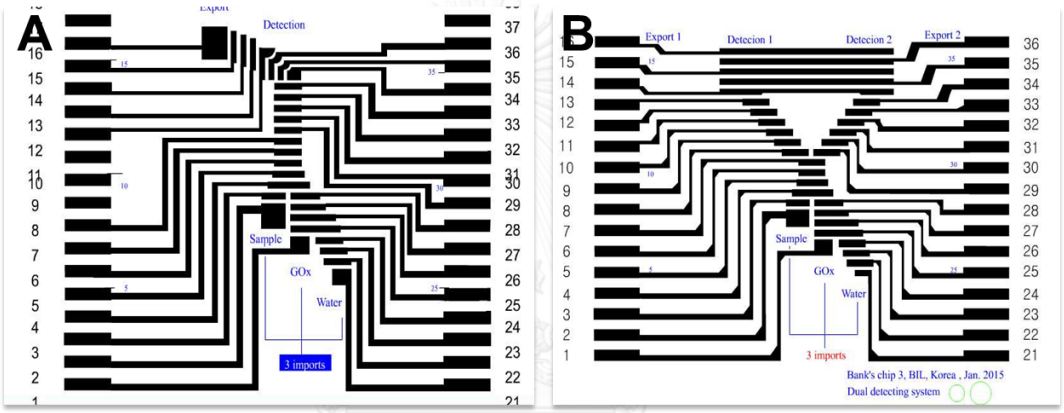

Figure 4.22 The designed paper-chips A) one detection zone and B) dual detection zone

Figure 4.23 shows the snapshots from the continuous actuation for paper chip coupled with multiprobe electrochemical detection. One detection zone of paper-chip coupled with multi-working electrode is showed in Figure 4.23A. This designed paper-chip can detect 3 analytes within one drop of sample, however; it used a large volume of sample (70 µL). Therefore, dual detection zone with small overall volume was developed. The snapshots from designed paper-chip for dual detection zone are shown in Figure 4.23B.

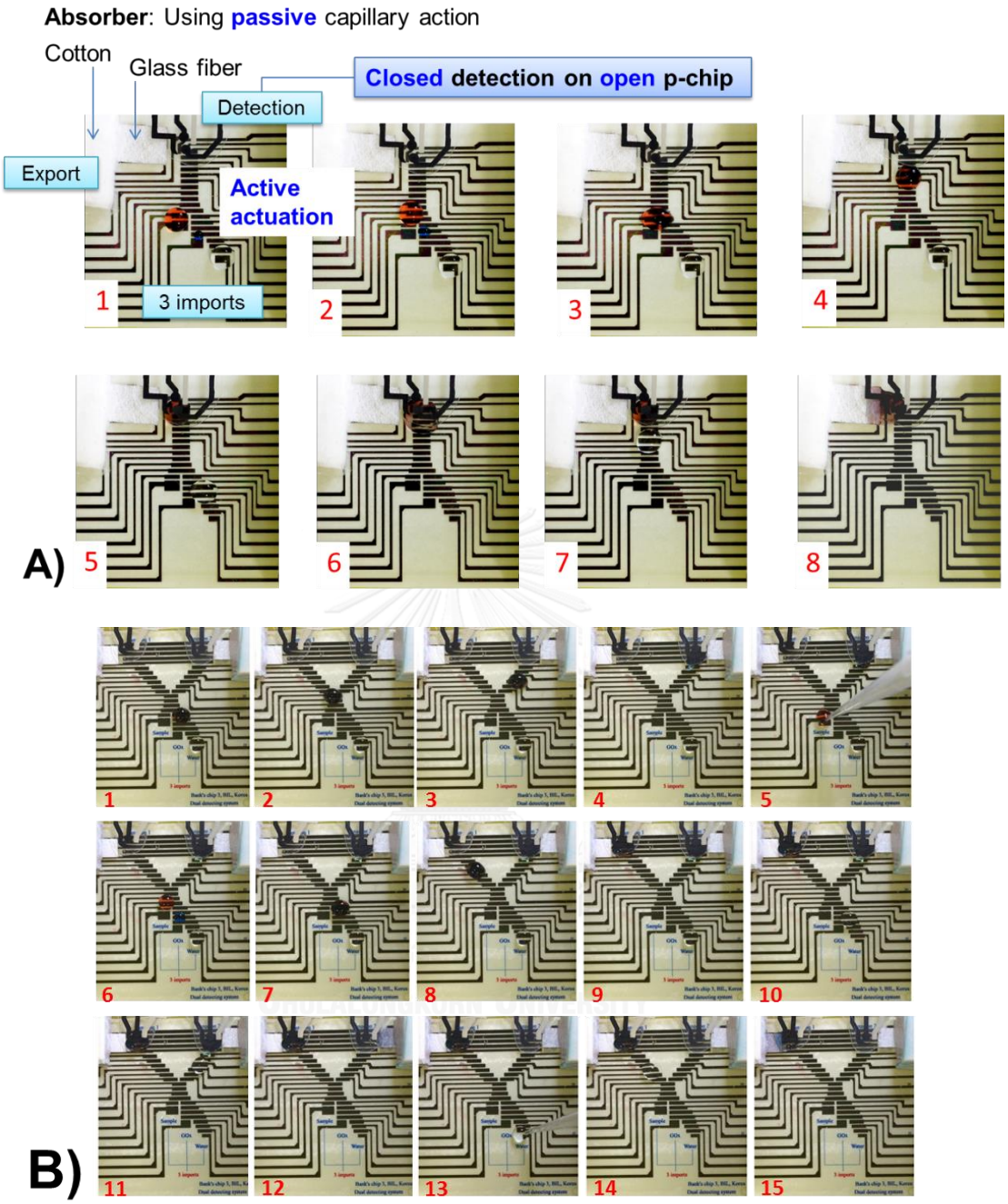

Figure 4.23 The snapshots from designed paper-chip with A) one detection zone and B) dual detection zone

4.3.2 Glucose detection

20 µL of sample (mixture of glucose, DA and UA) and 3 µL of 292 U mL^{-1} GOx were dropped on APOC at an import zone. The sample and GOx drops were automatically mixed via drop movement and incubated for 4 min, and then the mixture solution was moved to detect at a detection zone (CoPc electrode). The determination of hydrogen peroxide (H_2O_2) product obtained from the oxidation of glucose can be used for the indirect quantification of glucose using amperometry, which is frequently employed for monitoring low levels of glucose in biological fluids. CoPc was selected as a mediator for glucose detection because of its high sensitivity for an electrochemical detection of H_2O_2. Initially, H_2O_2 detection potential was investigated and optimized as shown in Figure 4.24A. The criteria for selecting of the optimal detection potential were based on achieving the lowest detection limit while avoiding interference species in the complex biological fluids. Glucose was reacted with GOx, and the current signal of H_2O_2 was measured at the detection potential between +0.1 and +0.8 V (vs Ag/AgCl). The result shows that the current signal of H_2O_2 significantly increased as the detection potential increased; however, the background current also increased. Therefore, the signal-to-background ratio was investigated as shown in Figure 4.24B. The optimal potential of +0.4 V is a compromise between the highest signal for glucose detection and the lowest background current. To investigate the analytical performance of CoPc modified SPCE for glucose detection, different concentrations of glucose were measured and the amperometric responses were recorded at the steady state current of 100 s to create a calibration plot for glucose detection. As shown in Figure 4.25, the linear range for glucose detection was observed in a range of 0.05—6 mM with a correlation coefficient of 0.992 and the limit of detection (LOD) of 0.05 mM. LOD was measured as concentration which produced the signal at 3 times of the standard deviation of background (n = 5).

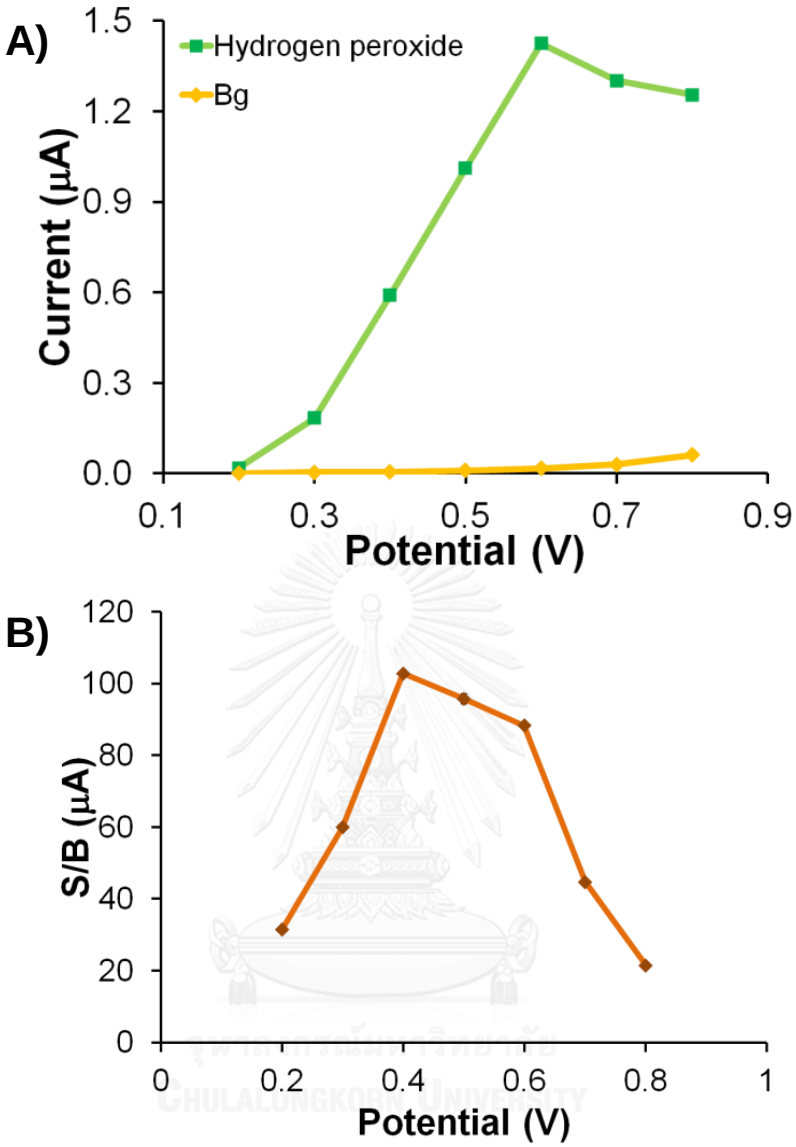

Figure 4.24 (A) Hydrodynamic voltammograms of 1.0 mM H_2O_2 (green line) and background (yellow line) in 0.01 M PBS pH 7.4 at a 100 s sampling time measured on a CoPc-modified SPCE and (B) hydrodynamic voltammogram of the signal-to-background ratios (S/B) extracted from the data in Figure 4.24A.

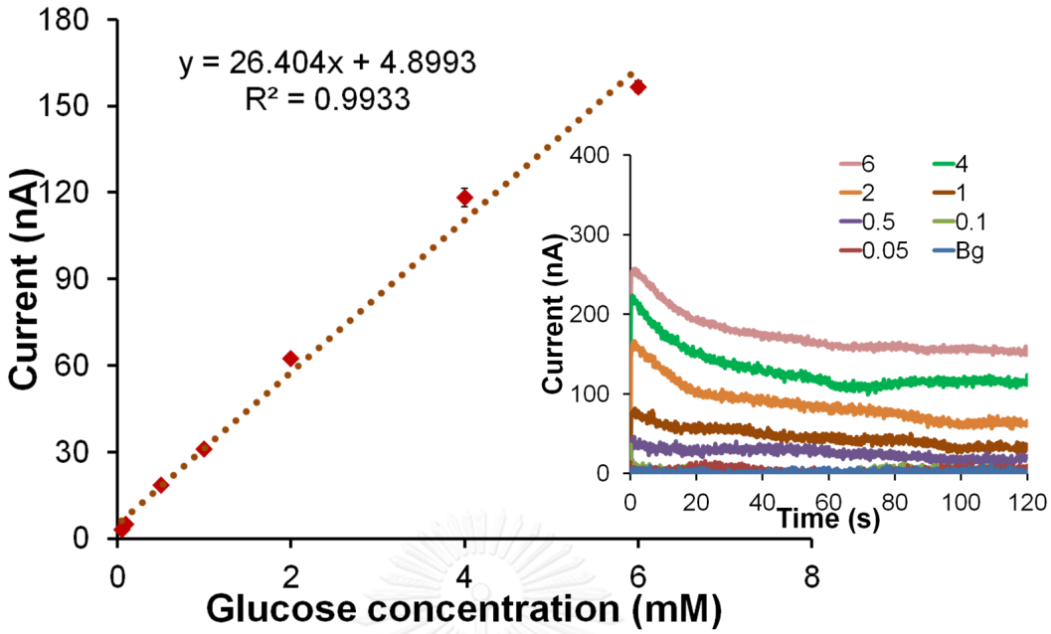

Figure 4.25 Linearity of glucose in a range of 0.05- 6 mM on CoPc modified electrode in 0.01 M PBS using +0.4 V as a detection potential and amperometric response as shown in the inset.

Previously, it has been reported that AA is a common interfering molecule for the detection of glucose in complex biological fluids (*e.g.,* human serum, plasma). Therefore, selective determination of glucose in the presence of AA was investigated using the highest anticipated concentrations of AA (80 μM) in human serum. As shown in Figure 4.26, an amperometric response of a mixture of glucose and AA using +0.4 V as detection potential shows negligible effect on the current response of 1 mM glucose. The reproducibility and stability of CoPc electrode were studied using amperometric detection of 1 mM glucose.

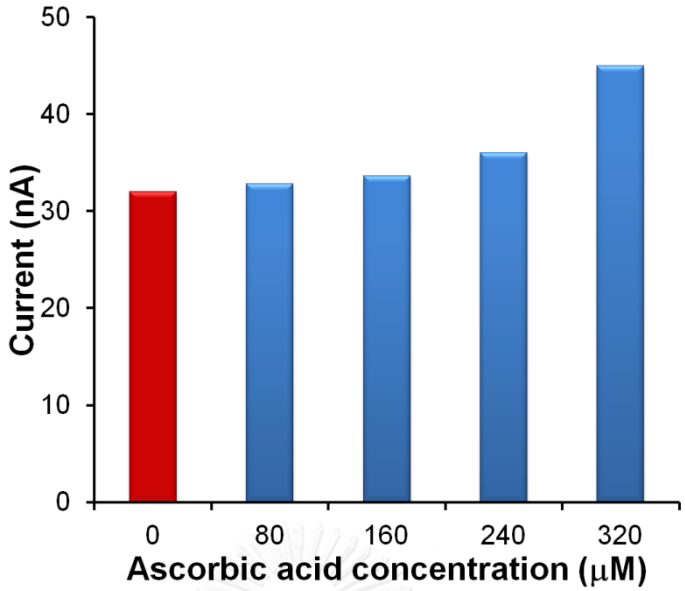

Figure 4.26 The interference effect of different concentrations of AA (0, 80, 160, 240 and 320 μM) in the detection of 1 mM glucose.

The relative standard deviation (RSD) of all glucose concentrations in the linear range were found between 1.3 % and 3.2 % (n = 5), indicating the acceptable reproducibility for CoPc modified SPCE. A similar experiment was performed with three devices, and the %RSD was found to be 1.6 %.

4.3.3 Dopamine and uric acid detection

After the detection of glucose, the drop of sample at the detection zone was continuously detected DA and UA by square wave anodic stripping voltammetry (SWASV) on Au/rGO modified SPCE by switching the detection potential from CoPc to Au/rGO electrode. Au nanoparticles and GO were modified on SPCE surface by electrodeposition and drop casting, respectively. GO was reduced to form rGO by cyclic voltammetry to enhance the conductivity. The surface of Au/rGO modified electrode was characterized by SEM as shown in Figure 4.27A and B. The surface of SPCE was covered with wrinkles graphene sheet that unique morphology is highly beneficial in

maintaining a large electroactive surface area. [76] After electrodeposition of Au, the Au nanoparticle was uniformly formed (gray color dot) on the surface of rGO electrode as shown in Figure 4.27B. The average size of Au nanoparticle is determined as 251.4±0.1 nm. As shown in Figure 4.28A, cyclic voltammograms of 2 mM $[Fe(CN)_6]^{3-/4-}$ on different electrodes including unmodified, Au, rGO and Au/rGO modified electrodes were measured. The highest anodic and cathodic currents of 2 mM $[Fe(CN)_6]^{3-/4-}$ were observed on Au/rGO modified electrode indicating the high sensitivity of the system. The presence of rGO reduces the peak-to-peak potential separation (ΔE_p) comparing to unmodified and Au modified electrodes, indicating that rGO can accelerate the electron transfer kinetics of this system. Compared to rGO modified electrode, incorporation of Au nanoparticles increases the signal current in the detection of 2 mM $[Fe(CN)_6]^{3-/4-}$. In electrochemical impedance spectra, the electron transfer resistance (R_{ct}) can be quantified using the semicircle diameter of Nyquist plot of impedance spectra. From Faradaic impedance spectra obtained upon the stepwise modification as shown in Figure 4.28B, when rGO and Au are modified onto a SPCE surface, the semicircle dramatically decreases compared to an unmodified electrode suggesting that the rGO and Au can accelerate the electron transfer between electrodes and $[Fe(CN)_6]^{3-/4-}$ solution.

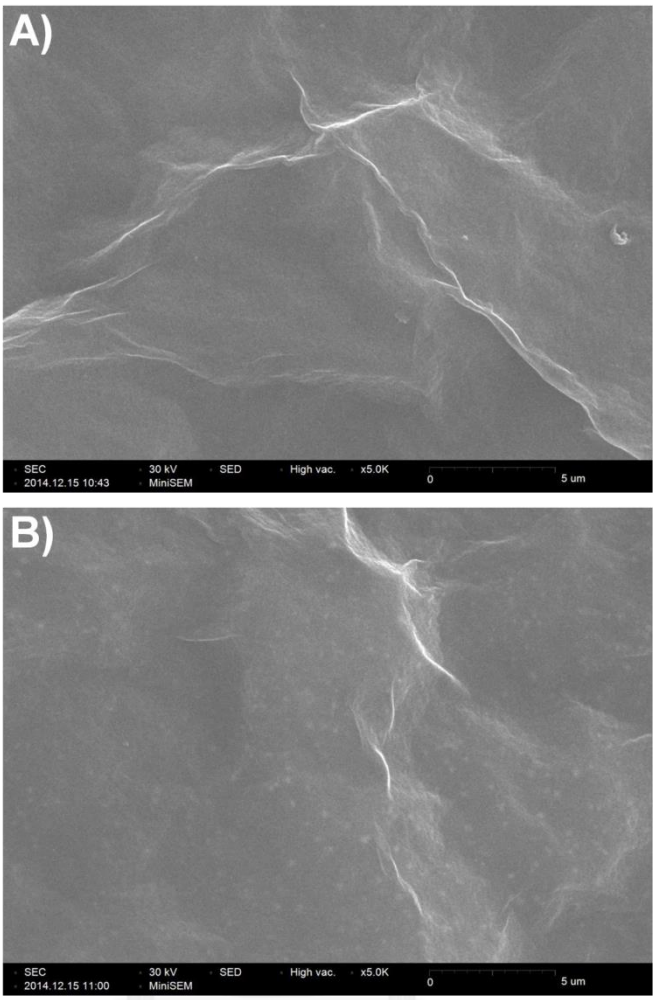

Figure 4.27 SEM image of (A) rGO and (B) Au/rGO modified SPCE.

As we know, DA and UA have similar oxidation potential, therefore; the separation of these species is important. To establish a selective and sensitive method for DA and UA detection, Au/rGO modified electrode was selected to simultaneously detect the mixture of DA and UA. The performance of Au/rGO modified electrode was investigated using SWASV for the detection of DA and UA. The peak currents obtained from Au/rGo modified electrode comparing with unmodified, Au and rGO modified electrodes demonstrated that the presence of rGO and Au can significantly increase the current response and decrease the peak potential of DA and UA. Moreover, the mixture of DA and UA can be separate indicating that the

presence of rGO and Au accelerates the electron transfer of this system as shown in Figure 4.28C. The peak potential of DA and UA were found to be 0.10±0.01 and 0.27±0.02 V (n=5), respectively.

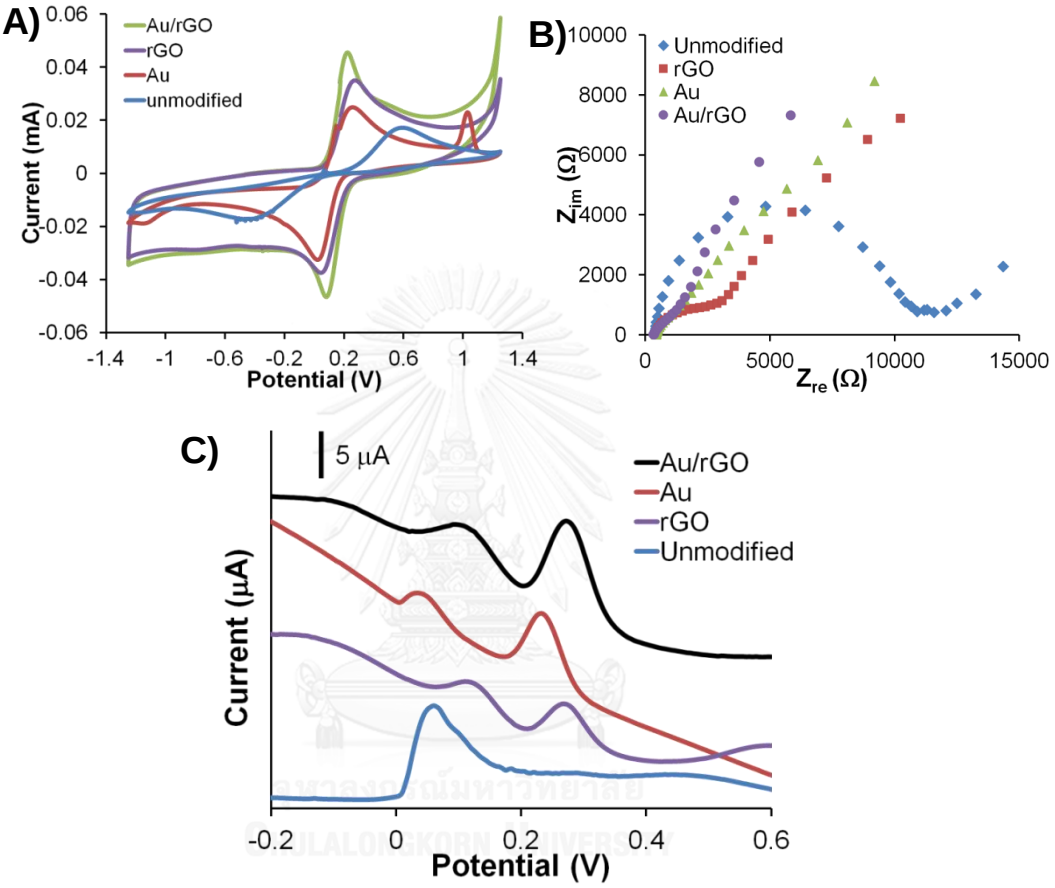

Figure 4.28 (A) Cyclic voltammogram and (B) Faradaic impedance spectra of 2.0 mM $[Fe(CN)_6]^{3-/4-}$ in 0.1 M KCl, and (C) SWASV of DA and UA in 0.01 M PBS buffer pH 7.4 measured on an unmodified electrode, and electrodes functionalized with Au, rGO and Au/rGO.

SWASV was selected to record the anodic currents of DA and UA on Au/rGO modified electrode because it is sensitive and can be used for simultaneous determination of the analyte mixture. The electro-oxidation process of DA and UA in the mixture solution was investigated by changing the concentration of one species, whereas another species was fixed. The SWASV was recorded at various concentrations of DA on Au/rGO modified electrode in the presence of 100 μM UA. As shown in Figure 4.29A, the peak current of DA was linear in a concentration range between 1 and 100 μM (R^2 = *0.998*) with a detection limit of 0.5 μM. Furthermore, it could be seen that the location of the peak current for UA was almost constant during the changing of the concentration of DA. For UA determination, similarly as shown in Figure 4.29B, the anodic peak currents of UA increased linearly with the increasing of UA concentrations (5 to 400 μM, R^2 = *0.998*) while the peak current of 5 μM DA still unchanged, and LOD was found to be 5 μM. Therefore, Au/rGO modified electrode is independent for the simultaneous detection of DA and UA in biological fluid.

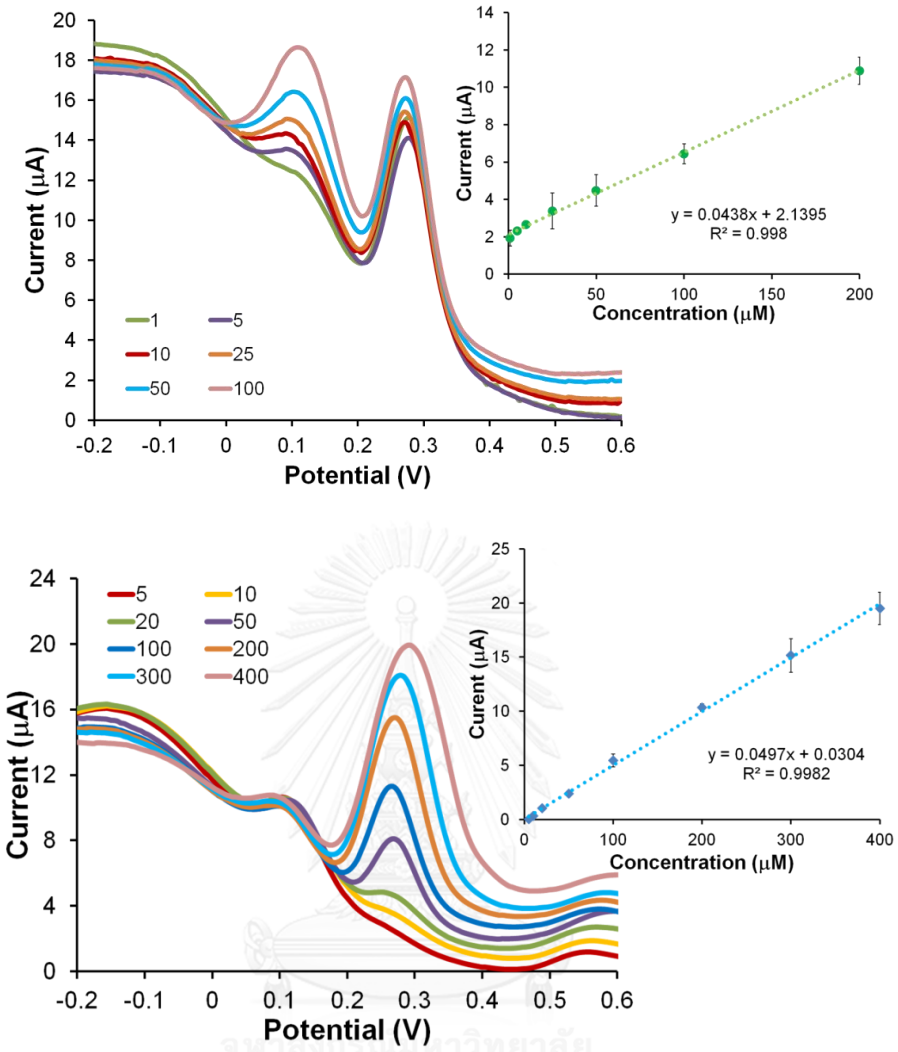

Figure 4.29 Square wave voltammogram of (A) DA (1 to 100 μM) in the presence of 100 μM UA, and (B) UA (5 to 400 μM) in the presence of 5 μM DA, and linear plot is shown in the insets.

Selective determination of DA and UA in the presence of AA was investigated using the highest anticipated concentrations of AA (80 μM) in human serum. It can be found that no significant interference of 80 μM AA was observed for the detection of mixture of 50 μM DA and UA. Moreover, the effect of AA was studied by increasing the amount of AA while fixing the concentration of DA and UA at 50 μM using the error approximately 5% as a criterion. It was found that no effect occurred in the increasing of AA

concentrations until 500 μM, indicating that Au/rGO modified electrode has an excellent selectivity for DA and UA detection.

4.3.4 Sample analysis

Human serum was chosen as a real sample for investigation of the reliability of this proposed system. The standard addition method was used to test the recovery. Three human serums containing spiked glucose, DA and UA were analyzed on 3 independently prepared electrodes. The analytical results are summarized in Table 4.6. The recovery range from 103.8 to 117.1 %, and RSD (n=3) were below 6% indicating this system is highly accurate.

Table 4.6 Simultaneous determination of glucose, DA and UA in human serum samples (n = 3)

Analyte	Added Concentration (mM)	Measured Concentration (mM)	% Recovery	% RSD
glucose	1	1.15±0.02	117.1	2.6
	2	2.35±0.03	115.3	0.9
	3	3.41±0.01	113.2	0.2
dopamine	10	10.95±0.11	109.5	1.1
	20	21.08±0.67	105.4	3.2
	40	41.52±1.16	103.8	2.8
uric acid	50	52.40±1.51	104.8	2.9
	70	74.03±3.90	105.8	5.3
	100	110.1±3.46	110.1	3.2

CHAPTER V
CONCLUSION

The main objective of this dissertation is to develop the paper-based biosensor coupled with electrochemical detection for the determination of biomarkers in biological samples. Under the optimal conditions, paper-based biosensor of these systems was successful. These results indicate that the developed paper-based biosensors provide a wide linear range and acceptable detection limit for biomarker detection. The detail of various type of paper-based sensors were evaluated as summarized as following;

5.1 Novel Paper-Based Cholesterol Biosensor Using Graphene/ Polyvinylpyrrolidone/Polyaniline Nanocomposite

A novel nanocomposite based on G/PVP/PANI has been prepared and used for the modification of a paper-based cholesterol biosensor. The high conductivity and large surface area of the droplet-like nanostructures of the G/PVP/PANI-modified electrode significantly improves the electrochemical sensitivity for the detection of H_2O_2 and cholesterol. Under optimum conditions, a high-sensitivity, wide linear range and low limit of detection for cholesterol is achieved. The interferences in the detection of cholesterol are easily eliminated by using SDS. In addition, this sensing system is successfully applied for the determination of cholesterol in human serum. This novel and sensitive paper-based biosensor might be an alternative tool for cholesterol screening in medical diagnosis due to its simplicity, low cost, disposability and portability.

5.2 Sensitive Electrochemical Sensor using a Graphene-Polyaniline Nanocomposite for Simultaneous Detection of Zn(II), Cd(II), and Pb(II)

Transparency film and filter paper based device are used and compared in the determination of heavy metal ions including Zn(II), Cd(II) and Pb(II). G/PANI

nanocomposite has been employed in the modification of electrochemical sensor. Along with square wave anodic stripping voltammetry (SWASV), the high conductivity and large surface area of the droplet-like structures of G/PANI nanocomposite modified electrode significantly improves the electrochemical sensitivity in the determination of Zn(II), Cd(II) and Pb(II). In addition, Nafion is coated on the G/PANI nanocomposite modified electrode for increasing sensitive detection of Zn(II), Cd(II) and Pb(II). Under optimum conditions, a high-sensitivity, wide linear range and low limit of detection for Zn(II), Cd(II), and Pb(II) are achieved. Moreover, Nafion coated G/PANI nanocomposite modified electrode is successfully applied to detect Zn(II), Cd(II), and Pb(II) in human serum sample. This developed electrochemical sensor might be an alternative device for heavy metals determination in medical diagnosis.

5.3 Active Paper Chips for Electrochemical Multiprobe Detections

Active paper-based microfluidic chips driven by electrowetting are fabricated. The potential of using active paper chips biosensor to simultaneously detect the dopamine and uric acid biomarkers in human serum is demonstrated for first time. Instead of using the passive capillary force of normal paper-based device, an active paper chips is perfectly used to transport a single or a group of digital liquid drops by programmed trajectories. The pattern of paper is carefully designed to allow the well-mixing between glucose and glucose oxidase enzyme for producing the hydrogen peroxide product and high through put to transport to the detection zone. To enhance the electrochemical signal, Au/rGO and CoPc are accomplished to modify the electrode for the simultaneous detection of dopamine and uric acid and glucose, respectively.

REFERENCES

[1] Rios, A., Escarpa, A., and Simonet, B. Miniaturization in Analytical Chemistry. in Miniaturization of Analytical Systems, pp. 1-38: John Wiley & Sons, Ltd, 2009.

[2] Liu, J.-S., Liu, C., Guo, J.-H., and Wang, L.-D. Electrostatic bonding of a silicon master to a glass wafer for plastic microchannel fabrication. Journal of Materials Processing Technology 178(1–3) (2006): 278-282.

[3] Poenar, D.P., Iliescu, C., Carp, M., Pang, A.J., and Leck, K.J. Glass-based microfluidic device fabricated by parylene wafer-to-wafer bonding for impedance spectroscopy. Sensors and Actuators A: Physical 139(1–2) (2007): 162-171.

[4] Dungchai, W., Chailapakul, O., and Henry, C.S. Electrochemical Detection for Paper-Based Microfluidics. Analytical Chemistry 81(14) (2009): 5821-5826.

[5] Apilux, A., Dungchai, W., Siangproh, W., Praphairaksit, N., Henry, C.S., and Chailapakul, O. Lab-on-Paper with Dual Electrochemical/Colorimetric Detection for Simultaneous Determination of Gold and Iron. Analytical Chemistry 82(5) (2010): 1727-1732.

[6] Mentele, M.M., Cunningham, J., Koehler, K., Volckens, J., and Henry, C.S. Microfluidic Paper-Based Analytical Device for Particulate Metals. Analytical Chemistry 84(10) (2012): 4474-4480.

[7] Geim, A.K. and Novoselov, K.S. The rise of graphene. Nat Mater 6(3) (2007): 183-191.

[8] Harish, C., Sreeharsha, V.S., Santhosh, C., Ramachandran, R., Saranya, M., Vanchinathan, T.M., Govardhan, K., and Grace, A.N. Synthesis of Polyaniline/Graphene Nanocomposites and Its Optical, Electrical and Electrochemical Properties. Advanced Science, Engineering and Medicine 5(2) (2013): 140-148.

[9] Aragay, G. and Merkoçi, A. Nanomaterials application in electrochemical detection of heavy metals. Electrochimica Acta 84(0) (2012): 49-61.

[10] Wei, Y., Gao, C., Meng, F.-L., Li, H.-H., Wang, L., Liu, J.-H., and Huang, X.-J. SnO2/Reduced Graphene Oxide Nanocomposite for the Simultaneous Electrochemical Detection of Cadmium(II), Lead(II), Copper(II), and Mercury(II): An Interesting Favorable Mutual Interference. The Journal of Physical Chemistry C 116(1) (2011): 1034-1041.

[11] Ruecha, N., Rangkupan, R., Rodthongkum, N., and Chailapakul, O. Novel paper-based cholesterol biosensor using graphene/polyvinylpyrrolidone/polyaniline nanocomposite. Biosensors and Bioelectronics 52(0) (2014): 13-19.

[12] Rodthongkum, N., Ruecha, N., Rangkupan, R., Vachet, R.W., and Chailapakul, O. Graphene-loaded nanofiber-modified electrodes for the ultrasensitive determination of dopamine. Analytica Chimica Acta 804(0) (2013): 84-91.

[13] Wang, L., Lu, X., Lei, S., and Song, Y. Graphene-based polyaniline nanocomposites: preparation, properties and applications. Journal of Materials Chemistry A 2(13) (2014): 4491-4509.

[14] Saini, D. and Basu, T. Synthesis and characterization of nanocomposites based on polyaniline-gold/graphene nanosheets. Applied Nanoscience 2(4) (2012): 467-479.

[15] Ko, H., Lee, J., Kim, Y., Lee, B., Jung, C.-H., Choi, J.-H., Kwon, O.-S., and Shin, K. Active Digital Microfluidic Paper Chips with Inkjet-Printed Patterned Electrodes. Advanced Materials 26(15) (2014): 2335-2340.

[16] Vargas-Bernal, R., Herrera-Pérez, G., and Rodríguez-Miranda, E. Evolution and Expectations of Enzymatic Biosensors for Pesticides. Pesticides - Advances in Chemical and Botanical Pesticides. 2012.

[17] Hamidi-Asl, E., Palchetti, I., Hasheminejad, E., and Mascini, M. A review on the electrochemical biosensors for determination of microRNAs. Talanta 115(0) (2013): 74-83.

[18] Ding, L., Bond, A.M., Zhai, J., and Zhang, J. Utilization of nanoparticle labels for signal amplification in ultrasensitive electrochemical affinity biosensors: A review. Analytica Chimica Acta 797(0) (2013): 1-12.

[19] Pohanka, M. Cholinesterases in Biorecognition and Biosensors Construction: A Review. Analytical Letters 46(12) (2013): 1849-1868.

[20] Marazuela, M. and Moreno-Bondi, M. Fiber-optic biosensors – an overview. Analytical and Bioanalytical Chemistry 372(5-6) (2002): 664-682.

[21] Soylak, M. and Kizil, N. Determination of some heavy metals by flame atomic absorption spectrometry before coprecipitation with neodymium hydroxide. J AOAC Int 94(3) (2011): 978-84.

[22] Maciel, J.V., Knorr, C.L., Flores, E.M.M., Müller, E.I., Mesko, M.F., Primel, E.G., and Duarte, F.A. Feasibility of microwave-induced combustion for trace element determination in Engraulis anchoita by ICP-MS. Food Chemistry 145(0) (2014): 927-931.

[23] Furia, E., Aiello, D., Di Donna, L., Mazzotti, F., Tagarelli, A., Thangavel, H., Napoli, A., and Sindona, G. Mass spectrometry and potentiometry studies of Pb(ii)-, Cd(ii)- and Zn(ii)-cystine complexes. Dalton Transactions 43(3) (2014): 1055-1062.

[24] Lee, G.-J., Kim, C.K., Lee, M.K., and Rhee, C.K. Simultaneous Voltammetric Determination of Zn, Cd and Pb at Bismuth Nanopowder Electrodes with Various Particle Size Distributions. Electroanalysis 22(5) (2010): 530-535.

[25] Ouyang, R., Zhu, Z., Tatum, C.E., Chambers, J.Q., and Xue, Z.-L. Simultaneous stripping detection of Zn(II), Cd(II) and Pb(II) using a bimetallic Hg–Bi/single-walled carbon nanotubes composite electrode. Journal of Electroanalytical Chemistry 656(1–2) (2011): 78-84.

[26] Injang, U., Noyrod, P., Siangproh, W., Dungchai, W., Motomizu, S., and Chailapakul, O. Determination of trace heavy metals in herbs by sequential injection analysis-anodic stripping voltammetry using screen-printed carbon nanotubes electrodes. Analytica Chimica Acta 668(1) (2010): 54-60.

[27] Rattanarat, P., Dungchai, W., Cate, D., Volckens, J., Chailapakul, O., and Henry, C.S. Multilayer Paper-Based Device for Colorimetric and Electrochemical Quantification of Metals. Analytical Chemistry 86(7) (2014): 3555-3562.

[28] Krolicka, A., Bobrowski, A., Kalcher, K., Mocak, J., Svancara, I., and Vytras, K. Study on Catalytic Adsorptive Stripping Voltammetry of Trace Cobalt at Bismuth Film Electrodes. Electroanalysis 15(23-24) (2003): 1859-1863.

[29] Jothimuthu, P., Wilson, R., Herren, J., Haynes, E., Heineman, W., and Papautsky, I. Lab-on-a-chip sensor for detection of highly electronegative heavy metals by anodic stripping voltammetry. Biomedical Microdevices 13(4) (2011): 695-703.

[30] Lu, Y., Shi, W., Jiang, L., Qin, J., and Lin, B. Rapid prototyping of paper-based microfluidics with wax for low-cost, portable bioassay. Electrophoresis 30(9) (2009): 1497-1500.

[31] Carrilho, E., Martinez, A.W., and Whitesides, G.M. Understanding Wax Printing: A Simple Micropatterning Process for Paper-Based Microfluidics. Analytical Chemistry 81(16) (2009): 7091-7095.

[32] Lu, Y., Shi, W., Qin, J., and Lin, B. Fabrication and Characterization of Paper-Based Microfluidics Prepared in Nitrocellulose Membrane By Wax Printing. Analytical Chemistry 82(1) (2010): 329-335.

[33] Abe, K., Suzuki, K., and Citterio, D. Inkjet-Printed Microfluidic Multianalyte Chemical Sensing Paper. Analytical Chemistry 80(18) (2008): 6928-6934.

[34] de Pedro, S., Cadarso, V.J., Muñoz-Berbel, X., Plaza, J.A., Sort, J., Brugger, J., Büttgenbach, S., and Llobera, A. PDMS-based, magnetically actuated variable optical attenuators obtained by soft lithography and inkjet printing technologies. Sensors and Actuators A: Physical 215(0) (2014): 30-35.

[35] Kit-Anan, W., Olarnwanich, A., Sriprachuabwong, C., Karuwan, C., Tuantranont, A., Wisitsoraat, A., Srituravanich, W., and Pimpin, A. Disposable paper-based electrochemical sensor utilizing inkjet-printed Polyaniline modified screen-printed carbon electrode for Ascorbic acid detection. Journal of Electroanalytical Chemistry 685(0) (2012): 72-78.

[36] Cho, H., Parameswaran, M., and Yu, H.-Z. Fabrication of microsensors using unmodified office inkjet printers. Sensors and Actuators B: Chemical 123(2) (2007): 749-756.

[37] Li, M., Li, Y.-T., Li, D.-W., and Long, Y.-T. Recent developments and applications of screen-printed electrodes in environmental assays—A review. Analytica Chimica Acta 734(0) (2012): 31-44.

[38] Ricci, F., Amine, A., Tuta, C.S., Ciucu, A.A., Lucarelli, F., Palleschi, G., and Moscone, D. Prussian Blue and enzyme bulk-modified screen-printed electrodes for hydrogen peroxide and glucose determination with improved storage and operational stability. Analytica Chimica Acta 485(1) (2003): 111-120.

[39] Hu, T., Zhang, X.-E., Zhang, Z.-P., and Chen, L.-Q. A Screen-Printed Disposable Enzyme Electrode System for Simultaneous Determination of Sucrose and Glucose. Electroanalysis 12(11) (2000): 868-870.

[40] Dungchai, W., Chailapakul, O., and Henry, C.S. A low-cost, simple, and rapid fabrication method for paper-based microfluidics using wax screen-printing. Analyst 136(1) (2011): 77-82.

[41] Chiu, M.-H., Wu, H., Chen, J.-C., Muthuraman, G., and Zen, J.-M. Disposable Screen-Printed Carbon Electrodes for Dual Electrochemiluminescence/Amperometric Detection: Sequential Injection Analysis of Oxalate. Electroanalysis 19(22) (2007): 2301-2306.

[42] Bakker, E. and Qin, Y. Electrochemical Sensors. Analytical Chemistry 78(12) (2006): 3965-3984.

[43] Kimmel, D.W., LeBlanc, G., Meschievitz, M.E., and Cliffel, D.E. Electrochemical Sensors and Biosensors. Analytical Chemistry 84(2) (2011): 685-707.

[44] Bleam, W.F. Chapter 8 - Redox Chemistry. in Bleam, W.F. (ed.)Soil and Environmental Chemistry, pp. 321-370. Boston: Academic Press, 2012.

[45] Panero, S. ELECTROCHEMICAL THEORY | Thermodynamics. in Garche, J. (ed.)Encyclopedia of Electrochemical Power Sources, pp. 1-7. Amsterdam: Elsevier, 2009.

[46] Sohail, M. and De Marco, R. ELECTRODES | Ion-Selective Electrodes. in Reference Module in Chemistry, Molecular Sciences and Chemical Engineering: Elsevier, 2013.

[47] Lovrić, M. and Komorsky-Lovrić, Š. Theory of square wave voltammetry of three step electrode reaction. Journal of Electroanalytical Chemistry 735(0) (2014): 90-94.

[48] Tiwari, I., Singh, M., Pandey, C.M., and Sumana, G. Electrochemical genosensor based on graphene oxide modified iron oxide–chitosan hybrid nanocomposite for pathogen detection. Sensors and Actuators B: Chemical 206(0) (2015): 276-283.

[49] Adeloju, S.B. AMPEROMETRY. in Poole, P.W.T. (ed.)Encyclopedia of Analytical Science (Second Edition), pp. 70-79. Oxford: Elsevier, 2005.

[50] Bard, A.J. and Faulkner, L.R. Fundamentals and Applications. 2nd ed. New York, USA: Jonh Wiley & Sons, 2001.

[51] Skoog, D.A., Holler, F.J., and Nieman, T.A. Principles of Instrumental Analysis. New York, USA: Harcourt Brace College, 1998.

[52] Orazem, M.E. and Bernard, T. Electrochemical Impedance Spectroscopy. John Wiley & Sons,, 2008.

[53] Prins, M.W.J., Welters, W.J.J., and Weekamp, J.W. Fluid Control in Multichannel Structures by Electrocapillary Pressure. Science 291(5502) (2001): 277-280.

[54] Hao, C., Liu, Y., Chen, X., He, Y., Li, Q., Li, K.Y., and Wang, Z. Electrowetting on liquid-infused film (EWOLF): Complete reversibility and controlled droplet oscillation suppression for fast optical imaging. Sci. Rep. 4 (2014).

[55] Cho, S.K., Moon, H., and Chang-Jin, K. Creating, transporting, cutting, and merging liquid droplets by electrowetting-based actuation for digital microfluidic circuits. Microelectromechanical Systems, Journal of 12(1) (2003): 70-80.

[56] Arya, S.K., Datta, M., and Malhotra, B.D. Recent advances in cholesterol biosensor. Biosensors and Bioelectronics 23(7) (2008): 1083-1100.

[57] Dey, R.S. and Raj, C.R. Development of an Amperometric Cholesterol Biosensor Based on Graphene−Pt Nanoparticle Hybrid Material. The Journal of Physical Chemistry C 114(49) (2010): 21427-21433.

[58] Eguílaz, M., Villalonga, R., Agüí, L., Yáñez-Sedeño, P., and Pingarrón, J.M. Gold nanoparticles: Poly(diallyldimethylammonium chloride)–carbon nanotubes composites as platforms for the preparation of electrochemical enzyme biosensors: Application to the determination of cholesterol. Journal of Electroanalytical Chemistry 661(1) (2011): 171-178.

[59] van Staden, J.F. and van Staden, R.I.S. Flow-injection analysis systems with different detection devices and other related techniques for the in vitro and in vivo determination of dopamine as neurotransmitter. A review. Talanta 102(0) (2012): 34-43.

[60] Studer, L., Psylla, M., Bühler, B., Evtouchenko, L., Vouga, C.M., Leenders, K.L., Seiler, R.W., and Spenger, C. Noninvasive dopamine determination by reversed phase HPLC in the medium of free-floating roller tube cultures of rat fetal ventral mesencephalon: A tool to assess dopaminergic tissue prior to grafting. Brain Research Bulletin 41(3) (1996): 143-150.

[61] Liu, L., Li, Q., Li, N., Ling, J., Liu, R., Wang, Y., Sun, L., Chen, X.H., and Bi, K. Simultaneous determination of catecholamines and their metabolites related to Alzheimer's disease in human urine. Journal of Separation Science 34(10) (2011): 1198-1204.

[62] Puumala, T. and Sirviö, J. Changes in activities of dopamine and serotonin systems in the frontal cortex underlie poor choice accuracy and impulsivity of rats in an attention task. Neuroscience 83(2) (1998): 489-499.

[63] Jakel, R.J. and Maragos, W.F. Neuronal cell death in Huntington's disease: a potential role for dopamine. Trends in Neurosciences 23(6) (2000): 239-245.

[64] Song, P., Mabrouk, O.S., Hershey, N.D., and Kennedy, R.T. In Vivo Neurochemical Monitoring Using Benzoyl Chloride Derivatization and Liquid Chromatography–Mass Spectrometry. Analytical Chemistry 84(1) (2012): 412-419.

[65] Uutela, P., Karhu, L., Piepponen, P., Käenmäki, M., Ketola, R.A., and Kostiainen, R. Discovery of Dopamine Glucuronide in Rat and Mouse Brain Microdialysis Samples Using Liquid Chromatography Tandem Mass Spectrometry. Analytical Chemistry 81(1) (2009): 427-434.

[66] Shou, M., Ferrario, C.R., Schultz, K.N., Robinson, T.E., and Kennedy, R.T. Monitoring Dopamine in Vivo by Microdialysis Sampling and On-Line CE-Laser-Induced Fluorescence. Analytical Chemistry 78(19) (2006): 6717-6725.

[67] Liu, Y.-M., Wang, C.-Q., Mu, H.-B., Cao, J.-T., and Zheng, Y.-L. Determination of catecholamines by CE with direct chemiluminescence detection. ELECTROPHORESIS 28(12) (2007): 1937-1941.

[68] Hu, Y., Xu, W., Li, J., and Li, L. Determination of 5-hydroxytryptamine in serum by electrochemiluminescence detection with the aid of capillary electrophoresis. Luminescence 27(1) (2012): 63-68.

[69] Li, L., Liu, H., Shen, Y., Zhang, J., and Zhu, J.-J. Electrogenerated Chemiluminescence of Au Nanoclusters for the Detection of Dopamine. Analytical Chemistry 83(3) (2011): 661-665.

[70] Grundmann, M., Rothenhöfer, M., Bernhardt, G., Buschauer, A., and Matysik, F.-M. Fast counter-electroosmotic capillary electrophoresis–time-of-flight mass spectrometry of hyaluronan oligosaccharides. Analytical and Bioanalytical Chemistry 402(8) (2012): 2617-2623.

[71] Khan, M.M.I., Haque, A.-M.J., and Kim, K. Electrochemical determination of uric acid in the presence of ascorbic acid on electrochemically reduced graphene oxide modified electrode. Journal of Electroanalytical Chemistry 700(0) (2013): 54-59.

[72] Erden, P.E. and Kılıç, E. A review of enzymatic uric acid biosensors based on amperometric detection. Talanta 107(0) (2013): 312-323.

[73] Ojani, R., Alinezhad, A., and Abedi, Z. A highly sensitive electrochemical sensor for simultaneous detection of uric acid, xanthine and hypoxanthine based on poly(l-methionine) modified glassy carbon electrode. Sensors and Actuators B: Chemical 188(0) (2013): 621-630.

[74] Chen, J.C., Chung, H.H., Hsu, C.T., Tsai, D.M., Kumar, A.S., and Zen, J.M. A disposable single-use electrochemical sensor for the detection of uric acid in human whole blood. Sensors and Actuators B: Chemical 110(2) (2005): 364-369.

[75] Wang, C., Du, J., Wang, H., Zou, C.e., Jiang, F., Yang, P., and Du, Y. A facile electrochemical sensor based on reduced graphene oxide and Au nanoplates modified glassy carbon electrode for simultaneous detection of ascorbic acid,

dopamine and uric acid. Sensors and Actuators B: Chemical 204(0) (2014): 302-309.

[76] Yang, L., Liu, D., Huang, J., and You, T. Simultaneous determination of dopamine, ascorbic acid and uric acid at electrochemically reduced graphene oxide modified electrode. Sensors and Actuators B: Chemical 193(0) (2014): 166-172.

[77] Temoçin, Z. Modification of glassy carbon electrode in basic medium by electrochemical treatment for simultaneous determination of dopamine, ascorbic acid and uric acid. Sensors and Actuators B: Chemical 176(0) (2013): 796-802.

[78] Rattanarat, P., Dungchai, W., Siangproh, W., Chailapakul, O., and Henry, C.S. Sodium dodecyl sulfate-modified electrochemical paper-based analytical device for determination of dopamine levels in biological samples. Analytica Chimica Acta 744(0) (2012): 1-7.

[79] Lim, S.S., Vos, T., Flaxman, A.D., Danaei, G., Shibuya, K., Adair-Rohani, H., AlMazroa, M.A., Amann, M., Anderson, H.R., Andrews, K.G., Aryee, M., Atkinson, C., Bacchus, L.J., Bahalim, A.N., Balakrishnan, K., Balmes, J., Barker-Collo, S., Baxter, A., Bell, M.L., Blore, J.D., Blyth, F., Bonner, C., Borges, G., Bourne, R., Boussinesq, M., Brauer, M., Brooks, P., Bruce, N.G., Brunekreef, B., Bryan-Hancock, C., Bucello, C., Buchbinder, R., Bull, F., Burnett, R.T., Byers, T.E., Calabria, B., Carapetis, J., Carnahan, E., Chafe, Z., Charlson, F., Chen, H., Chen, J.S., Cheng, A.T.-A., Child, J.C., Cohen, A., Colson, K.E., Cowie, B.C., Darby, S., Darling, S., Davis, A., Degenhardt, L., Dentener, F., Des Jarlais, D.C., Devries, K., Dherani, M., Ding, E.L., Dorsey, E.R., Driscoll, T., Edmond, K., Ali, S.E., Engell, R.E., Erwin, P.J., Fahimi, S., Falder, G., Farzadfar, F., Ferrari, A., Finucane, M.M., Flaxman, S., Fowkes, F.G.R., Freedman, G., Freeman, M.K., Gakidou, E., Ghosh, S., Giovannucci, E., Gmel, G., Graham, K., Grainger, R., Grant, B., Gunnell, D., Gutierrez, H.R., Hall, W., Hoek, H.W., Hogan, A., Hosgood Iii, H.D., Hoy, D., Hu, H., Hubbell, B.J., Hutchings, S.J., Ibeanusi, S.E., Jacklyn, G.L., Jasrasaria, R., Jonas, J.B., Kan, H., Kanis, J.A., Kassebaum, N., Kawakami, N., Khang, Y.-H., Khatibzadeh, S., Khoo, J.-P., Kok, C., Laden, F., Lalloo, R., Lan, Q., Lathlean, T.,

Leasher, J.L., Leigh, J., Li, Y., Lin, J.K., Lipshultz, S.E., London, S., Lozano, R., Lu, Y., Mak, J., Malekzadeh, R., Mallinger, L., Marcenes, W., March, L., Marks, R., Martin, R., McGale, P., McGrath, J., Mehta, S., Memish, Z.A., Mensah, G.A., Merriman, T.R., Micha, R., Michaud, C., Mishra, V., Hanafiah, K.M., Mokdad, A.A., Morawska, L., Mozaffarian, D., Murphy, T., Naghavi, M., Neal, B., Nelson, P.K., Nolla, J.M., Norman, R., Olives, C., Omer, S.B., Orchard, J., Osborne, R., Ostro, B., Page, A., Pandey, K.D., Parry, C.D.H., Passmore, E., Patra, J., Pearce, N., Pelizzari, P.M., Petzold, M., Phillips, M.R., Pope, D., Pope Iii, C.A., Powles, J., Rao, M., Razavi, H., Rehfuess, E.A., Rehm, J.T., Ritz, B., Rivara, F.P., Roberts, T., Robinson, C., Rodriguez-Portales, J.A., Romieu, I., Room, R., Rosenfeld, L.C., Roy, A., Rushton, L., Salomon, J.A., Sampson, U., Sanchez-Riera, L., Sanman, E., Sapkota, A., Seedat, S., Shi, P., Shield, K., Shivakoti, R., Singh, G.M., Sleet, D.A., Smith, E., Smith, K.R., Stapelberg, N.J.C., Steenland, K., Stöckl, H., Stovner, L.J., Straif, K., Straney, L., Thurston, G.D., Tran, J.H., Van Dingenen, R., van Donkelaar, A., Veerman, J.L., Vijayakumar, L., Weintraub, R., Weissman, M.M., White, R.A., Whiteford, H., Wiersma, S.T., Wilkinson, J.D., Williams, H.C., Williams, W., Wilson, N., Woolf, A.D., Yip, P., Zielinski, J.M., Lopez, A.D., Murray, C.J.L. and Ezzati, M. A comparative risk assessment of burden of disease and injury attributable to 67 risk factors and risk factor clusters in 21 regions, 1990–2010: a systematic analysis for the Global Burden of Disease Study 2010. The Lancet 380(9859) (2012): 2224-2260.

[80] Loomis, D., Grosse, Y., Lauby-Secretan, B., Ghissassi, F.E., Bouvard, V., Benbrahim-Tallaa, L., Guha, N., Baan, R., Mattock, H., and Straif, K. The carcinogenicity of outdoor air pollution. The Lancet Oncology 14(13) (2013): 1262-1263.

[81] Heyland, D.K., Jones, N., Cvijanovich, N.Z., and Wong, H. Zinc Supplementation in Critically Ill Patients: A Key Pharmaconutrient? Journal of Parenteral and Enteral Nutrition 32(5) (2008): 509-519.

[82] Jacob, R.A., Spinozzi, G.M., Simon, V.A., Kelley, D.S., Prior, R.L., Hess-Pierce, B., and Kader, A.A. Consumption of Cherries Lowers Plasma Urate in Healthy Women. The Journal of Nutrition 133(6) (2003): 1826-1829.

[83] Salomao, R., Brunialti, M.K.C., Gomes, N.E., Mendes, M.E., Diaz, R.S., Komninakis, S., Machado, F.R., da Silva, I.D.C.G., and Rigato, O. Toll-like receptor pathway signaling is differently regulated in neutrophils and peripheral mononuclear cells of patients with sepsis, severe sepsis, and septic shock*. Critical Care Medicine 37(1) (2009): 132-139 10.1097/CCM.0b013e318192fbaf.

[84] Cvijanovich, N., Shanley, T.P., Lin, R., Allen, G.L., Thomas, N.J., Checchia, P., Anas, N., Freishtat, R.J., Monaco, M., Odoms, K., Sakthivel, B., and Wong, H.R. Validating the genomic signature of pediatric septic shock. Physiol genomics 34(1) (2008): 127-134.

[85] Plum, L.M., Rink, L., and Haase, H. The Essential Toxin: Impact of Zinc on Human Health. International Journal of Environmental Research and Public Health 7(4) (2010): 1342-1365.

[86] Guallar, E., Silbergeld, E.K., Navas-Acien, A., Malhotra, S., Astor, B.C., Sharrett, A.R., and Schwartz, B.S. Confounding of the Relation between Homocysteine and Peripheral Arterial Disease by Lead, Cadmium, and Renal Function. American Journal of Epidemiology 163(8) (2006): 700-708.

[87] Navas-Acien, A., Selvin, E., Sharrett, A.R., Calderon-Aranda, E., Silbergeld, E., and Guallar, E. Lead, Cadmium, Smoking, and Increased Risk of Peripheral Arterial Disease. Circulation 109(25) (2004): 3196-3201.

[88] Jacquillet, G., Barbier, O., Cougnon, M., Tauc, M., Namorado, M.C., Martin, D., Reyes, J.L., and Poujeol, P. Zinc protects renal function during cadmium intoxication in the rat. Am J Physiol Renal Physiol 290(1) (2006): F127-37.

[89] Lanphear, B.P., Dietrich, K.N., and Berger, O. Prevention of Lead Toxicity in US Children. Ambulatory pediatrics 3(1) (2003): 27-36.

[90] Ruecha, N., Siangproh, W., and Chailapakul, O. A fast and highly sensitive detection of cholesterol using polymer microfluidic devices and amperometric system. Talanta 84(5) (2011): 1323-1328.

[91] Shin, Y.J. and Kameoka, J. Amperometric cholesterol biosensor using layer-by-layer adsorption technique onto electrospun polyaniline nanofibers. Journal of Industrial and Engineering Chemistry 18(1) (2012): 193-197.

[92] Rattanarat, P., Dungchai, W., Siangproh, W., Chailapakul, O., and Henry, C.S. Sodium dodecyl sulfate-modified electrochemical paper-based analytical device for determination of dopamine levels in biological samples. Analytica Chimica Acta 744 (2012): 1-7.

[93] Zhang, P., Han, X., Kang, L., Qiang, R., Liu, W., and Du, Y. Synthesis and characterization of polyaniline nanoparticles with enhanced microwave absorption. RSC Advances 3(31) (2013): 12694-12701.

[94] Kwon, O.-S., Kim, H., Ko, H., Lee, J., Lee, B., Jung, C.-H., Choi, J.-H., and Shin, K. Fabrication and characterization of inkjet-printed carbon nanotube electrode patterns on paper. Carbon 58(0) (2013): 116-127.

[95] Karuwan, C., Sriprachuabwong, C., Wisitsoraat, A., Phokharatkul, D., Sritongkham, P., and Tuantranont, A. Inkjet-printed graphene-poly(3,4-ethylenedioxythiophene):poly(styrene-sulfonate) modified on screen printed carbon electrode for electrochemical sensing of salbutamol. Sensors and Actuators B-Chemical 161(1) (2012): 549-555.

[96] Manjunatha, R., Shivappa Suresh, G., Savio Melo, J., D'Souza, S.F., and Venkatarangaiah Venkatesha, T. An amperometric bienzymatic cholesterol biosensor based on functionalized graphene modified electrode and its electrocatalytic activity towards total cholesterol determination. Talanta 99(0) (2012): 302-309.

[97] Aravind, S.S.J., Baby, T.T., Arockiadoss, T., Rakhi, R.B., and Ramaprabhu, S. A cholesterol biosensor based on gold nanoparticles decorated functionalized graphene nanoplatelets. Thin Solid Films 519(16) (2011): 5667-5672.

[98] Ahmadalinezhad, A. and Chen, A. High-performance electrochemical biosensor for the detection of total cholesterol. Biosensors and Bioelectronics 26(11) (2011): 4508-4513.

[99] Singh, J., Srivastava, M., Kalita, P., and Malhotra, B.D. A novel ternary NiFe2O4/CuO/FeO-chitosan nanocomposite as a cholesterol biosensor. Process Biochemistry 47(12) (2012): 2189-2198.

[100] Saxena, U., Chakraborty, M., and Goswami, P. Covalent immobilization of cholesterol oxidase on self-assembled gold nanoparticles for highly sensitive

amperometric detection of cholesterol in real samples. Biosensors and Bioelectronics 26(6) (2011): 3037-3043.

[101] Gomathi, P., Ragupathy, D., Choi, J.H., Yeum, J.H., Lee, S.C., Kim, J.C., Lee, S.H., and Ghim, H.D. Fabrication of novel chitosan nanofiber/gold nanoparticles composite towards improved performance for a cholesterol sensor. Sensors and Actuators B: Chemical 153(1) (2011): 44-49.

[102] Safavi, A. and Farjami, F. Electrodeposition of gold–platinum alloy nanoparticles on ionic liquid–chitosan composite film and its application in fabricating an amperometric cholesterol biosensor. Biosensors and Bioelectronics 26(5) (2011): 2547-2552.

[103] Dey, R.S. and Raj, C.R. Development of an Amperometric Cholesterol Biosensor Based on Graphene-Pt Nanoparticle Hybrid Material. Journal of Physical Chemistry C 114(49) (2010): 21427-21433.

[104] Parmar, M., Balamurugan, C., and Lee, D.-W. PANI and Graphene/PANI Nanocomposite Films — Comparative Toluene Gas Sensing Behavior. Sensors 13(12) (2013): 16611-16624.

[105] Rana, U. and Malik, S. Graphene oxide/polyaniline nanostructures: transformation of 2D sheet to 1D nanotube and in situ reduction. Chemical Communications 48(88) (2012): 10862-10864.

[106] Dimovasilis, P.A. and Prodromidis, M.I. Bismuth-dispersed xerogel-based composite films for trace Pb(II) and Cd(II) voltammetric determination. Analytica Chimica Acta 769(0) (2013): 49-55.

[107] Rico, M.Á.G., Olivares-Marín, M., and Gil, E.P. Modification of carbon screen-printed electrodes by adsorption of chemically synthesized Bi nanoparticles for the voltammetric stripping detection of Zn(II), Cd(II) and Pb(II). Talanta 80(2) (2009): 631-635.

[108] Li, M., Li, D.-W., Li, Y.-T., Xu, D.-K., and Long, Y.-T. Highly selective in situ metal ion determination by hybrid electrochemical “adsorption–desorption” and colorimetric methods. Analytica Chimica Acta 701(2) (2011): 157-163.

[109] Koper, A. and Grabarczyk, M. Electrochemical determination of bismuth with use of a Bi(III)-cupferron complexation system and elimination of interferences

connected with the presence of organic substances in natural samples. Journal of Electroanalytical Chemistry 663(2) (2011): 67-71.

[110] Keawkim, K., Chuanuwatanakul, S., Chailapakul, O., and Motomizu, S. Determination of lead and cadmium in rice samples by sequential injection/anodic stripping voltammetry using a bismuth film/crown ether/Nafion modified screen-printed carbon electrode. Food Control 31(1) (2013): 14-21.

[111] Legeai, S. and Vittori, O. A Cu/Nafion/Bi electrode for on-site monitoring of trace heavy metals in natural waters using anodic stripping voltammetry: An alternative to mercury-based electrodes. Analytica Chimica Acta 560(1–2) (2006): 184-190.

[112] Zhao, D., Guo, X., Wang, T., Alvarez, N., Shanov, V.N., and Heineman, W.R. Simultaneous Detection of Heavy Metals by Anodic Stripping Voltammetry Using Carbon Nanotube Thread. Electroanalysis 26(3) (2014): 488-496.

[113] Wu, Y., Li, N.B., and Luo, H.Q. Simultaneous measurement of Pb, Cd and Zn using differential pulse anodic stripping voltammetry at a bismuth/poly(p-aminobenzene sulfonic acid) film electrode. Sensors and Actuators B: Chemical 133(2) (2008): 677-681.

[114] Xiao, L., Xu, H., Zhou, S., Song, T., Wang, H., Li, S., Gan, W., and Yuan, Q. Simultaneous detection of Cd(II) and Pb(II) by differential pulse anodic stripping voltammetry at a nitrogen-doped microporous carbon/Nafion/bismuth-film electrode. Electrochimica Acta 143(0) (2014): 143-151.

[115] Zhu, L., Xu, L., Huang, B., Jia, N., Tan, L., and Yao, S. Simultaneous determination of Cd(II) and Pb(II) using square wave anodic stripping voltammetry at a gold nanoparticle-graphene-cysteine composite modified bismuth film electrode. Electrochimica Acta 115(0) (2014): 471-477.

[116] Chen, L., Su, Z., He, X., Liu, Y., Qin, C., Zhou, Y., Li, Z., Wang, L., Xie, Q., and Yao, S. Square wave anodic stripping voltammetric determination of Cd and Pb ions at a Bi/Nafion/thiolated polyaniline/glassy carbon electrode. Electrochemistry Communications 15(1) (2012): 34-37.

[117] Herrero, E., Arancibia, V., and Rojas–Romo, C. Simultaneous determination of Pb2+, Cd2+ and Zn2+ by adsorptive stripping voltammetry using Clioquinol as a chelating-adsorbent agent. Journal of Electroanalytical Chemistry 729(0) (2014): 9-14.

[118] Goullé, J.-P., Mahieu, L., Castermant, J., Neveu, N., Bonneau, L., Lainé, G., Bouige, D., and Lacroix, C. Metal and metalloid multi-elementary ICP-MS validation in whole blood, plasma, urine and hair. Forensic Science International 153(1): 39-44.

VITA

Miss Nipapan Ruecha was born in May 12, 1985 in Bangkok, Thailand. She is a smallest daughter of Maj. Boonthavee Ruecha and Mrs. Saowalux Yimprasert. She finished elementary shool and high school from Khemapittaya School and Wat Khemapirataram School, respectively. She received her Bachelor Degree with 2nd Honor in Science, majoring in General Science (Chemistry Minor) from Kasetsart University in 2006. After that, she worked in quantitative analysis at Atlantic Pharmaceutical Co., Ltd. for 11 month. In 2009, she finished Master degree in Petrochemistry and Polymer Science, Chulalongkorn University. She received the financial support for her Ph.D. program in Macromolecular Science from Chulalongkorn University Dutsadi Phiphat Scholarship. Miss Nipapan Ruecha was visited in Henry's research lab, Department of Chemistry, Colorado State University, USA. Moreover, she was also internship student at Biological Interfaces Lab (Prof. Kwanwoo Shin) in Sogang University, South Korea. Her research interest areas focus on Microfluidics device (e.g. paper-based device and polymeric device), biosensor using electrochemistry and colorimetry and nanocomposite for sensor development.